NAVAL POSTGRADUATE SCHOOL

MONTEREY, CALIFORNIA

THESIS

SINTERING OF ADDITIVELY MANUFACTURED HYDROXYAPATITE EMBEDDED WITH BORON NITRIDE NANOTUBES

by

Nathan J. Matalavage

June 2023

Thesis Advisor: Troy Ansell
Second Reader: Chanman Park

THIS PAGE INTENTIONALLY LEFT BLANK

REPORT DOCUMENTATION PAGE	*Form Approved OMB No. 0704-0188*

1. AGENCY USE ONLY *(Leave blank)*	**2. REPORT DATE** June 2023	**3. REPORT TYPE AND DATES COVERED** Master's thesis

4. TITLE AND SUBTITLE SINTERING OF ADDITIVELY MANUFACTURED HYDROXYAPATITE EMBEDDED WITH BORON NITRIDE NANOTUBES	**5. FUNDING NUMBERS**
6. AUTHOR(S) Nathan J. Matalavage	
7. PERFORMING ORGANIZATION NAME(S) AND ADDRESS(ES) Naval Postgraduate School Monterey, CA 93943-5000	**8. PERFORMING ORGANIZATION REPORT NUMBER**
9. SPONSORING / MONITORING AGENCY NAME(S) AND ADDRESS(ES) N/A	**10. SPONSORING / MONITORING AGENCY REPORT NUMBER**

11. SUPPLEMENTARY NOTES The views expressed in this thesis are those of the author and do not reflect the official policy or position of the Department of Defense or the U.S. Government.

12a. DISTRIBUTION / AVAILABILITY STATEMENT Approved for public release. Distribution is unlimited.	**12b. DISTRIBUTION CODE** A

13. ABSTRACT (maximum 200 words)

As technologies like hypersonics develop, the need for advanced ceramic and composite materials becomes more urgent. These materials must have unique geometries and exceptional materials properties like high melting (or decomposition) temperature, low thermal conductivity, and high thermal shock resistance. In many cases, the only way to achieve the required geometry is by additive manufacturing. Furthermore, ceramic parts often need to be reinforced with nanoparticles to achieve the desired properties. This presents an issue since the high temperature of ceramic post-processing can degrade or even destroy these nanoparticles. This thesis sought to identify a method to sinter a 3D-printed ceramic while keeping the embedded nanoparticles intact. This work focused on hydroxyapatite [$Ca_{10}(PO_4)_6(OH)_2$] embedded with boron nitride nanotubes (BNNTs). The samples were heat treated in argon using a tube furnace. The temperature and the sintering medium were varied to determine the ideal process. After post-processing, the samples were evaluated using X-ray diffraction, scanning electron microscope analysis, and the Archimedes method. No significant trends in the density were noted throughout testing; however, it was found that samples that were sintered in a boron nitride powder medium displayed intact BNNTs post-sintering. This demonstrated that BNNTs can survive temperatures far above their oxidation point if the environment is carefully controlled.

14. SUBJECT TERMS BNNT, boron nitride nanotubes, alumina, hydroxyapatite, additive manufactured ceramics, ceramic sintering	**15. NUMBER OF PAGES** 99
	16. PRICE CODE

17. SECURITY CLASSIFICATION OF REPORT Unclassified	**18. SECURITY CLASSIFICATION OF THIS PAGE** Unclassified	**19. SECURITY CLASSIFICATION OF ABSTRACT** Unclassified	**20. LIMITATION OF ABSTRACT** UU

NSN 7540-01-280-5500

Standard Form 298 (Rev. 2-89)
Prescribed by ANSI Std. 239-18

THIS PAGE INTENTIONALLY LEFT BLANK

Approved for public release. Distribution is unlimited.

SINTERING OF ADDITIVELY MANUFACTURED HYDROXYAPATITE EMBEDDED WITH BORON NITRIDE NANOTUBES

Nathan J. Matalavage
Ensign, United States Navy
BS, United States Naval Academy, 2022

Submitted in partial fulfillment of the
requirements for the degree of

MASTER OF SCIENCE IN MECHANICAL ENGINEERING

from the

NAVAL POSTGRADUATE SCHOOL
June 2023

Approved by: Troy Ansell
Advisor

Chanman Park
Second Reader

Brian S. Bingham
Chair, Department of Mechanical and Aerospace Engineering

THIS PAGE INTENTIONALLY LEFT BLANK

ABSTRACT

As technologies like hypersonics develop, the need for advanced ceramic and composite materials becomes more urgent. These materials must have unique geometries and exceptional materials properties like high melting (or decomposition) temperature, low thermal conductivity, and high thermal shock resistance. In many cases, the only way to achieve the required geometry is by additive manufacturing. Furthermore, ceramic parts often need to be reinforced with nanoparticles to achieve the desired properties. This presents an issue since the high temperature of ceramic post-processing can degrade or even destroy these nanoparticles. This thesis sought to identify a method to sinter a 3D-printed ceramic while keeping the embedded nanoparticles intact. This work focused on hydroxyapatite [$Ca_{10}(PO_4)_6(OH)_2$] embedded with boron nitride nanotubes (BNNTs). The samples were heat treated in argon using a tube furnace. The temperature and the sintering medium were varied to determine the ideal process. After post-processing, the samples were evaluated using X-ray diffraction, scanning electron microscope analysis, and the Archimedes method. No significant trends in the density were noted throughout testing; however, it was found that samples that were sintered in a boron nitride powder medium displayed intact BNNTs post-sintering. This demonstrated that BNNTs can survive temperatures far above their oxidation point if the environment is carefully controlled.

THIS PAGE INTENTIONALLY LEFT BLANK

TABLE OF CONTENTS

LIST OF FIGURES

LIST OF TABLES

THIS PAGE INTENTIONALLY LEFT BLANK

LIST OF ACRONYMS AND ABBREVIATIONS

BNNT	Boron Nitride Nanotube
BSE	Backscatter Electrons
CFM	Craniofacial Microsomia
CNT	Carbon Nanotube
DOD	Department of Defense
ETD	Everhart-Thornley Detector
SE	Secondary Electrons
SEM	Scanning Electron Microscope
UNREP	Underway Replenishment
XRD	X-Ray Diffractometer

THIS PAGE INTENTIONALLY LEFT BLANK

ACKNOWLEDGMENTS

First, I would like to thank my advisor, Dr. Troy Ansell, for guiding me through the thesis process and teaching me more about materials science than I ever thought possible. Creating a thesis project from scratch is hard enough, but doing so in a single year would have been next to impossible without his mentorship and expertise. I would also like to thank Dr. Ansell for spending the time to train me on each piece of equipment used during this project. The skills I learned helped me better understand the topics covered and will undoubtedly help me throughout my career. I wish every Naval Postgraduate School student could be advised by such an exceptional professor. I would also like to thank my second reader, Dr. Chanman Park, for taking the time to ensure I uphold the great standards of the Naval Postgraduate School.

Finally, I would like to thank all the staff of the Naval Postgraduate School and the institution itself. It is a true privilege to be able study at the postgraduate level, especially directly after finishing my undergraduate degree. This is an opportunity rarely given to members of the Armed Service immediately following their commissioning and it is something I am eternally grateful for.

THIS PAGE INTENTIONALLY LEFT BLANK

I. MOTIVATION

A. WEAR RESISTANCE

Wear is among the costliest issues encountered by industrialized nations. It was estimated in 2020 that mechanical wear and its associated negative effects accounted for a 1–4% loss in Gross Domestic Product in industrialized nations [1]. This equates to US$210.6–US$842.4 billion in losses in 2020 alone. Wear is the gradual loss of material caused by the friction between two surfaces. If left untreated, wear will lead to part deformation, which can result in part failure. The effects of wear are particularly acute in the Department of Defense (DOD). The demands of the military require reliable systems with service lives that far exceed those found in the private sector. Over the years this has caused the DOD to spend millions to prevent wear. While wear cannot be prevented outright, there are several methods to mitigate its effects such as lubrication and coatings. In many situations lubricants are unable to be used, which leaves coatings as one of the few mitigation options. Recently, the DOD has increased interest in ceramic coatings for metallic parts prone to wear. Ceramics are less susceptible to wear due to their typically greater hardness than metals. In addition to reducing material loss due to wear, these ceramic coats can often be reapplied to further increase the service life of the part. By reducing the frequency at which parts need to be replaced the DOD can save billions each year with the help of ceramic coatings.

B. CORROSION RESISTANCE

Corrosion and wear typically go hand-in-hand, with the latter acting as a catalyst for the prior. Wear often results in bear metal surfaces that when exposed to the elements leads to corrosion. Since 2012 corrosion and its effects cost the DOD $20.9 billion annually [2]. Corrosion is especially problematic for the U.S. Navy, as the maritime environment accelerates corrosion of metallic surfaces. Corrosion affects everything from the hull of a ship to the coolant pipes in a naval reactor. When considering its wide range of effects, corrosion poses one of the largest obstacles to fleet readiness. Corrosion is “the destruction or deterioration of a material because of a reaction with its environment” [3]. In its most

basic form corrosion can be broken up into two reactions, an oxidation reaction, and a reduction reaction, as seen in Figure 1.

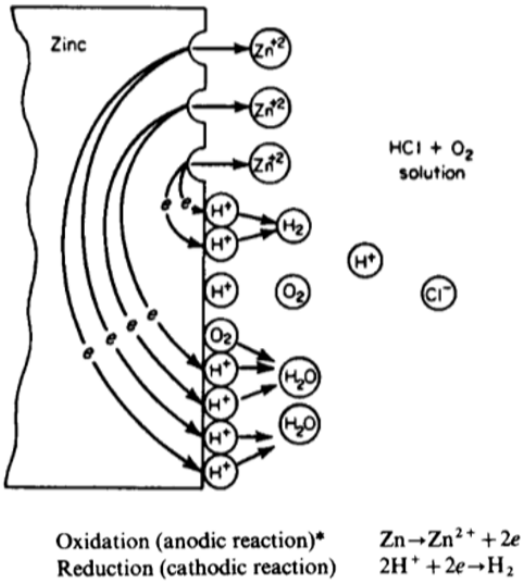

Figure 1. Diagram of Zinc Undergoing Corrosion in an Acidic Environment. Source: [3].

For these reactions to occur four things must be present, an oxidizing agent (cathode), a reducing agent (anode), an electrolytic solution, and a way for electrons to move between the cathode and the anode [3]. In the maritime environment, the metals aboard a ship act as the anode and typically hydrogen in the environment as the cathode. When these are combined with seawater as an electrolytic solution and a route for electrons to move, it breeds the perfect conditions for corrosion. Substantial research has been conducted into preventing these conditions by using metals less likely to oxidize and/or isolating the metals with a barrier. The latter of the two is more pertinent to DOD applications due to the costly nature of corrosion resistance metals. By far the most common example of corrosion barriers is paint. It is cheap and easy to apply; however, any chips or scratches result in the conditions for corrosion being met. Ceramic coatings can provide a similar barrier with a much higher resistance to chips, scratches, and wear.

C. HYDROPHOBICITY

Hydrophobicity is defined as a material where "the contact angle is more than 90 degrees" for a water droplet resting on the surface [4]. Beyond reducing corrosion, hydrophobicity has some other benefits. One of the most promising areas for research with hydrophobic materials is their ability to reduce drag. One study in 2022 found that hydrophobic SiO_2/HLR-Si was able to reduce drag up to 23.4% in water [5]. By reducing the drag on the hull of ships, the efficiency with which they move through the water can be greatly reduced. This could reduce the fuel required to operate a vessel. In the case of the Navy, a reduction in fuel consumption would lead to less frequent UNREPs and port calls, and a massive reduction in overall cost to operate. Hydroxyapatite by itself is typically hydrophilic, demonstrating a contact angle of 10^{o}-100^{o} [6]. However, with the addition of nanoparticles like BNNTs, the contact angle of any ceramic, hydroxyapatite included, can be greatly increased. BNNTs are extremely hydrophobic, with some orientations displaying contact angles above 170^{o}, an example of this can be seen in Figure 2 [7]. With the addition of even a small weight percent of BNNTs, hydroxyapatite's hydrophobicity could be greatly improved making it an ideal choice as a coating.

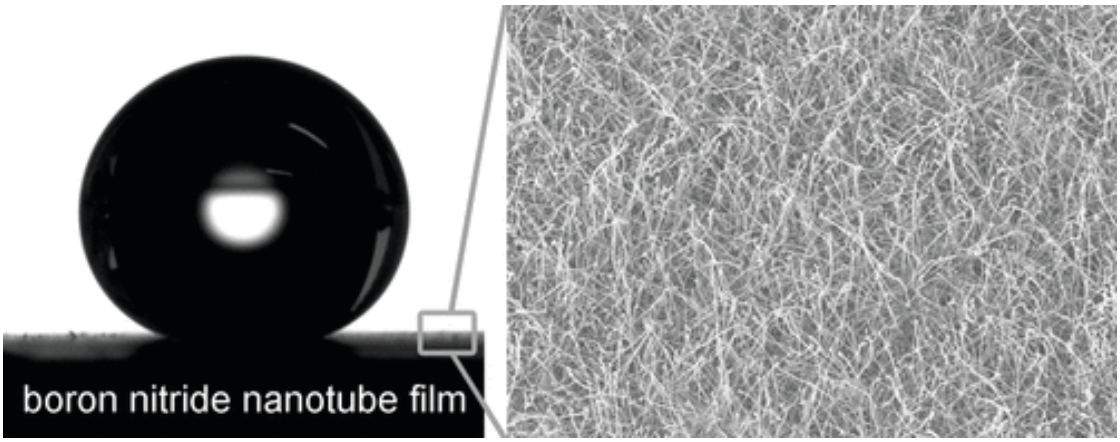

Figure 2. Water Droplet Resting on a Boron Nitride Nanotube Film. Source: [7].

D. THERMAL CONDUCTIVITY

Ceramics have long been used in high temperature applications due to their ability to withstand temperatures that would melt most metals; however, ceramics fail to conduct heat like metals. The room temperature thermal conductivity of copper is 380 W/m-k, while a typical industrial ceramic like aluminum oxide only has a thermal conductivity of 26 W/m-k [8]. With many high temperature applications emerging like hypersonics, the need has arisen for a material that can withstand incredibly high temperatures while also being able to conduct this heat. The solution to this problem lies in ceramic matrix composites with additives like BNNT.

While the thermal properties due to the addition of BNNTs have not been studied in depth in ceramics, they have been researched in engineering polymers. In one study from 2011, the addition of BNNTs to a polyvinyl alcohol polymeric composite resulted in a ~270% increase in thermal conductivity [9]. If comparable results can be replicated in a ceramic medium it would aid development of ceramics for high temperature applications. Another interesting property of BNNTs is their anisotropic thermal conductivity. This means that the orientation of the BNNT affects the thermal conductivity. The greatest thermal conductivity is axially along the BNNT's length. As a result, if the BNNTs are all oriented in a certain direction, then the material will demonstrate much better thermal conductivity along that direction, as can be seen in Figure 3. This can allow for the design of directionally conducting materials, which can be used in anything from hypersonics to computer cooling systems.

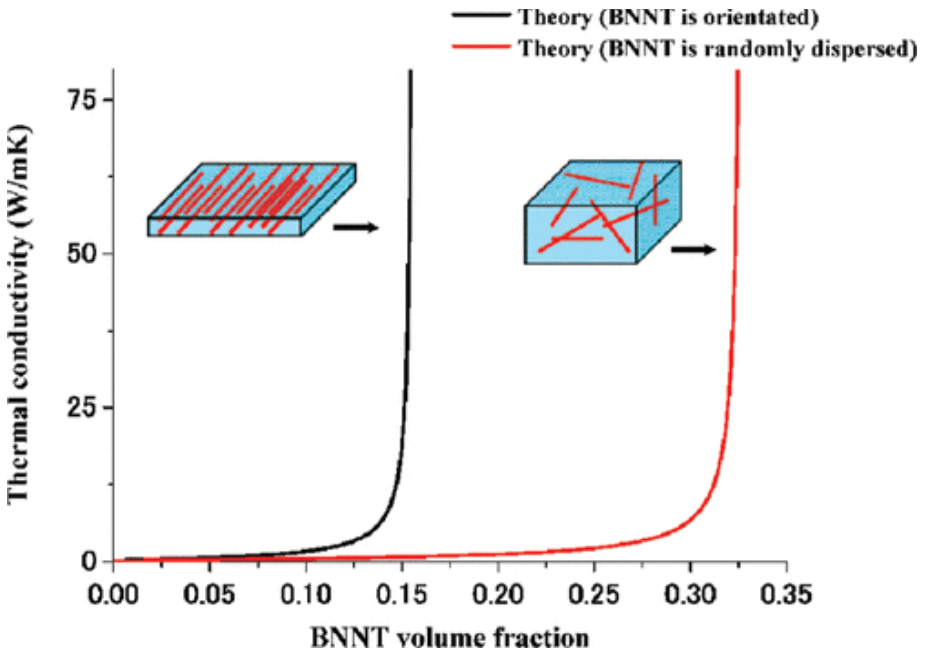

Figure 3. Estimated Thermal Conductivity for Two BNNT Orientations. Source: [10].

E. OBJECTIVE

The objective of this thesis is to show that hydroxyapatite and by extension other ceramics can be properly sintered, while preventing the oxidation of the BNNTs within the ceramic. This is a challenge because most ceramics require sintering temperature well in excess of 1000ºC, while BNNTs begin to oxidize at ~900ºC when oxygen is present [11]. In the case of hydroxyapatite, the ideal sintering temperature is ~1250ºC [12]. As a result, the sintering of hydroxyapatite must be done in an oxygen-free environment to ensure the BNNTs remain intact. With confirmation that hydroxyapatite can be sintered without oxidizing the BNNTs, the way can be paved for future research into ceramics with BNNT additives.

THIS PAGE INTENTIONALLY LEFT BLANK

II. BACKGROUND

A. ADDITIVE MANUFACTURING WITH CERAMICS

1. Materials

Additive manufacturing is one of the fastest growing fields in engineering. Initially, additive manufacturing research focused on polymers and metals; however, new emerging techniques have allowed the printing of ceramics. Ceramic additive manufacture is still in its infancy when compared to metals and polymers. The major drawback of printed ceramics is the porosity of the parts and the costly process of sintering to correct the porosity [13]. This is the result of the printing process; all techniques required some sort of binding agent or solvent. This results in a porous part after the polymer binder is removed. While additive manufactured ceramics do have some disadvantages, they excel in material variability. Any ceramic can be used given it is paired with a binding agent that it will not react with. Common ceramics that are used in additive manufacturing are alumina, zirconia, and silicon-based ceramics [14]. In this thesis a ceramic called hydroxyapatite will be used.

2. Printing Techniques

Additive manufactured ceramics are primarily made using four techniques fused filament fabrication, inkjet, binder jetting, and stereolithography [14]. Fused filament fabrication (FFF) works by melting and extruding a polymer loaded with high levels of ceramic particles. Inkjet uses hundreds to thousands of nozzles that deposit ceramic particles suspended in a solvent, which evaporates as it contacts the heated build plate [14]. Binder jetting works by electively depositing a liquid adhesive to a bed of ceramic powder. Stereolithography uses UV light to cure photosensitive resin that is loaded with ceramic powder. Inkjet can create the highest resolution parts, but it is the slowest; while stereolithography is common and has good resolution, it cannot create fully enclosed parts that are hollow. The method that was used to print the parts used in this thesis, is a proprietary system by Lithoz, but is an adaptation of stereolithography.

3. Post-Processing

The post-processing required for additively manufactured ceramics is like that required for traditionally manufactured ceramics. The first portion in the post-processing of 3-D printed ceramics is to remove the polymer binding agent. This is most often done in two steps. First, a preconditioning step removes some of the binding agents that have a lower boiling point. This is then followed by a debinding step that completely removes the remaining binding agent. These steps are only required when a binding agent is used. Most traditionally made advanced ceramics are fabricated by pressing a powder into shape in a die. In many cases the part can retain its shape after pressing without the use of a binding agent [15]. These parts do not require any preconditioning or debinding like 3-D printed parts. The second part is known as sintering the "green" ceramic is heated to near its melting point and held at that temperature for an extended period of time. During this time, the ceramic grains within the part will fuse together with neighboring grains, creating a final part with a high density and low porosity.

4. Applications

Ceramics in general have a unique and in many applications desirable set of material properties. They are typically more resistant to wear and corrosion than most metals; however, they are often difficult to work with due to their brittle nature. 3-D printing allows for the fabrication of ceramics with advanced geometries that would have been impossible to achieve using older methods. The possible applications for 3-D printing are broad from medical implants to aerospace engineering. In the medical field, additively manufactured ceramic bone and teeth replacement allow doctors to treat unique patients quickly and relatively affordably [16]. In aerospace engineering, organizations like NASA are using 3-D printing to create ceramic parts that are complex, durable, and heat resistant to aid in the development in space travel [16]. The energy industry is using additive manufacturing to create custom ceramic insulators in advanced electronics [16]. The global 3-D printed ceramic market was estimated to be worth $186.4 million in 2022 and is expected to grow to $1.246 billion by 2030 [17]. This highlights how quickly this industry is growing and how vital it is that the United States stays at the forefront of research.

B. HYDROXYAPATITE

1. Chemical Composition

Hydroxyapatite is a common medical grade ceramic that is often used as a bone replacement and regeneration [18]. The chemical formula of hydroxyapatite is $Ca_{10}(PO_4)_6(OH)_2$, which is very similar to that of human bone, resulting in high biocompatibility [19]. A pictorial representation of the chemical formula for hydroxyapatite can be seen in Figure 4.

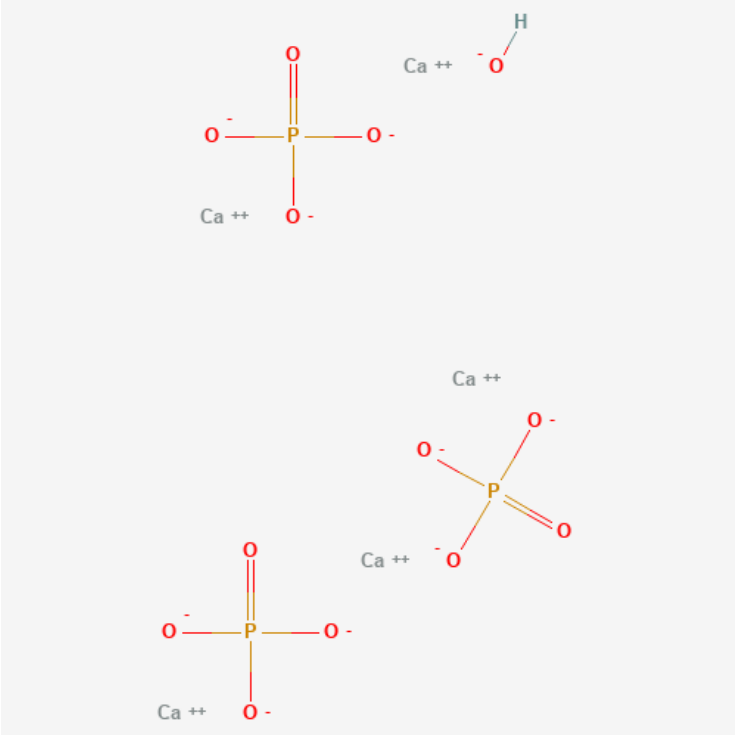

Figure 4. Chemical Structure of Hydroxyapatite. Source: [19].

2. Microstructure

Hydroxyapatite forms a hexagonal structure with a $P6_3/m$ space group, which is represented in Figure 5 [20]. The lattice parameters of a standard hydroxyapatite crystal are a=b=0.937 nm, c=0.688 nm, α=β=90º, and γ=120º [20]. Hydroxyapatite is typically stable, resulting in good biocompatibility; however, under dihydroxylation conditions other compounds such as tricalcium phosphate, tetracalcium phosphate, and calcium oxide

can form [21]. These other compounds typically do not form until hydroxyapatite reaches temperatures more than 1300ºC [22]. These temperatures will not be reached during the sintering process, so the formation of these compounds is rarely a concern.

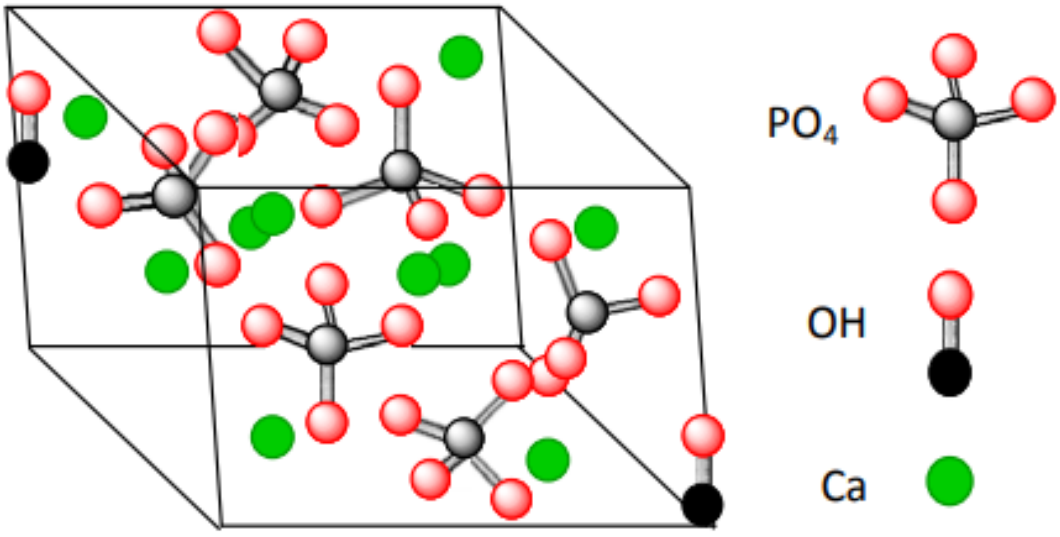

Figure 5. Crystal Structure of Hydroxyapatite. Source: [20].

3. Properties

As ceramic hydroxyapatite follows the typical trends found in the properties of ceramic materials. Hydroxyapatite typically has a density somewhere between 3.05-3.15 g/cm^3, with the variation being due to the porosity of the sample [23]. Its melting point is between 1500ºC and 1670ºC depending upon the structure; however, hydroxyapatite will typically begin to decompose into other compounds before reaching its melting point [24]. This decomposition typically occurs above 1360ºC; however, hydroxyapatite can release its OH^- group at temperatures as low as 1000ºC [25]. As for mechanical properties, hydroxyapatite has a compressive strength of 350–450 MPa, while it has a tensile strength of only 38–48 MPa. This disparity is consistent with most ceramics [23]. Its flexural strength is 100–120 MPa [23]. Hydroxyapatite has a modulus of elasticity of 7–13 GPa and a shear modulus of 2.76-5.12 GPa [23]. Compared to the modulus values of a typical steel,

which are orders of magnitude larger, hydroxyapatite like all ceramics are hard and brittle materials.

4. Applications

Hydroxyapatite is almost exclusively used in the medical and dental fields. Due to its similarity to bone and its biocompatibility, hydroxyapatite is most used as a bio-ceramic coating and a bone filler [26]. Bio-ceramic coatings are used to help inorganic implants integrate with the body. In the case of join replacements, the metallic replacements often fail to properly bond to adjoining bone. To correct this, bio-ceramic coatings are applied to metal implants, resulting in far better bonding to natural bone [27]. Hydroxyapatite makes an ideal bio-ceramic coating since it is bioactive and promotes the growth of natural bone. Bone fillers act in an analogous way to bone within the body. When large enough sections of bone are removed during surgery, a bone filler is often required. Bone fillers act as a scaffold for new bone growth to occur [28]. As a result, it is vital for the material used to be osteoconductive, or able for bone to grow on [28]. Hydroxyapatite is ideal for this application due to its similarities to actual bone.

C. BORON NITRIDE NANOTUBES

1. Chemical Composition

In this project the hydroxyapatite used contained 4 vol% boron nitride nanotubes. BNNTs are a recent development in materials science. First theorized in 1994 by Marvin Cohen, BNNTs were first synthesized the following year by Alex Zettl at the University of California, Berkeley [29]. Since then, a large amount of research has been done to improve the synthesis process. Scientists have been able to standardize techniques to produce defect free BNNTs on a much larger scale than in 1995. BNNTs are made of hexagonal lattice of Boron and Nitride arranged in a tubular form with an average diameter of above 5 nm, an example shown in Figure 6. Depending upon the synthesis process BNNTs can display differing diameters, lengths, and number of walls.

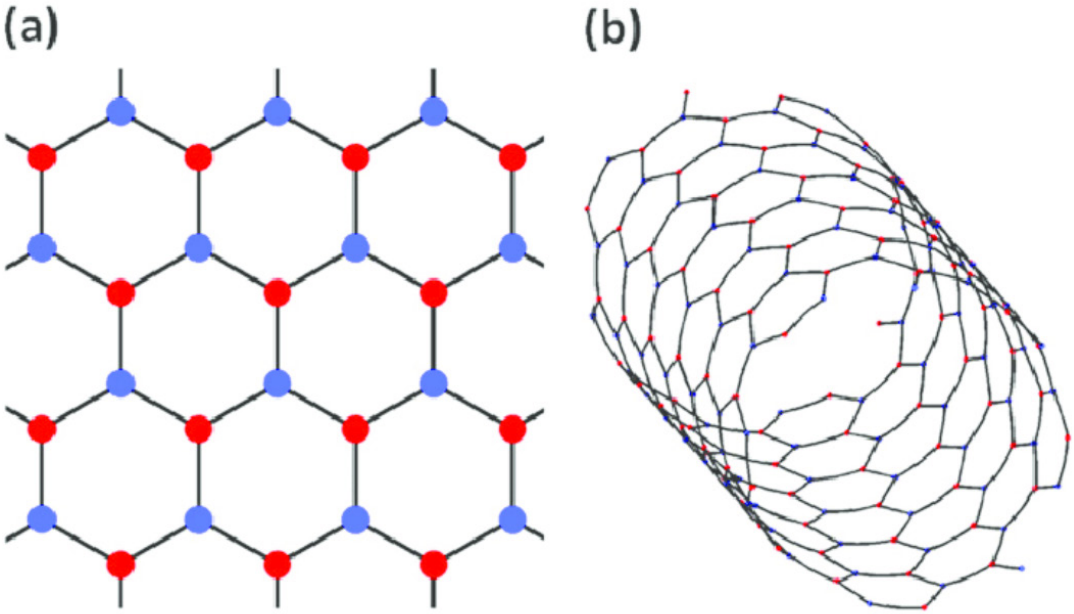

Figure 6. (a) Boron Nitride Sheet and (b) Boron Nitride Nanotube. Source: [30].

2. Microstructure

Boron nitride forms a hexagonal crystal structure with lattice parameters of a=b=0.250 nm, c=0.666 nm, α=β=90º, and γ=120º [31]. In the case of BNNTs the hexagonal lattice comes in the form of a tube; however, the base structure remains the same. BNNTs and all nanotubes are classified as 1D nanomaterials. 1D nanomaterials are defined as particles that are confined to the nanoscale in two dimensions [32]. In the case of BNNTs the cross section is confined to 1–100 nm in both dimensions, while the length in the dimension along the tube can be greater than 100 nm. BNNTs are incredibly stable compounds when compared to other nanoparticles. The most common way in which BNNTs breakdown is via oxidation. This typically only occurs at temperatures above 700ºC with oxygen present.

3. Properties

The main purpose behind nanoparticles like BNNTs is to improve the properties of the materials they are added to. BNNTs have a density from 1.9 to 2.1 g/cm^3; however, this

can vary in unique configurations [33]. BNNTs, like many nanomaterials, have exceptional mechanical properties. When just 0.15 wt% BNNTs were added to a methacrylate-based resin, the tensile strength increased from 52.28 ± 15.14 MPa to 65.47 ± 13.00 MPa [32]. Another area where BNNTs excel is in thermal properties. BNNTs have high thermal stability, resisting any oxidation up to 700ºC, while other nanomaterials like carbon nanotubes (CNT) begin to oxidize around 400ºC [32]. In a perfectly oxygen free environment BNNTs do not decompose up to 1900ºC [34]. This indicates that any degradation of the BNNTs at the temperature range in question is due to oxidation and not decomposition. Unlike CNTs, which are semi-conductive, BNNTs are excellent insulators with a bandgap of 6 eV [32]. This large bandgap means that when excited, BNNTs will emit a high energy photon, usually in the ultraviolet range. Due to the recent discovery of BNNTs, a lot of ongoing research is required to better understand the electrical and optical uses for BNNTs.

4. Applications

Due to their remarkable properties, the applications for BNNTs are endless. The most common use for BNNTs is as an additive to improve material properties of metals, ceramics, and polymers. Even a small weight percent of BNNTs can improve material strength, thermal conductivity, hydrophobicity, and much more. One area of increased interest in the last few years is hypersonics. Much of the recent research into BNNTs centers around how it can be used to improve the thermal resistance of hypersonic materials. There is also evidence that aligned BNNTs can be used to improve thermal conductivity in a single dimension within a material, leading to direction thermal conductivity [10]. In the field of advanced electronics BNNTs, in conjunction with other nanomaterials, are being used to create nano transistors and switches to radically improve computing power [35]. Another innovative field of BNNTs applications is in medicine. Due to their unique geometry BNNTs can be used to delivery drug to a very target area of the body, aiding in cancer treatment [32]. Research is also being conducted to use a BNNT-gelatin-glucose structure as a scaffold in tissue engineering [32]. BNNTs can be for their anti-bacterial properties and as components in biosensor [32]. These applications only scratch the surface for what is possible with BNNTs.

THIS PAGE INTENTIONALLY LEFT BLANK

III. EXPERIMENTAL METHODS

A. PART FABRICATION

The hydroxyapatite parts that were used in this thesis were produced by Lithoz. Lithoz is an Austrian based high-performance ceramic company that specializes in 3-D printing [36]. The parts used in this project were printed by Lithoz America, LLC using their LithaBone HA 480 ceramic with 4 vol% BNNTs. LithaBone HA 480 is a hydroxyapatite ceramic that is optimized for 3-D printing and follows ASTM F1185 Material Standards. Its primary intended uses according to Lithoz are CMF surgery, bone replacement implants, and neurosurgery [37]. These samples were printed using Lithoz's Lithography-based Ceramic Manufacturing (LCM) technology. The LCM technique works much like photocurable resin printers, as shown in Figure 7. A vat of ceramic-loaded liquid (slurry) is placed in a transparent bath. A build plate is then dipped into the slurry where a blue light selectively cures the slurry attaching it to the build plate. The build plate is then pulled up as the blue light selectively cures layer-by-layer, eventually resulting in a solid part [38]. At this point, the ceramic part is known as the green part. This means that the part still contains the polymer used to bind the ceramic particles together in the printing process. From this point several postprocessing steps are required to achieve the final part.

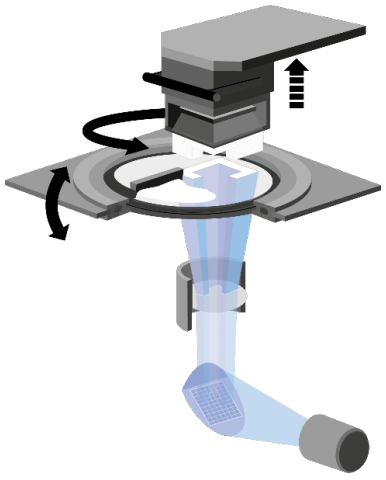

Figure 7. Lithoz's LCM Printing Diagram. Source: [38].

B. POST-PROCESSING

1. Preconditioning

The first major step in post-processing is called preconditioning. Preconditioning is an intermediate step that raises the temperature of the green part to a certain temperature causing some of the polymers with low boiling points to vaporize. In this case, Lithoz performed the preconditioning for these samples. The green parts were heat treated to 120ºC, resulting in partial organic removal. While this step does vaporize some resin, it leaves the majority intact within the sample, resulting in the need for a debinding step.

2. Debinding

The second step in post-processing is known as debinding or pre-sintering. This process finishes what preconditioning started by vaporizing all remaining polymers, leaving only the ceramic particles. Its second function is to pre-sinter the part. During the printing process, the ceramic particles are suspended in a slurry composed primarily of a polymer matrix. The polymer matrix is needed for the green part to hold its shape. When the sample is debinded all the polymer binding is removed. Pre-sintering causes the ceramic particles to begin to fuse together. For these samples, a peak debinding temperature of 1000ºC was required to ensure all polymers were vaporized. Half of the samples used in this thesis had been previously debinded by Lithoz at 1000ºC in air.

This presented a major issue since BNNTs will begin to breakdown due to oxidation when heated above 900ºC in air [39]. This occurs when the oxygen in the air forms boron oxide with the boron found in BNNTs, resulting in degradation of the nanotubes. The solution is to debind the samples in an oxygen free environment. In this case, an MTI OTF-1200X tube furnace was used to debind the samples in argon gas rather than air. The furnace used for this is shown in Figure 8. The samples were heated to 1000ºC over a 90-minute period (11.11ºC/min) and held at 1000ºC for 5 minutes. Initially the samples were debinded with no surrounding medium; however, due to poor density early samples some of the later samples were debinded in a bed of powder boron nitride under the same conditions. Once the 5-minute hold was complete, the sample was naturally cooled in the

furnace. By doing this, the BNNTs could be preserved while eliminating any polymer binder left in the samples.

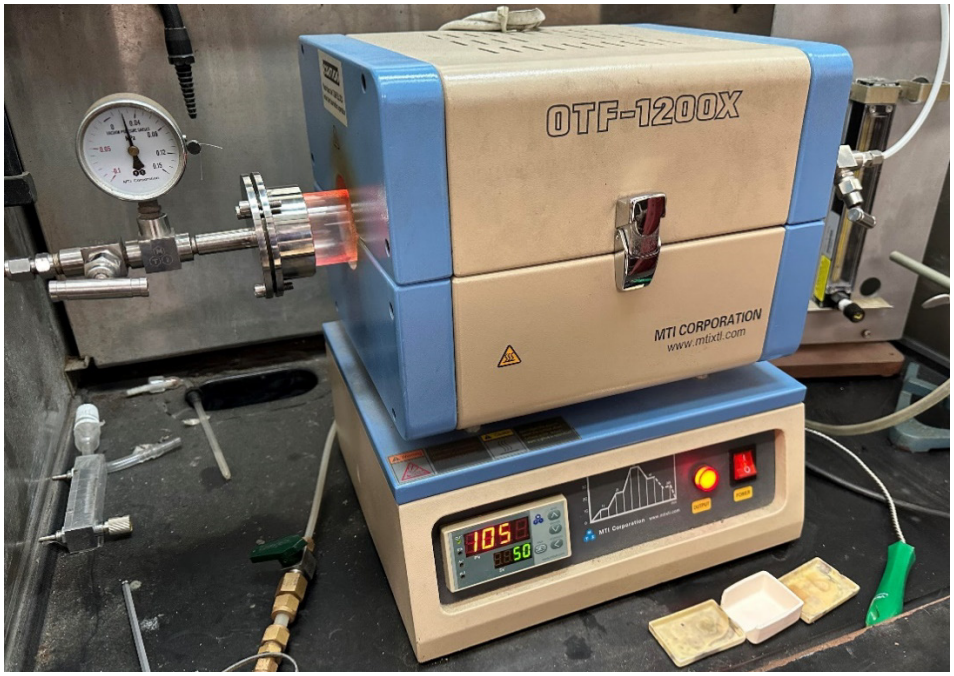

Figure 8. MTI OTF-1200X Tube Furnace

3. Sintering

The final and most crucial step in the post-processing of ceramics is sintering. Sintering is the process by which the individual particles slowly fuse together to form a solid, without fully melting the particles. This process allows the debinded part to densify, becoming cohesive, stronger, and less porous. The porosity and fragile nature of most ceramics mean that they are unusable without some sort of sintering process. The first step was to identify a sintering process and to test it with a small sample. Due to the limitations of the tube furnace, all temperatures were kept under 1100ºC. A dwell time of 2 hours was decided based upon research into prior experiments [12]. The paper cited used a 2ºC/min ramp rate; however, this was reduced to a uniform 90-minute ramp time due to equipment limitation. This significant reduction in ramp up time was determined to be acceptable due to the smaller size of these samples as compared to the samples found in the paper. To test

the process, an initial sample was debinded with no medium as explained above and was sintered at 1000ºC for 2 hours. Once the process was finalized, the first real batch of testing began.

The first batch of samples were sintered according to the values in Table 1. The purpose of batch one was to identify the ideal sintering temperature to achieve a satisfactory density. The five samples were sintered with no medium and allowed to cool in the furnace after the dwell time was reached. The density that resulted from the first batch was poorer than expected, this led to a second batch of sample sintering.

Table 1. Sintering Processes for Sample Batch 1.

	Sample 1	**Sample 2**	**Sample 3**	**Sample 4**	**Sample 5**
Sintering Temperature	900ºC	950ºC	1000ºC	1050ºC	1100ºC
Dwell Time	120 min	120 min	120 min	120 min	120 min
Ramp-Up Time	90 min	90 min	90 min	90 min	90 min

The second batch was used to determine how sintering the samples in a medium would affect the final density and if it could help protect the BNNTs. As explained, one sample was debinded in a bed of boron nitride alongside a sample debinded in no medium. The bed of boron nitride was compacted around the sample in the hope that it would prevent oxygen from reaching the sample while sintering. These two samples were then sintered at 1000ºC for two hours, just like Sample 3 in Batch 1. The two samples of Batch 2 then underwent the same rounds of testing as the samples in Batch 1.

The third batch was aimed at identifying whether BNNTs affect grain fusion and growth during the sintering process. To accomplish this, two samples were debinded in argon under the same conditions as the samples in previous batches. These samples were then sintered at 1000ºC for two hours, just as the samples in Batch 2. The first sample was the same hydroxyapatite with 4v% BNNTs that was used in the prior batches, while the second sample was a similar hydroxyapatite print with no BNNTs. Once the post-

processing was completed, these two samples underwent the same characterizations as the prior two batches.

C. MATERIAL CHARACTERIZATION

1. Archimedes Method

Using a Sartorius QUINTIX224-1S laboratory scale, the density of each sample was measured following Archimedes Method. The first step was to weigh each sample in air. Then a beaker of distilled water was placed on a scale and tared. Next each sample was submerged in water and weighed. With the density of water known, the density of each sample was calculated by using Archimedes Formula,

$$\rho_{sample} = \frac{\rho_{water} W_{in\ air}}{W_{in\ air} - W_{in\ water}}.$$

Once the density measurements were complete, each sample was placed in a Pelco 2251 Vacuum Desiccator at a pressure of -25 inHg gauge for 24 hours. This was done to ensure all moisture introduced to the sample during the Archimedes Method was removed before beginning the next step.

2. Scanning Electron Microscopy

Once the samples were removed from the vacuum desiccator, they were broken to create a fracture surface for analysis. The broken samples were then mounted on to ½'' aluminum specimen mounts using a double-sided adhesive patch. The samples were then sputter coated with a 5 nm thick 80/20 platinum/palladium layer in a Cressington Sputter Coater 208HR seen in Figure 9. Sputter coating is a process by which a thin layer of conductive material (typically a metal) is applied to a sample for scanning electron microscopy (SEM) imaging. An example of samples that have undergone sputter coating can be seen in Figure 10. This is done to prevent a phenomenon common in insulating materials known as charging. Charging occurs when the electrons emitted from the SEM beam strike the sample and remain trapped on the surface since the insulating material prohibits free electron movement through the sample. When this occurs the negatively charged surface interferes with the incoming beam causing bright sections of the sample

that drastically reduce the image quality. Sputter coating creates a conductive surface that prevents the sample from being overly charged with electrons.

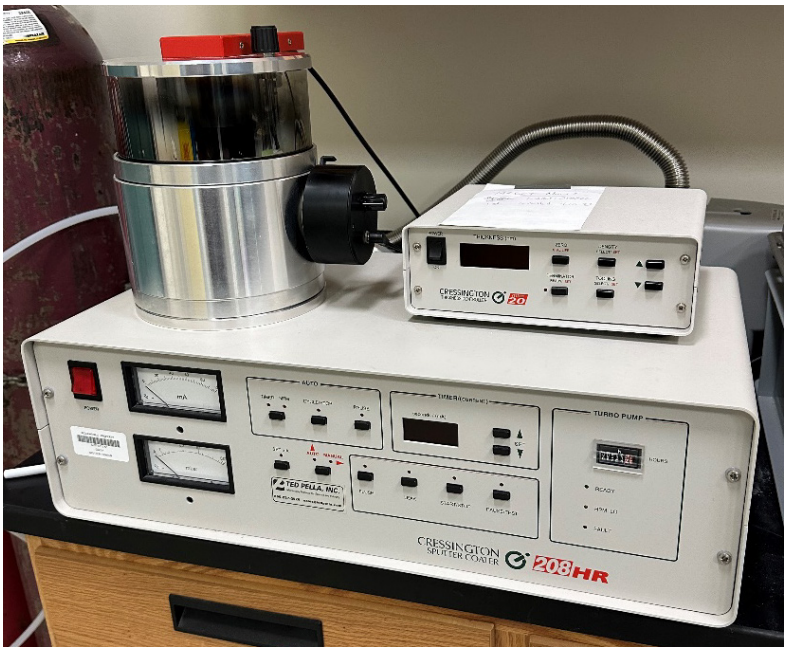

Figure 9. Cressington Sputter Coater 208HR

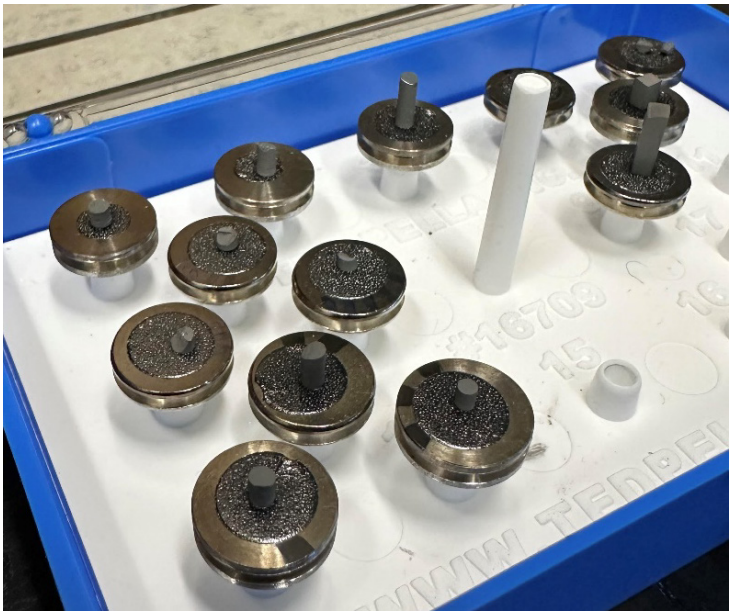

Figure 10. Fully Prepared SEM Samples

The SEM used in this work was the FEI Helios 5 UX SEM seen in Figure 11. Once the samples were loaded into the SEM, the electron beam was turned on and the Everhart-Thornley Detector (ETD) was selected. The ETD was used because it primarily detects secondary electrons (SE) rather than backscattered electrons (BSE). Secondary electrons provide more topographical information about the sample, while backscattered electrons provide more compositional information. In this case, secondary electrons are desired because a more topographical view of the sample allows for easier identification of BNNTs within the sample. The SEM was then used to manually scan the fracture surface for BNNTs and other features of interest. Once a feature was found an image was taken at x100000 magnification, then the magnification was reduced to half and another image was taken. This process was repeated until the magnification reached x500. This was done to standardize the images across the samples and to ensure a large quantity of images at various magnifications were captured. Each sample has several areas of interest imaged, with most samples having between 30 to 50 images. Once the imaging was complete the characterization process could move to the X-ray diffraction analysis.

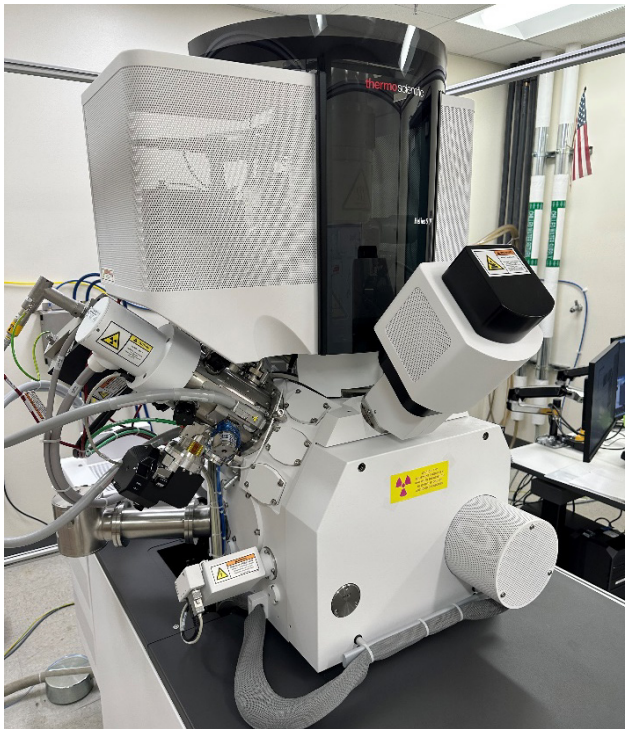

Figure 11. FEI Helios 5 UX SEM

3. X-Ray Diffraction

Powder x-ray diffraction (XRD) was used to investigate the crystal structure of the hydroxyapatite composites. XRD works by bombarding a sample with electrons at a range of angles. The electrons interact with the sample and are scattered at characteristic angles according to their microstructure and composition. The resulting XRD spectrum acts as a fingerprint, with each material having its own unique pattern. With this pattern, a material can be identified by comparing the spectrum to established XRD spectra in databases like Crystallography Open Database or the database established by the International Centre for Diffraction Data. Figure 12 and Figure 13 show the XRD spectra from hydroxyapatite and BNNTs, respectively. As can be seen, each spectrum is unique and can be different depending upon the material characterized.

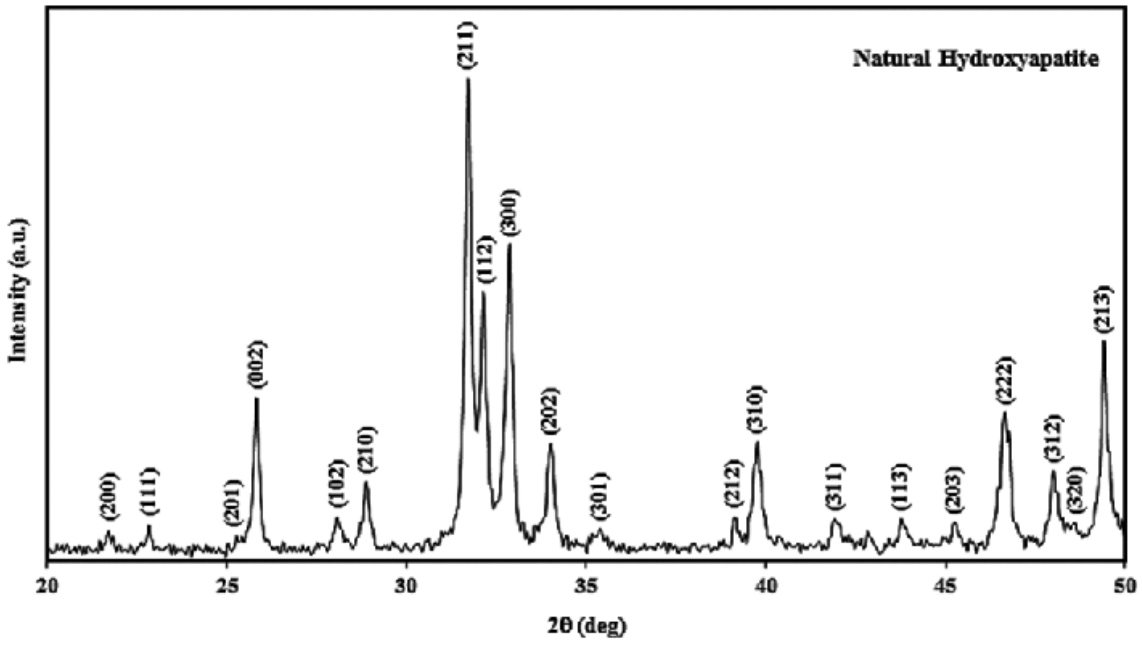

Figure 12. X-Ray Diffraction Spectrum for Hydroxyapatite. Source: [40].

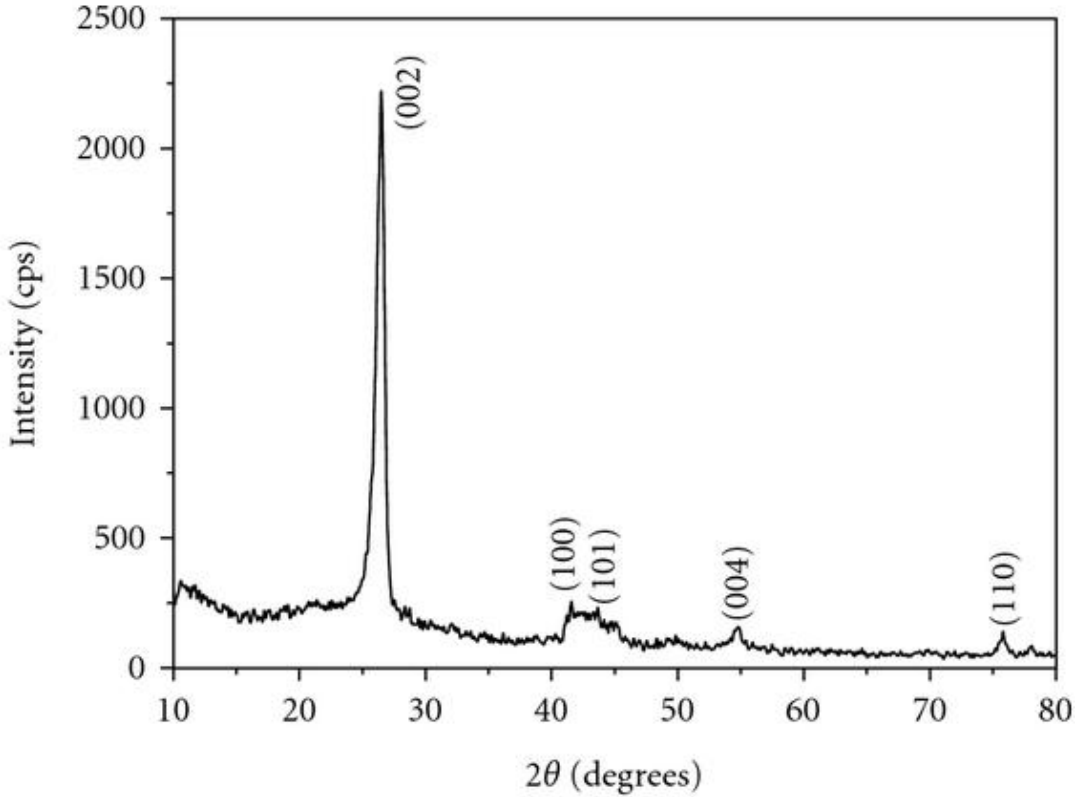

Figure 13. X-Ray Diffraction Spectrum for BNNTs. Source: [41].

The first step was to take the remaining part of each sample, that was not used for SEM analysis, and crush it into a fine powder. It is important that the power is fine and uniform, any larger uncrushed pieces can affect the XRD analysis. This was done using an agate mortar and pestle. Once the powder was crushed, it was carefully packed into a small well within a specimen holder. Next, the samples were loaded in the XRD, a Rigaku MiniFlex 600 X-Ray Diffractometer as seen in Figure 14. The XRD target used for analysis of the samples was copper (with a wavelength of 0.15418 nm) with a scan rate of 3º/minute. The scan was done over an angle range of 10º to 100º to capture all relevant peaks. At these settings, each XRD run took about 30 minutes.

Figure 14. Rigaku MiniFlex 600 X-Ray Diffractometer

IV. RESULTS

A. INITIAL TESTING

Before any post-processing of the initial sample to be sintered, a green sample (as printed), and a sample debinded in air were imaged using the SEM. An image from the green sample seen in Figure 15 shows an agglomerated mass of BNNTs in the sample, confirming that the BNNTs are in fact present. This also shows that rather than being uniformly dispersed in the hydroxyapatite, the BNNTs typically group together in agglomerated masses.

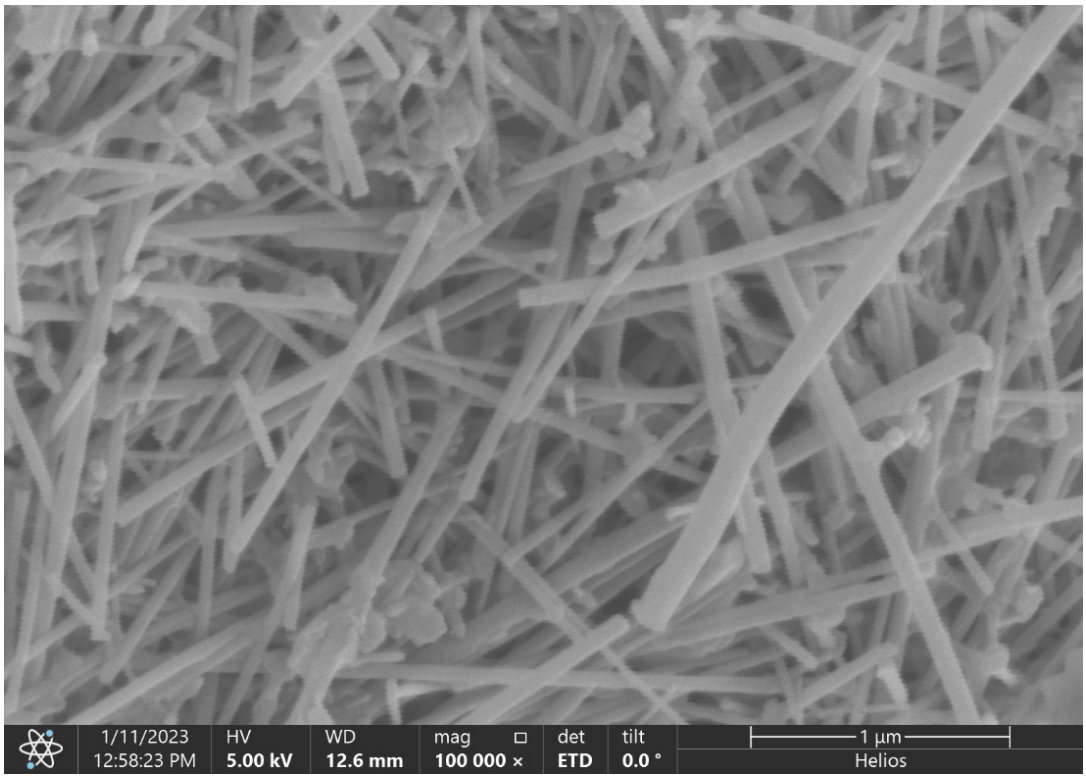

Figure 15. BNNT Agglomeration in Green Sample (x100000).

Figure 16 shows the typical grain structure within the green sample. While the sample looks like it has minimal porosity, it is the binding agent filling the gaps between hydroxyapatite grains. This becomes clear when the sample is debinded in air.

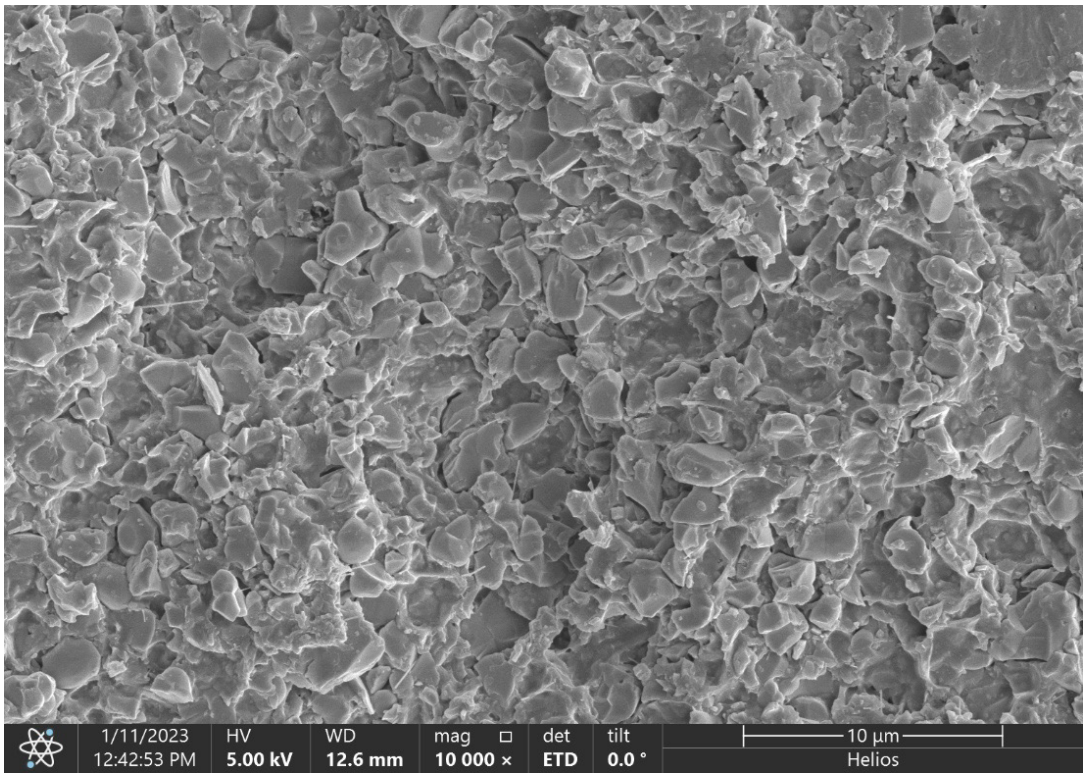

Figure 16. Grain Structure of Green Sample (x10000).

Figures 17 and 18 show the sample that was previously debinded in air by Lithoz. Lithoz debinded their samples at 1000ºC, using a ramp time of 90-minutes and a dwell time of 5 minutes. BNNTs begin to show damage in an oxygen environment at around 700ºC and complete oxidation at around 900ºC [39]. Since the debinding was done in air at a temperature of 1000ºC, the expectation was that no BNNTs survived. This was confirmed with the SEM. No BNNTs were found on the fractured surface of the sample; however, in their place were the structures seen in Figure 10. These structures do not match the hydroxyapatite grains in the sample, leading to the conclusion that they are the remnants of BNNTs post oxidization.

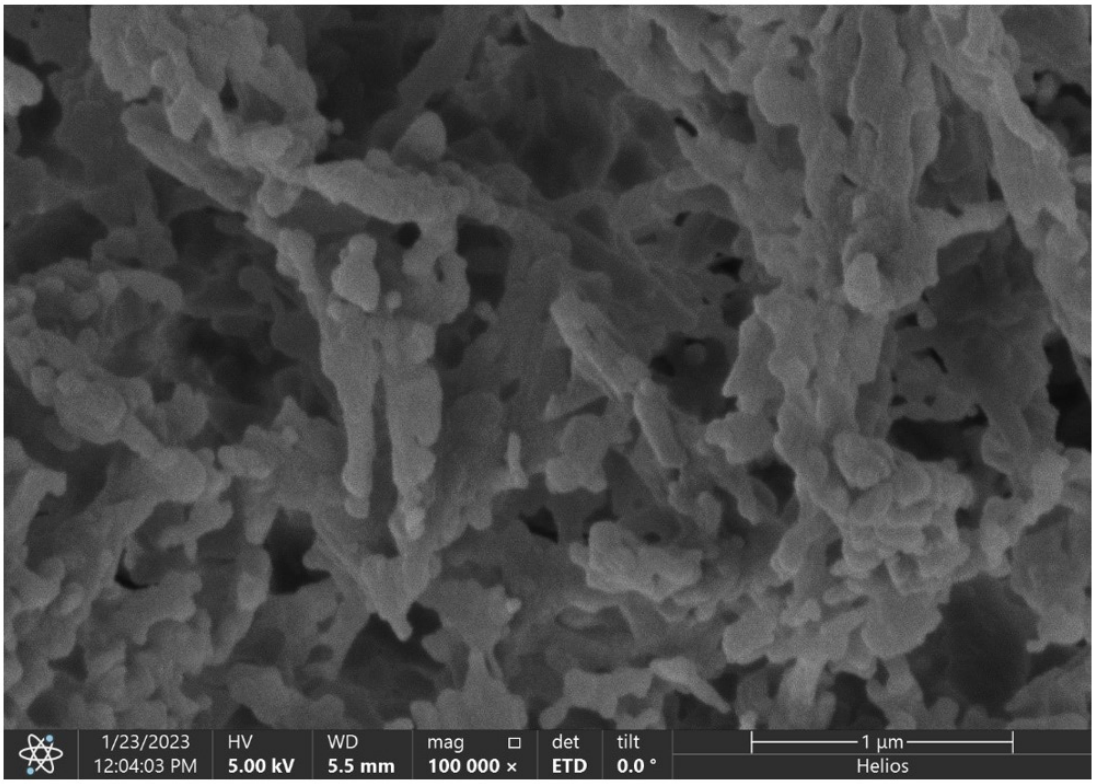

Figure 17. Oxidized BNNT Agglomeration in Sample Debinded in Air (x100000).

Figure 18 shows the grain structure of the sample debinded in air. When compared to Figure 16 there are several clear differences. First, there are no visible BNNTs present. Second, the grain structure in Figure 18 is far more porous due to the lack of the polymer binding agent. Third, the grains in Figure 18 show little to no evidence of fusion, indicating that sintering has not taken place. After the debinding step, the samples are at their lowest density. This is why sintering is a vital step for final part strength.

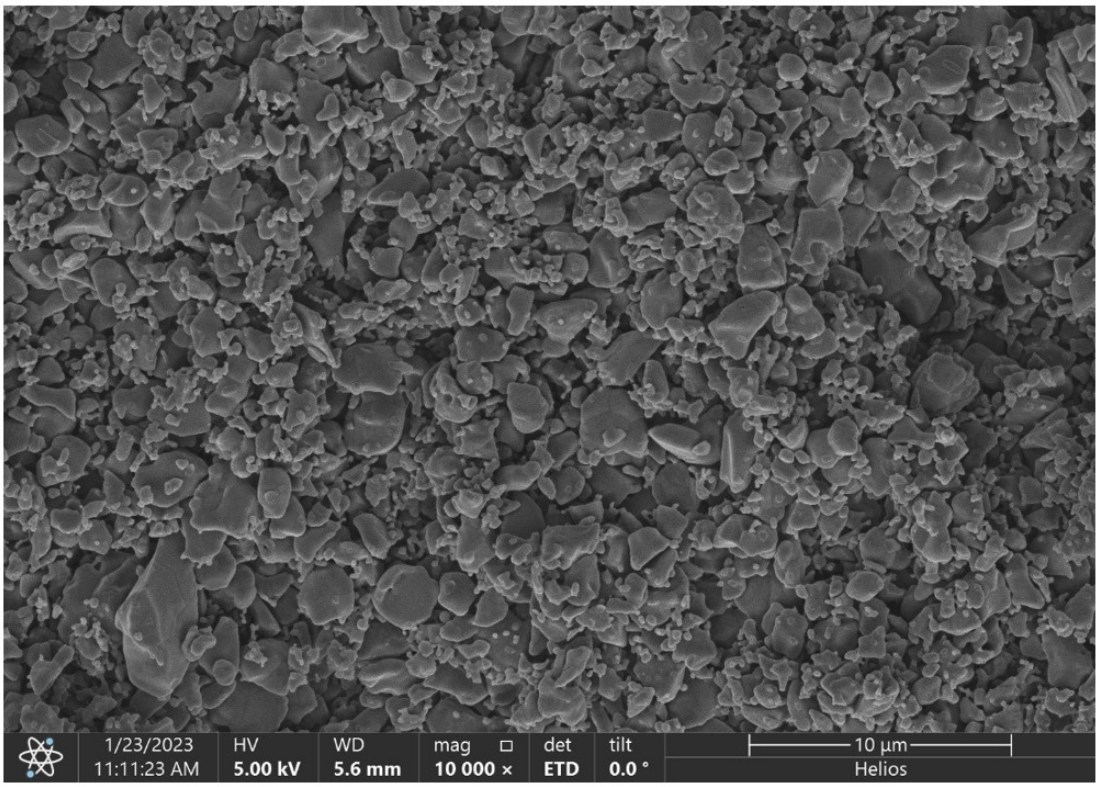

Figure 18. Grain Structure of Sample Debinded in Air (x10000).

Once it was identified that no BNNTs had survived the debinding process in air, as described in the experimental methods section, a sample was debinded in argon. The idea was to protect the BNNTs from air and thus ensure that no oxidation takes place. Figure 19 shows an agglomeration of BNNTs in the argon debinded sample. This proves that the BNNTs can survive the debinding process; however, when Figures 19 16 are compared, there are some differences. The BNNTs in Figure 19 appear to be shorter and damaged. This indicates that some oxygen could have been present in the furnace. This could be a result of a leak in the furnace or oxygen being formed during the vaporization of the polymer binding agent. The second possibly is difficult due to the binding agent being a proprietary blend. If oxygen was present, it was at a low enough concentration that some BNNTs were able to survive mostly intact.

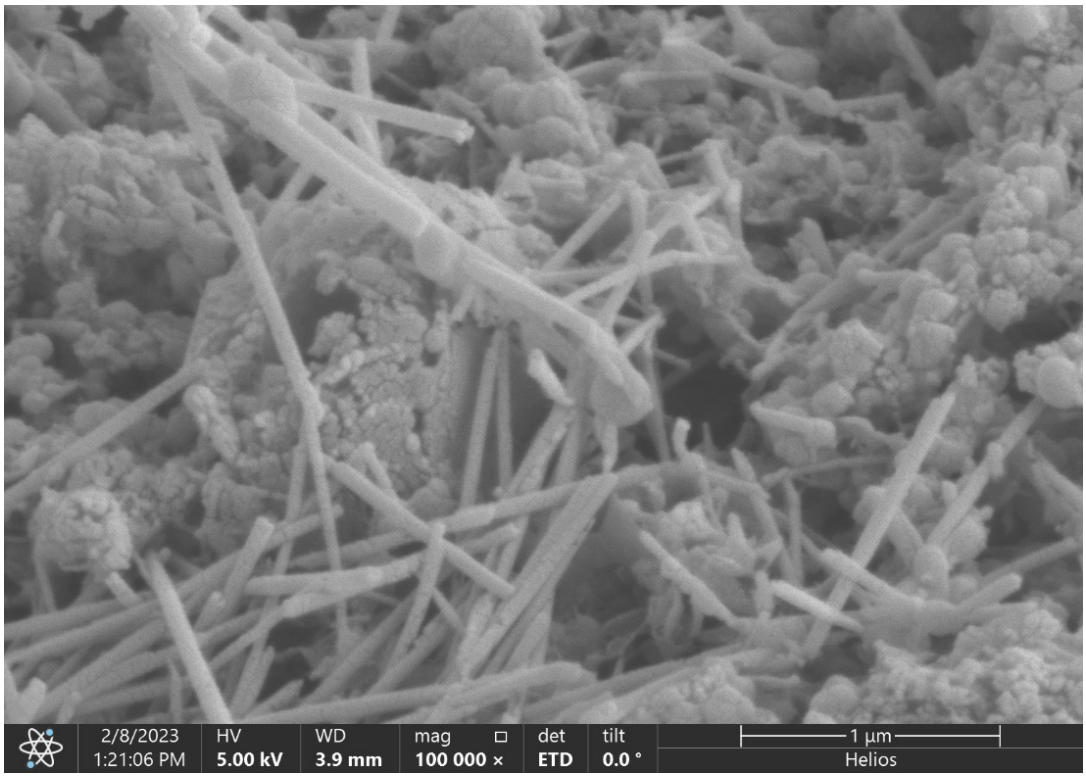

Figure 19. BNNT Agglomeration in Sample Debinded in Argon (x100000).

Figure 20 shows the grain structure of the sample debinded in argon. When compared to Figure 18, the two are similar. Both show unfused hydroxyapatite grains without the presence of the binder. Figure 20 also contains a region that resembles the structures in Figure 17, again indicating that some oxygen was present.

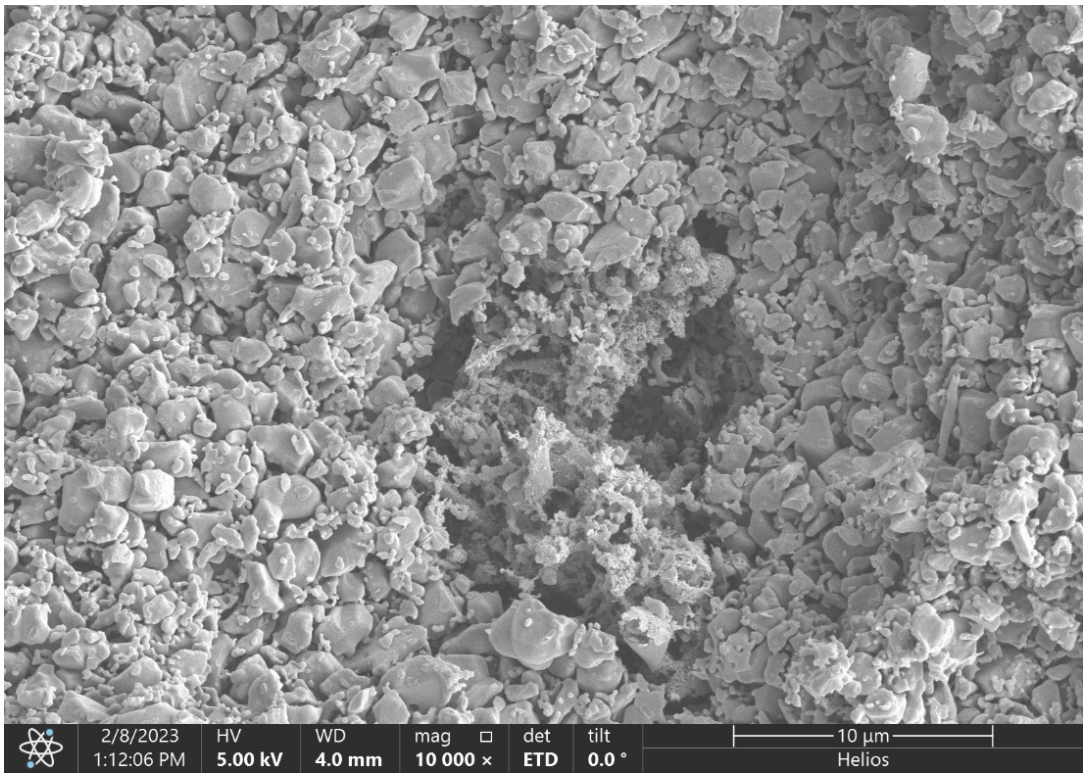

Figure 20. Grain Structure of Sample Debinded in Argon (x10000).

To confirm the results of the SEM analysis, each of these three samples underwent XRD analysis. The XRD spectra for all three samples are seen in Figure 21. As expected, all three samples have incredibly similar diffraction spectra; however, there is one major difference. Both debinded samples show nearly identical spectra with some slight variation in peak intensity, which is common across different samples. The difference is found in the spectrum of the green sample. Around a 2θ value of 27º there is a defined peak seen in red. This peak almost certainly corresponds to the presence of BNNTs as seen with the spectrum in Figure 13. BNNTs display a peak around 26.65º, depending upon the individual XRD settings and target [42]. This indicates that the green sample had enough BNNTs present to diffract a sufficient number of x-rays even though they are only 4 vol%. What is more interesting, is that this peak was not seen in the spectrum of the sample debinded in argon, despite intact BNNTs observed during SEM analysis. This indicates that the amount of BNNTs left intact was not sufficient to register a peak above background. This also confirms the hypothesis that some oxygen was present and caused

most of the BNNTs in the samples to oxidize. Aside from confirming the SEM data, this test showed that XRD is a reliable method to test for BNNTs even at a very small concentration like 4 vol%.

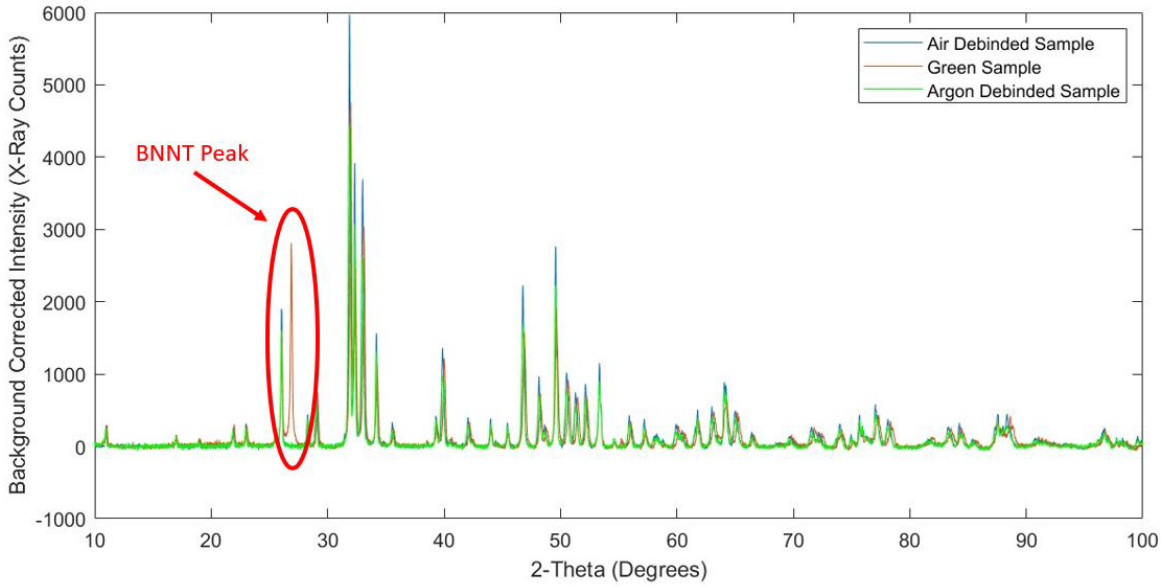

Figure 21. XRD Spectra from All Initial Testing Samples.

The initial testing confirmed that BNNTs could survive debinding; however, the presence of any oxygen results in partial and on some occasions complete oxidation of the BNNTs. The initial testing also highlighted the porosity of the hydroxyapatite after the removal of the polymer binding agent. This was the motivation behind the next round of testing, to identify the ideal temperature at which to sinter.

B. TEMPERATURE VARIATION TESTING

Due to the temperature limitations of the tube furnace, the maximum testing temperature was limited to 1100ºC. As a result, the five samples that were debinded in argon, were tested at 900ºC, 950ºC, 1000ºC, 1050ºC, and 1100ºC. Along with these samples, a control sample debinded in air was sintered alongside the argon-debinded samples. The samples in Batch 1 were exceedingly small. The sample were cylinders with a diameter of 0.25 cm and a thickness of 0.2 cm.

The first sample of Batch 1 was sintered for 2 hours at 900ºC with a 90-minute ramp-up time. Figure 22 shows the grain structure for this sample at two different magnifications. No BNNTs could be found within the 900ºC sample, further indicating a leak in the tube furnace. When comparing the grain structure in Figure 22 to those in Figures 18 20, there is a clear difference in porosity. The grains in Figure 22 show signs of fusion indicating sintering began. The sample still contains a large amount of porosity which indicates that it needed to be sintered for a longer period or at a higher temperature.

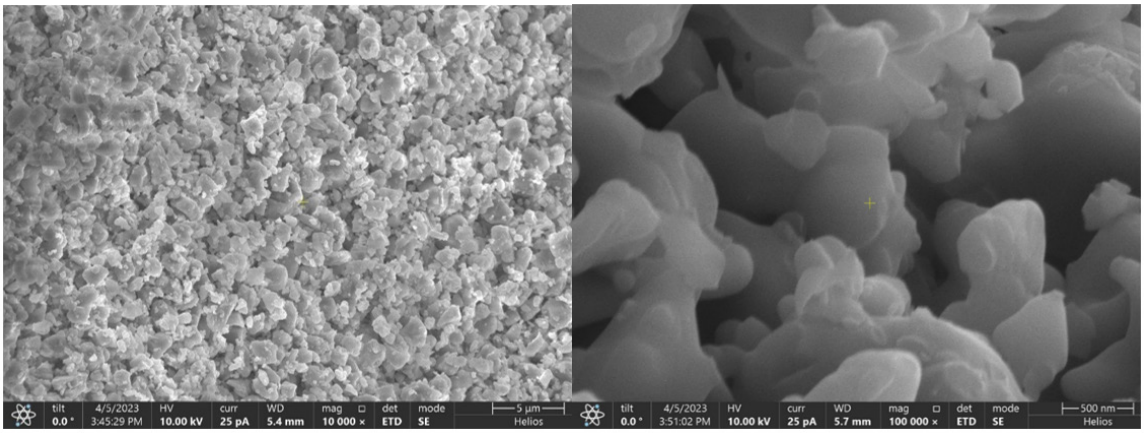

Figure 22. Grain Structure of 900ºC Sample.

The second sample of Batch 1 was sintered for 2 hours at 950ºC with a 90-minute ramp-up time. Figure 23 shows the grain structure for this sample at two separate locations. Much like the 900ºC sample, the 950ºC sample shows no signs of intact BNNTs; however, the structure in the right image of Figure 23 is likely the remnants of an oxidized BNNT agglomeration. The 950ºC sample does show some grain fusion, but it still contains a large amount of porosity.

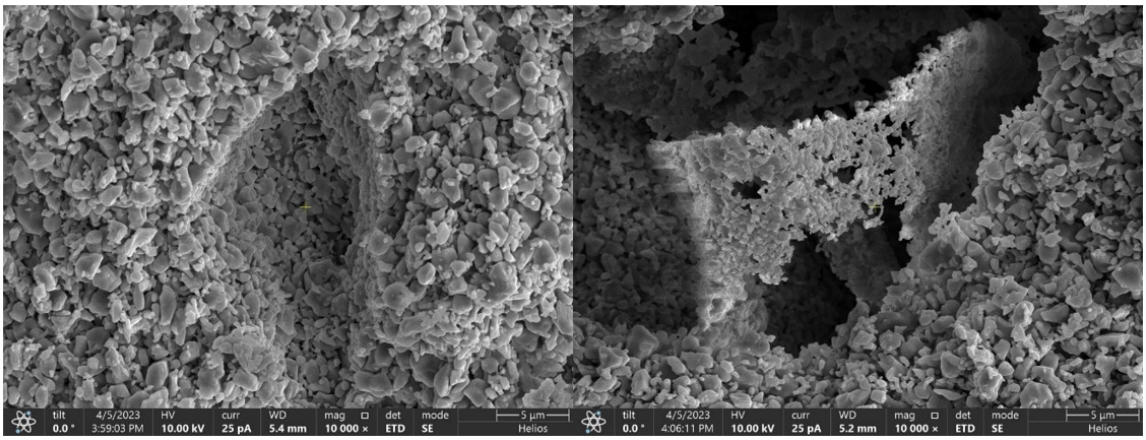

Figure 23. Grain Structure of 950ºC Sample.

The third sample of Batch 1 was sintered for 2 hours at 1000ºC with a 90-minute ramp-up time. Figure 24 shows the grain structure for this sample at two separate locations and magnifications. Much like the prior two samples the 1000ºC shows some sintering, but still below expectations. The key difference in this sample was the structuring in the right image of Figure 24. Based upon the size and shape, the structure is obviously a nanofiber of some sort. When the structure is compared to images of pre-heat treated BNNTs, they share the same size and general shape; however, the structure in Figure 24 seems to be distorted and damaged. The evidence indicates that this structure is an intermediate step in the oxidation of BNNTs. It is a result of enough oxygen being present to damage the BNNTs, but not enough to fully oxidize them.

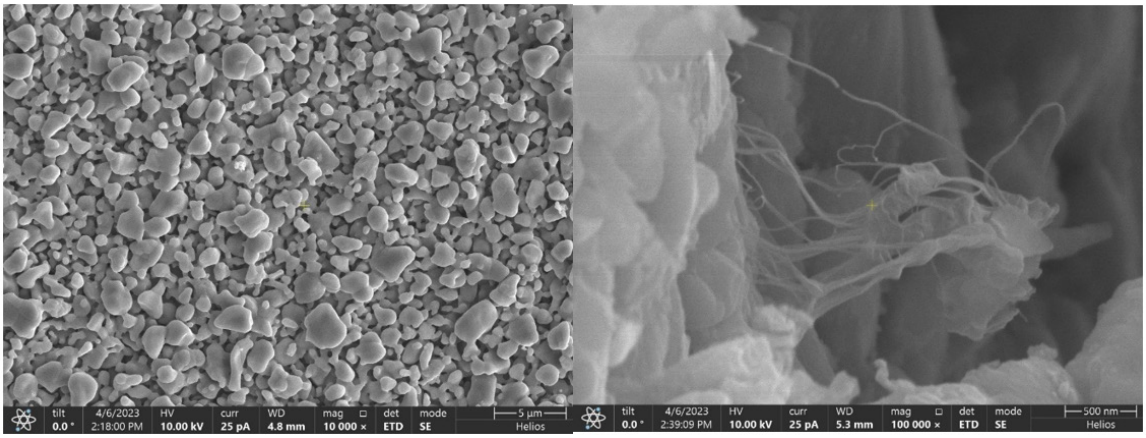

Figure 24. Grain Structure of 1000ºC Sample.

The fourth sample of Batch 1 was sintered for 2 hours at 1050ºC with a 90-minute ramp-up time. Figure 25 shows the grain structure for this sample at two separate locations. The two images in Figure 25 are like those in Figure 23. The left image shows the typical grain structure, which shows some grain fusion. The image on the right again shows what appears to be a fully oxidized BNNT agglomeration.

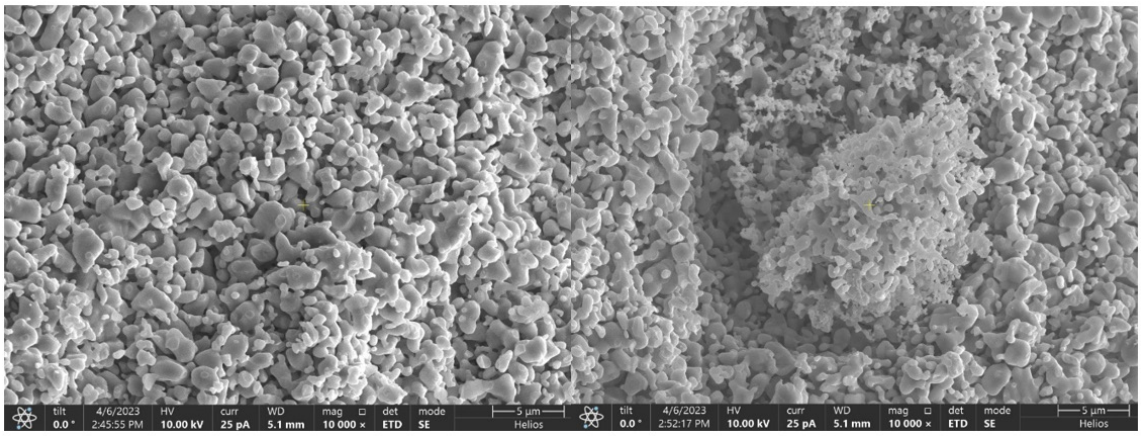

Figure 25. Grain Structure of 1050ºC Sample.

The fifth and final sample of Batch 1 was sintered for 2 hours at 1100ºC with a 90-minute ramp-up time. Figure 26 shows the grain structure for this sample at two separate locations and magnifications. While it is subjective, the grains in the 1100ºC appear to have

the most grain fusion, which fits with the expectations. Theoretically the highest temperature should have the highest levels of grain fusion and in turn density. The right image in Figure 26 contains a structure much like the one found in Figure 24. Again, it is likely BNNTs in some stage of oxidation. This example appears to have suffered more damage than the BNNTs in Figure 24, which fits with the increase in temperature.

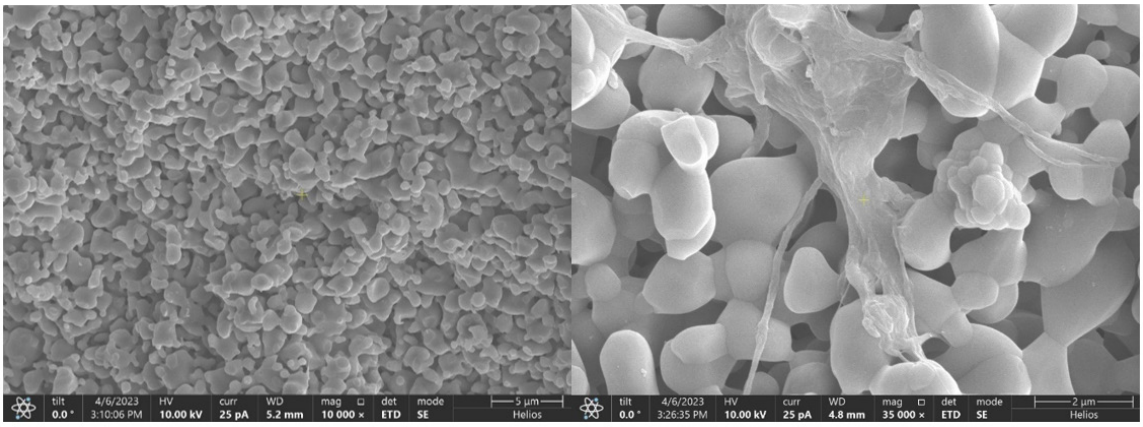

Figure 26. Grain Structure of 1100ºC Sample.

Only two sintered samples (1000ºC and 1100ºC) were found to have partially oxidized BNNTs, while the other three samples were found to contain completely oxidized BNNTs. It is more likely that all five samples contained BNNTs in some stage of oxidization. In the absence of other methods, the SEM can identify BNNTs on a fracture surface, but it cannot definitively determine the presence or absence of BNNTs in a sample. While Batch 1 failed to yield definitive proof that BNNTs survived the sintering process without severe damage, it did give insight into the process of BNNT oxidation and to the degrees of oxidation.

Along with the SEM imaging of the samples, the density for each was measured using Archimedes Method. The percent density values of the argon debinded samples and the control samples are listed in Table 2 and graphically in Figure 27. All argon debinded samples fell between 86%-91% density, while all control samples fell between 84%-89%. Unfortunately, the samples do not follow any kind of trend. This indicates that the dwell temperature had little to no effect on densification. Thus, the dwell time bears a stronger

influence on final density than the dwell temperature. The samples in Batch 1 were incredibly small, with an average volume of only 0.0075 cm^3. There is likely a significant error in the density calculation due to the sample's small size. This can be corrected in future testing with more samples or larger samples. While not ideal for final ceramic parts, the percent densities at these sintering temperatures are consistent with similar experiments in literature. In a similar experiment by G. Muralithran and S. Ramesh, the authors used sintering temperatures up to 1450ºC, which achieved a theoretical density of >99% in sintering temperatures above 1250ºC [12]. Due to the limitations on the tube furnace available the sintering temperature had to be kept under 1100ºC; however, for sintering temperatures below 1100ºC, the percent densities were found to be between 76%-83% [12]. The cited experiment used a traditional ceramic manufacturing method where hydroxyapatite powder was pressed into disc samples with a small amount of binder, while the samples used in this thesis were manufactured via 3-D printing. This is encouraging since additively manufactured ceramics often display more porosity; however, in this case they performed as well or better than traditional samples.

As previously mentioned, the samples in Batch 1 were small. As a result, after preparing the samples for SEM analysis there was not enough remaining material to conduct any XRD testing. This issue was noted, and the following batches used larger samples that contained ample remaining material for XRD analysis. Batch 1 provided confirmation that the BNNTs could partially survive sintering with severe damage and that the percent densities achieved were consistent with published literature. The motivation for Batch 2, was to understand how the sintering medium can affect the percent density of the sample and the preservation of BNNTs.

Table 2. Percent Density Values for Samples in Batch 1.

	Sample 1	Sample 2	Sample 3	Sample 4	Sample 5
Temperature	900ºC	950ºC	1000ºC	1050ºC	1100ºC
Argon Debinded Samples	87.39%	90.80%	86.69%	89.37%	86.69%
Air Debinded Samples	88.66%	87.94%	84.59%	88.08%	86.33%

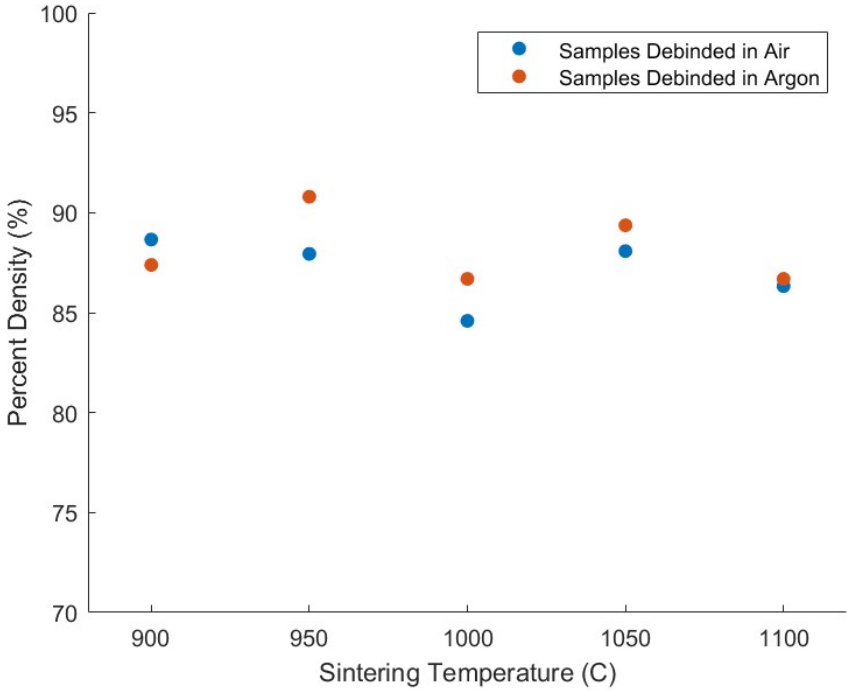

Figure 27. Percent Density Values for Samples in Batch 1.

C. SINTERING MEDIUM TESTING

Batch 2 focused on identifying whether sintering the hydroxyapatite samples in a medium resulted in differing percent densities and if it provides addition protection for the BNNTs. As explained in the experimental methods section, one sample was placed in a bed of boron nitride and covered completely, while the other sample was placed next to the

first without any medium. Both were larger than the samples were cylinders with a diameter of 0.232 cm and a length of 1.252 cm, larger than the samples in Batch 1. This was done to help eliminate some of the errors associated with the smaller samples. The two samples in Batch 2 were both debinded in argon following the same steps as Batch 1. Next, the samples were sintered at 1000ºC for 2 hours with a 90-minute ramp-up time. For Batch 2, the tube furnace was kept at about 0.2 MPa gauge pressure throughout the debinding and sintering processes. This was done to prevent air from entering the tube.

Figures 28 and 29 show the sample that was debinded and sintered without any medium. This sample, like the samples of Batch 1, were placed on a crucible and directly into the furnace with no surrounding medium. As expected, the sample with no medium shared many similarities to the samples in Batch 1. Figure 28 shows the remnants of a BNNT agglomeration post oxidation. No intact BNNTs could be found in the first sample, indicating that oxygen was present even after the precautions taken to lessen the effects of the leak. This demonstrates the difficulty in sintering ceramics while protecting BNNTs from oxidation. It highlights the need for a near perfect absence of oxygen, which is nearly impossible. As mentioned earlier the two most probable sources of oxygen in the furnace are a leak or the vaporization of the polymer binding agent, but there is a possible third source. The chemical formula of hydroxyapatite is $Ca_5(PO_4)_3(OH)$, and it contains a significant amount of oxygen. Hydroxyapatite can decompose at high temperatures typically above 1300ºC, but it can release OH^- ion at temperatures as low as 1000ºC [25]. It is possible that the oxygen in the hydroxide ion is reacting with the boron in the BNNTs and oxidizing. This could explain the structures seen in Figures 67–70 in the appendix. In these images the BNNTs seem to be fused to the hydroxyapatite grains. If the hydroxyapatite was decomposing and releasing hydroxide ions, then the BNNTs could have reacted to the ions that were diffusing out of the hydroxyapatite grains. This would result in the BNNTs almost bonding to the hydroxyapatite grains and becoming oxidized by the hydroxide ions, explaining the structures. Since the temperatures were kept lower than 1100ºC, it is likely that the amount of hydroxide ions being released is low. If this is what is occurring, no amount of oxygen elimination can protect the BNNTs. This would mean that hydroxyapatite is simply not suited for use with BNNTs and that a non-oxide

ceramic would be a better choice. To confirm this hypothesis more thermal analysis of hydroxyapatite would be required. Figure 29 shows the grain structure of the sample with no medium. There is no noticeable difference in the porosity in the sample when compared to the samples in Batch 1. There are significant signs of grain fusion, but large pores remain prevalent in the sample.

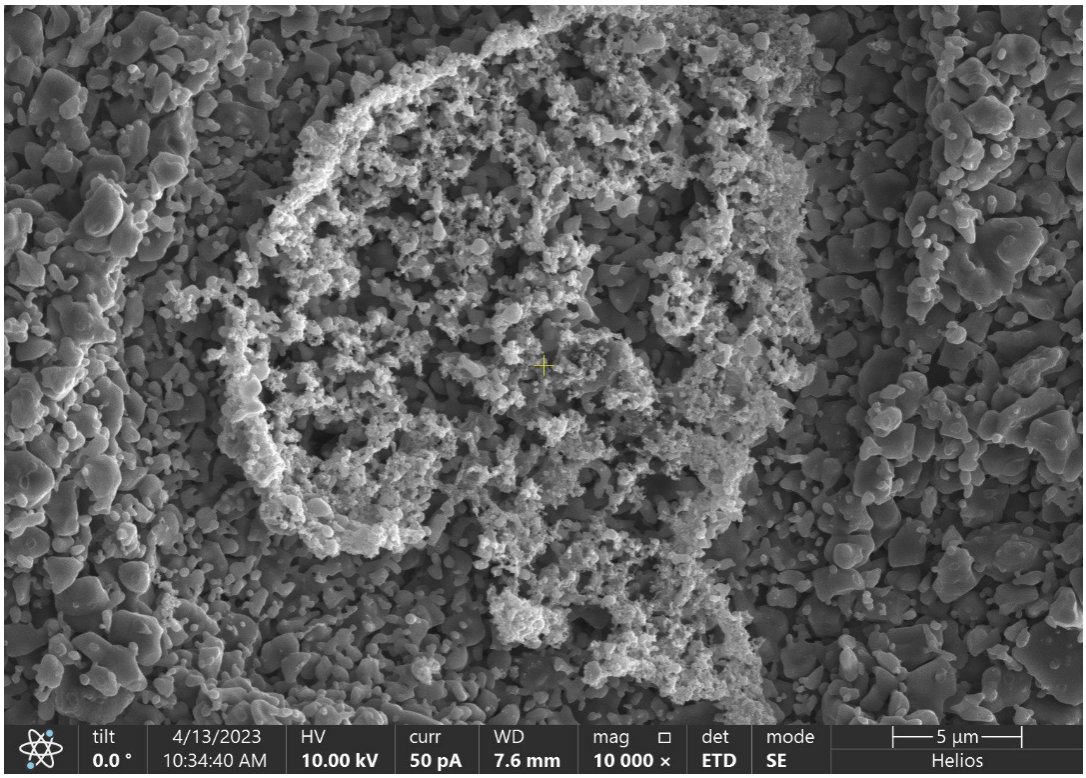

Figure 28. Fully Oxidized BNNT Agglomeration in Sample with No Medium.

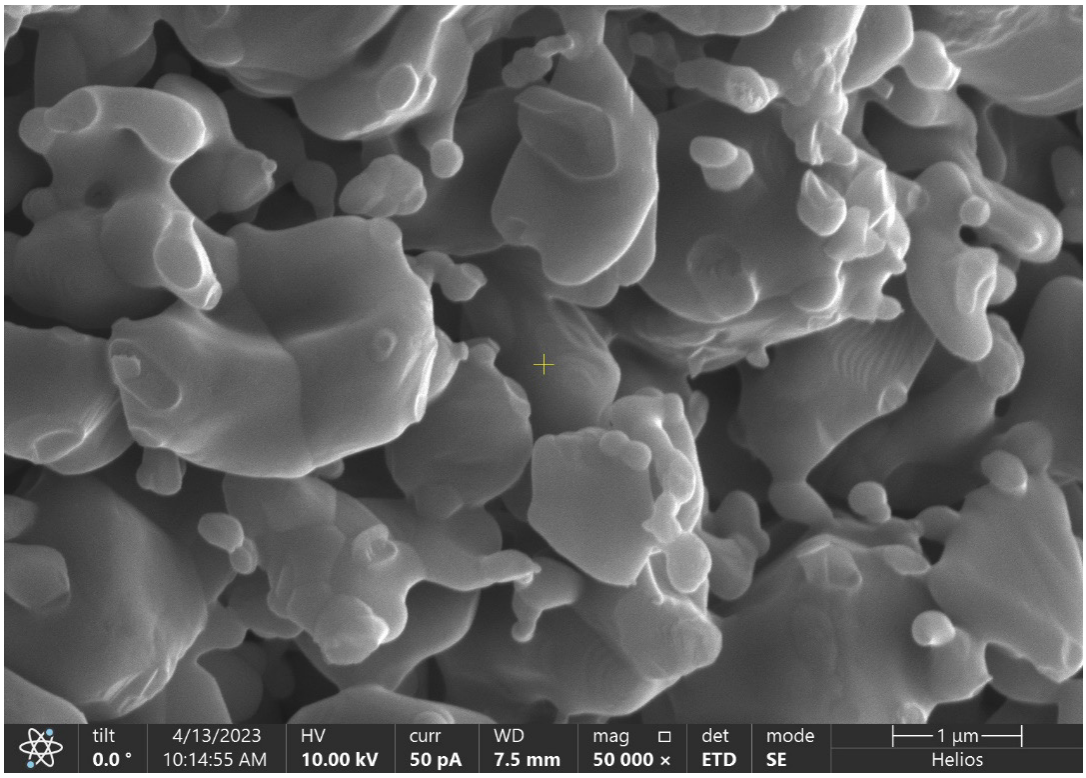

Figure 29. Grain Structure of Sample with No Medium (x50000)

Figures 30–32 show the sample that was debinded and sintered in a medium of boron nitride power. The grain structure of the boron nitride medium sample (Fig. 30) is almost identical to that found in Figure 29. This is as expected since both were debinded and sintered together under the exact same conditions; however, sintering this sample in medium had little to no effect on the grain fusion. Figures 31 and 32 show an agglomeration of what appeared to be perfectly intact BNNTs at two different magnifications. These images definitively show that the BNNTs can survive the debinding and sintering processes when exposed to the right environment. As can be seen from Figure 31. The BNNT agglomeration is large, indicating that it was not simply a stray BNNT that survived by chance. Figure 32 shows the same region at a higher magnification. As can be seen in the image, the BNNTs show little to no sign of oxidization damage. It is possible that by compacting the boron nitride powder around the sample, it created another layer of protection from oxygen. This indicates that any oxygen that contaminated the samples via the leak was prevented from reaching this sample by the boron nitride medium, while it

was allowed to oxidize the sample without a medium protecting it. The results from Batch 2, clearly demonstrate that it is best to sinter samples in a powder medium to reduce BNNT oxidation.

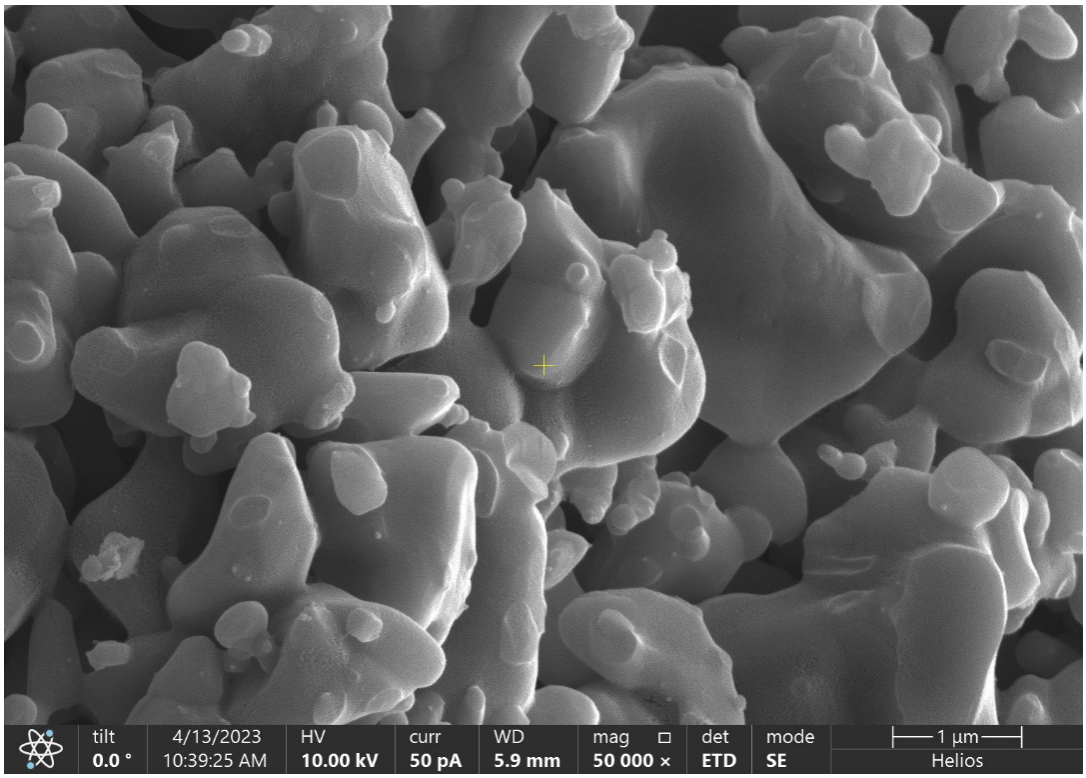

Figure 30. Grain Structure of Sample with the Boron Nitride Medium (x50000)

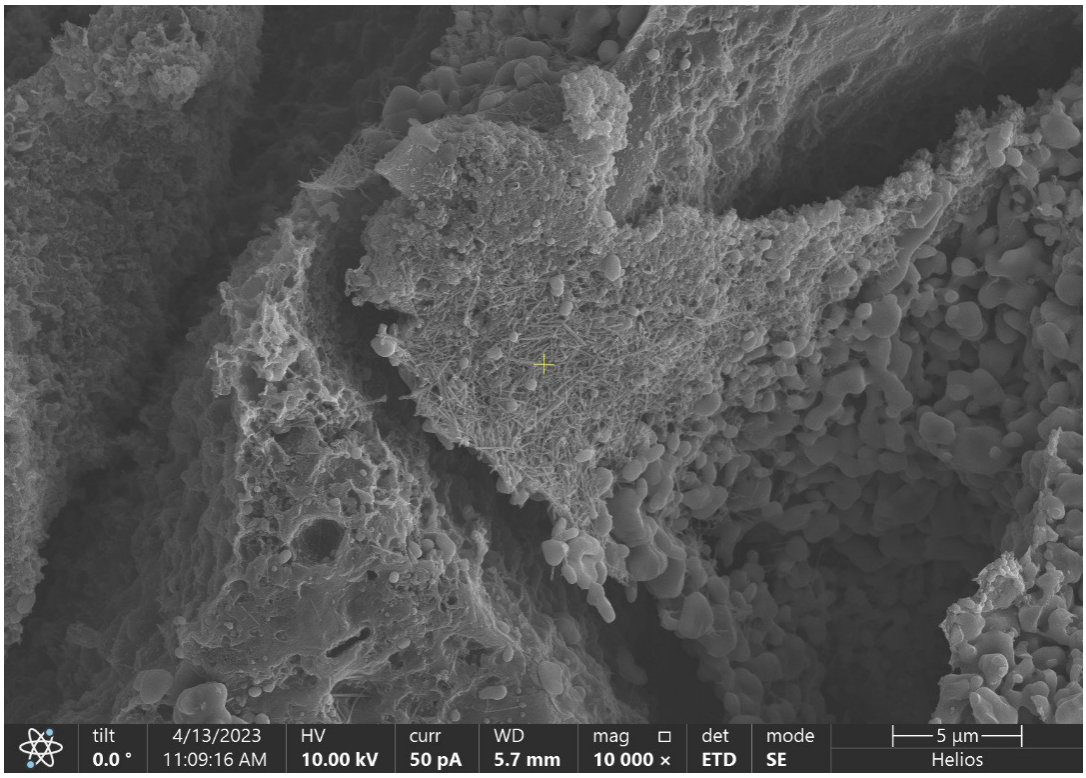

Figure 31. Agglomeration of Intact BNNTs in Sample with the Boron Nitride Medium (x10000)

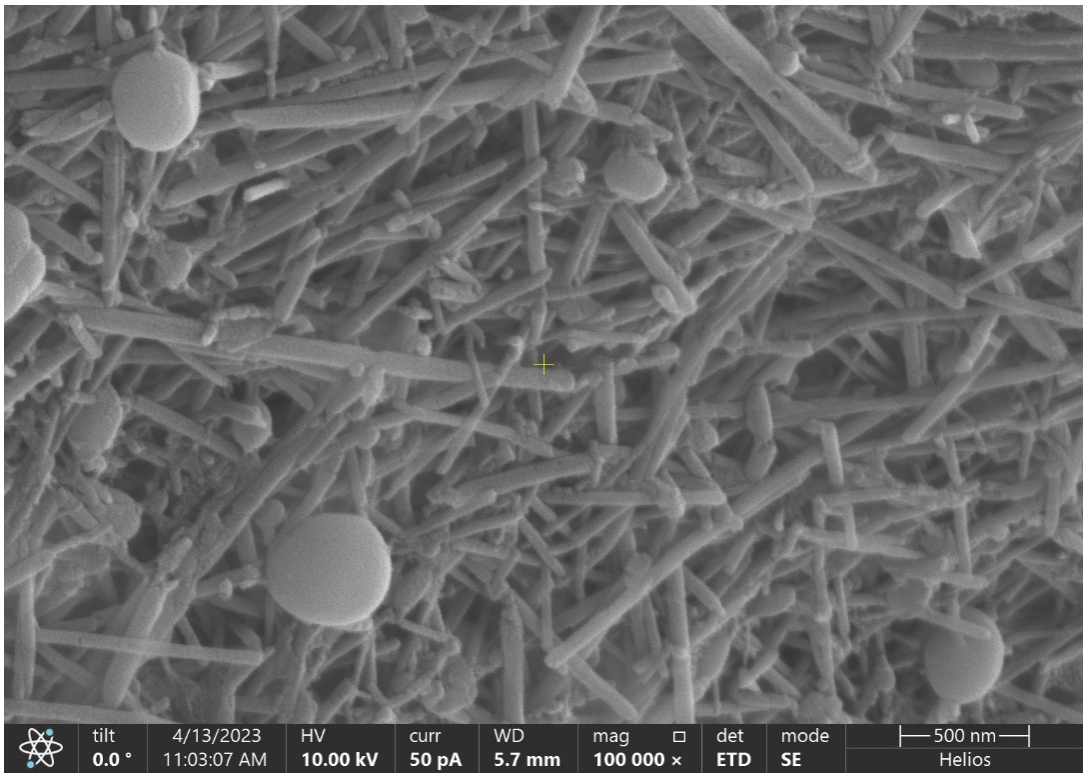

Figure 32. Agglomeration of Intact BNNTs in the Sample with Boron Nitride Medium (x100000)

Along with SEM analysis these samples were measured using the Archimedes method. The samples used in Batch 2 were an order of magnitude larger than those in Batch 1. The average sample volume for Batch 2 was 0.0539 cm^3. While still small, these larger samples are less prone to measurement errors. The percent densities were measured at 85.39% and 84.77% for the sample heated in no medium and the sample heated in boron nitride powder, respectively. With a difference of less than 1% theoretical density it is not possible to draw any solid conclusions as to which medium results in the best post-sintering density. To draw such conclusions several further rounds of testing are required with more samples and more types of medium.

The two samples of Batch 2 also underwent XRD analysis. The XRD spectra for both samples and for a green sample, for comparison, are in Figures 33 and 34. Figure 33 shows the entire spectra from 10º to 100º. The spectra are almost indistinguishable aside from some key differences highlighted in Figure 34. Figure 34 shows a region of interest

that contains three peaks that reveal information about the samples. This first being the peak around 26.65º that indicates the presence of BNNTs. The green sample displays a strong peak at around 26.65º; however, both samples from Batch 2 display a small but distinguishable peak at the sample angle. Interestingly, the sample with no medium displays a peak with more intensity, indicating that there were BNNTs present. It is easily possible that the SEM analysis did not uncover BNNTs in the sample by chance, since it only considers one fracture surface and not the whole sample. While smaller the peak is present in the spectrum for the sample with no medium, confirming the presence of BNNTs. Another point of interest are the two peaks at around 31.5º and 34.75º that were found in both Batch 2 samples but not in the green sample. This leads to the conclusion that some new compound was formed in the debinding and sintering process. The immediate suspect would be boron oxide from the oxidation of the BNNTs; however, boron trioxide (B_2O_3) typically has a high intensity peak around 31º using a Cu target [43]. This could explain the peak at 31.5º, but not the peak at 34.75º. The culprit of the 34.75º peak is likely another form of boron oxide compound boron suboxide (B_6O). Boron suboxide has a high intensity peak around 34.4º, which is close enough to explain the second unknown peak [43]. The fact that these peaks are present after sintering but not after debinding, indicates that the degradation of BNNTs is an extended process rather than a single reaction. The elevated temperatures of the debinding step causes the breakdown of the nanotube structure but is too brief to allow the oxygen present to oxidize a large amount of boron nitride. The longer dwell time during sintering allows for the full oxidization of the remnants of the BNNTs, resulting in substantial concentrations of compounds like boron trioxide and boron suboxide. This again highlights how delicate BNNTs are depending upon their environment. Even though several steps were taken to ensure an oxygen free environment, the small amount that was present was able to oxidize most of the BNNTs in the samples.

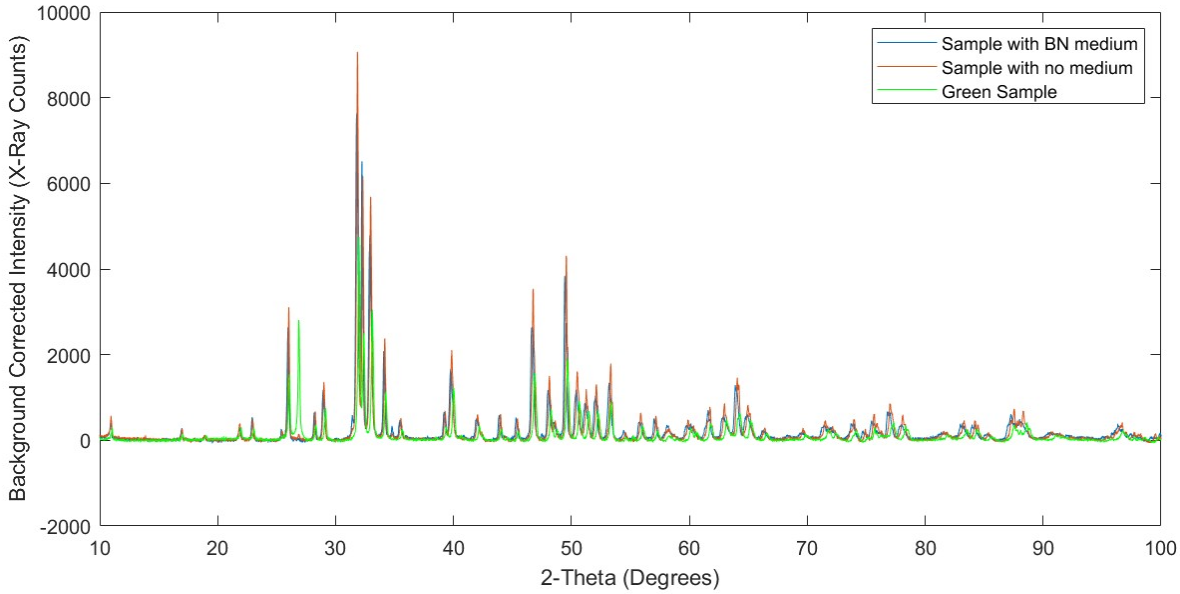

Figure 33. XRD Spectra from Batch 2.

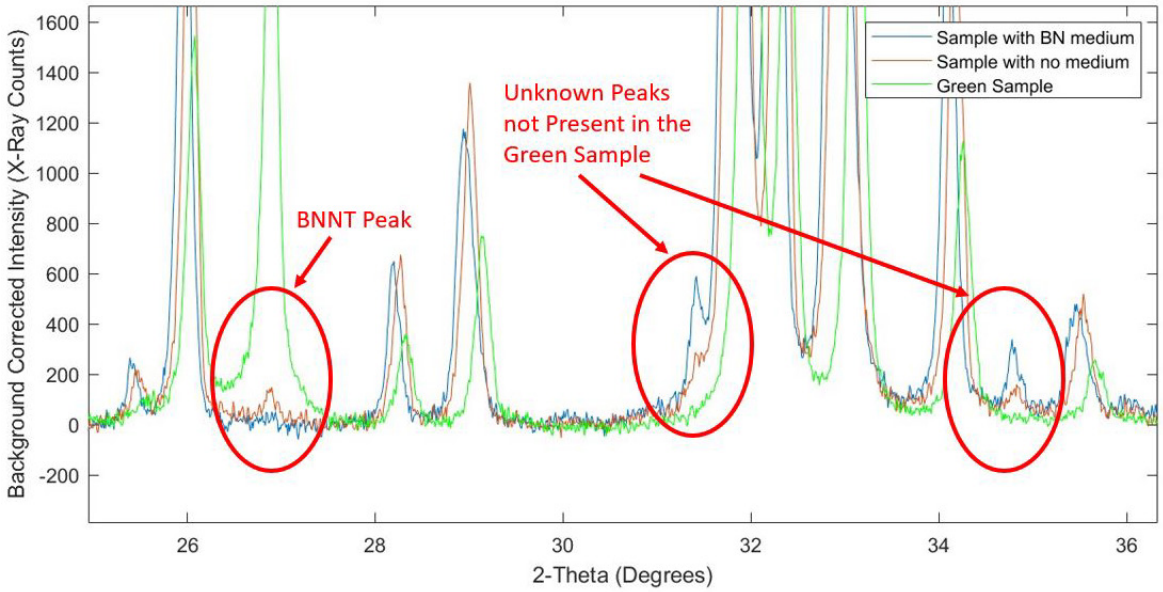

Figure 34. Region of Interest for Batch 2 XRD Spectra.

While the inconclusive density measurements were disappointing, the presence of intact post-sintering BNNTs demonstrates that it is possible to sinter a ceramic with BNNTs and have them survive. Due to sintering temperature limitations the final densities

of the samples have been poor compared to industry standards; however, it is important to better understand all the factors that contribute to the proper sintering of the hydroxyapatite. BNNTs are not typically sintered in ceramics, and they potentially could affect the grain fusion process. This question was the motivation behind the third batch of samples.

D. EFFECTS OF BNNTS ON SINTERING

Batch 3 focused on better understanding what effect the presence of BNNTs have on the grain fusion and growth process during sintering. The samples used in Batch 3 had the same geometry as the samples used in Batch 2, with a volume of about 0.0539 cm^3. Both samples were placed on a crucible with no medium and exposed to the same post-processing heat treatments as before. The samples were debinded as normal and sintered at 1000ºC for 2 hours, like the samples in Batch 2. Also like in Batch 2, the tube furnace was kept at about 0.2 MPa gauge pressure throughout the debinding and sintering processes. Once the samples were properly sintered, they underwent the sample characterization methods as before.

Figures 35 and 36 show the sample that contained 4 vol% of BNNTs before post-processing. Figure 35 shows the grain structure along the edge of the sample. This image was taken to see whether there was better grain fusion along the edge due to how heat takes time to penetrate the sample. As seen, there seems to be little to no difference in the grains at the immediate edge versus farther into the sample. As expected, the grains are similar to prior samples. Figure 36 shows the grains at the center of the sample. These grains have a unique structure throughout, which is likely the remains of oxidized BNNTs. These oxidized BNNT structures are different from ones seen before. This could be simply differences in samples, or the structures could be a different compound. As explained above the BNNTs appear to form two distinct compounds when oxidized. It is possible that earlier evidence of oxidation is one of these oxides and the structure in Figure 36 is the other. Further chemical analysis is required to determine exactly what the unknow structure in Figure 36 is. Thorough analysis of this sample yielded no evidence of any intact BNNTs.

This is consistent with the sample from Batch 2 that was sintered in the exact same manner, with no medium.

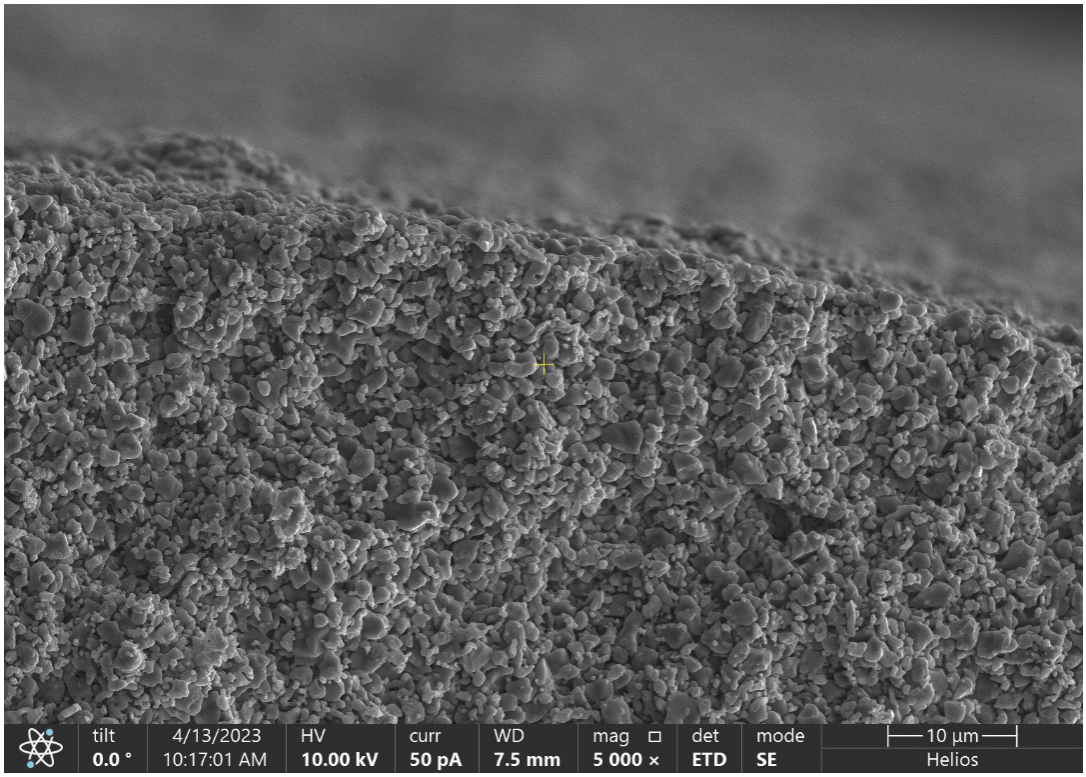

Figure 35. Grain Structure of Sample with BNNTs Along Sample Edge (x5000).

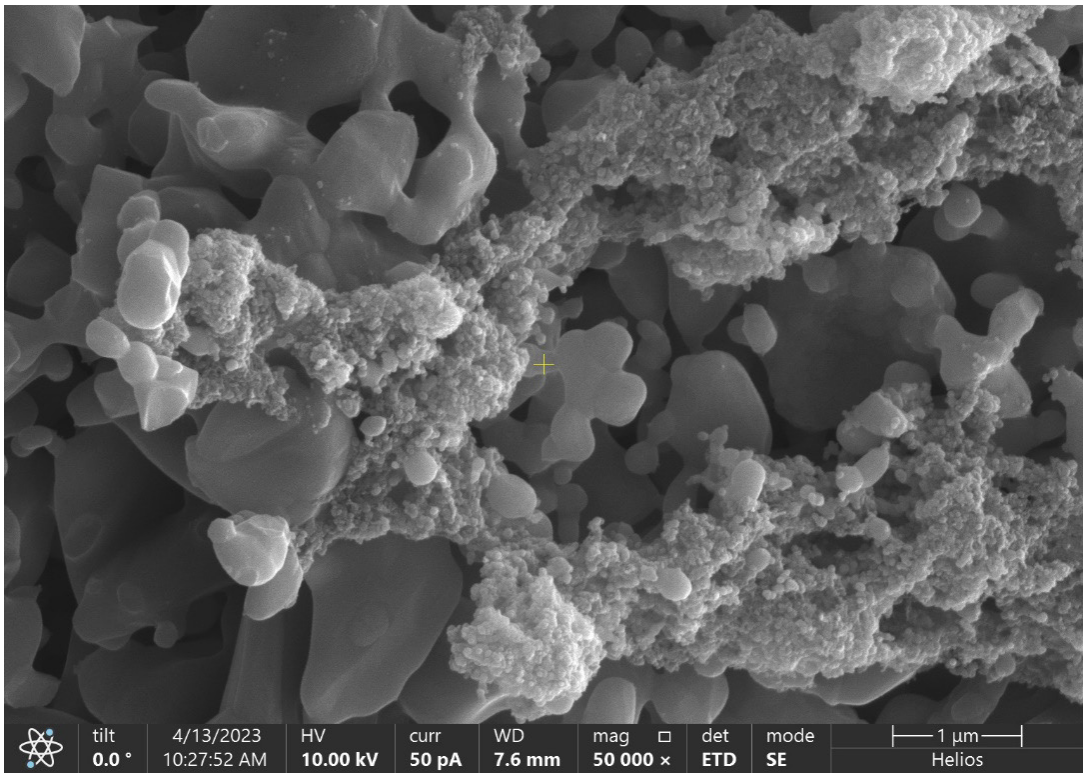

Figure 36. Grain Structure of Sample with BNNTs (x50000).

Figures 37 and 38 show the sample that was printed without BNNTs at all. Figure 37 shows the edge of the sample much like Figure 35. While it is completely subjective, the grains appear to show slightly more characteristics of fusion. This is especially apparent with comparing Figures 36 and 38. The sample without BNNTs appears to have a denser structure caused by more complete sintering. When this observation is coupled with the density measurements for both samples, it becomes clear that the sample without BNNTs was more completely sintered.

The hydroxyapatite sample with BNNTs displayed a percent density of 85.27%, which is consistent with earlier samples; however, the sample printed without BNNTs displayed a percent density of 91.86%. This is substantially higher than the sample with BNNTs and higher than any sample tested thus far. There are two possible explanations for this significant difference in percent densities. First, that the printed part used differing compound while printing since BNNTs were not present. It is likely that since BNNTs were not in the print slurry, a different mixture was used for the hydroxyapatite. It is also

possible that this mixture had a different hydroxyapatite loading within the slurry. If the loading was higher, more hydroxyapatite would be in the sample per unit volume. This higher starting density in the sample without BNNTs would result in higher post sintering density even if the rate of grain fusion for both samples was the same. The second explanation is that the presence of BNNTs in the sample disrupted the sintering process. It is possible that the BNNTs stood in the way of neighboring hydroxyapatite grains being able to fuse together. The BNNTs and boron oxidizes could hinder the hydroxyapatite grain from coming in contact, resulting in less grain fusion around BNNTs agglomerations. This would then lead to a lowered total density of the sample. While these two hypothetical causes of the density difference are possible, they require much more testing to confirm or dispel them.

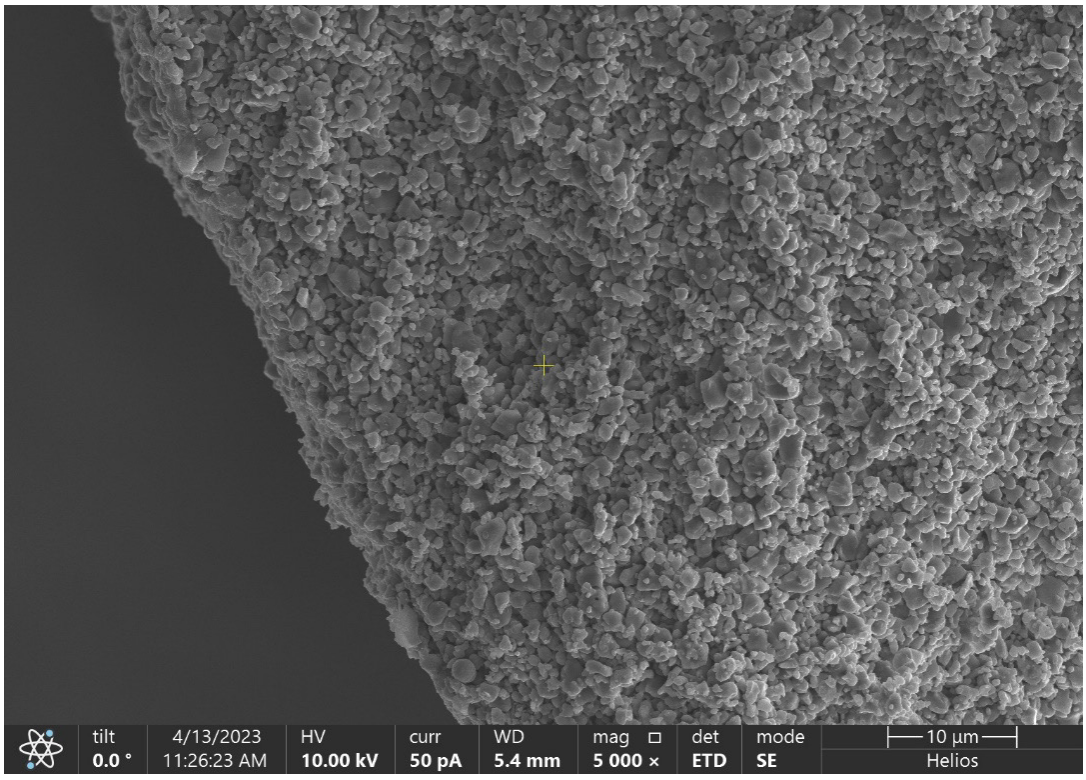

Figure 37. Grain Structure of Sample with No BNNTs Along Sample Edge (x5000).

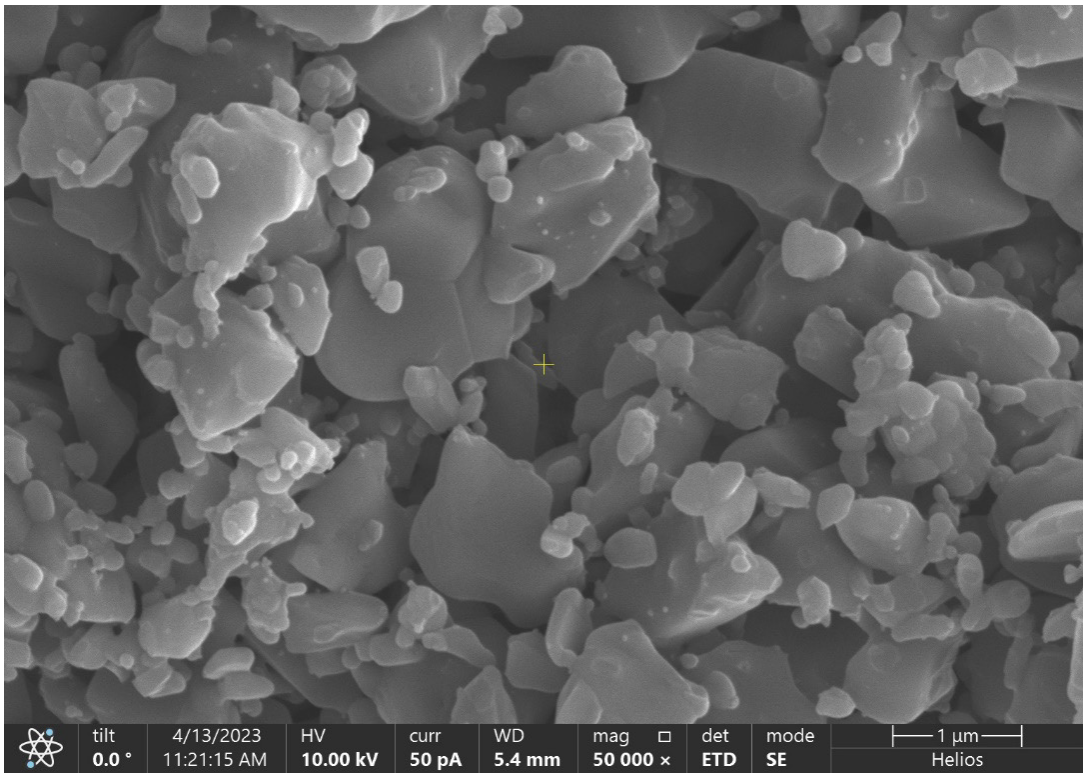

Figure 38. Grain Structure of Sample with No BNNTs (x50000).

Like previous samples, those in Batch 3 also underwent XRD analysis. Figure 39 shows the spectra of both samples in Batch 3 along with a green sample for comparison. Much like the sample sintered without a medium in Batch 2, the sample with BNNTs in Batch 3 displayed a BNNT peak around 26.65º. Neither sample yielded evidence of BNNTs following SEM analysis, yet both produced a BNNTs peak under XRD analysis. The sample with BNNTs also showed two boron oxide peaks indicating that oxidation took place. The spectrum from the sample with BNNTs was far less interesting. It followed the spectrum of the green sample exactly, with the only difference being peak intensities. These XRD results fall comfortably within expectations and provide surprises or further insights.

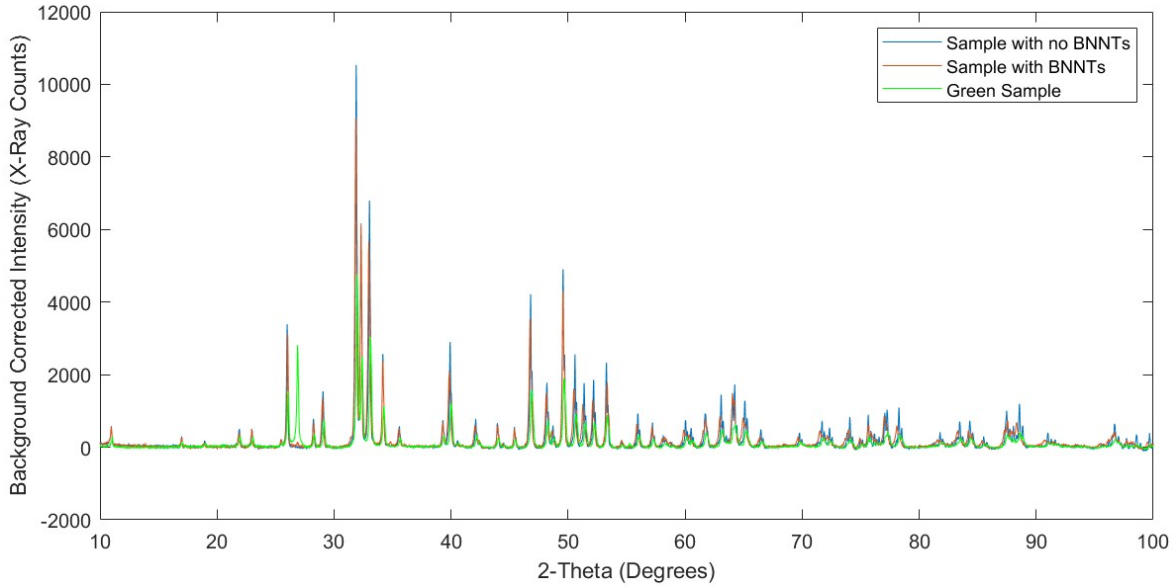

Figure 39. XRD Spectra for Batch 3.

Batch 3 sought to answer whether BNNTs had any effect on the sintering process of the hydroxyapatite grains. The samples seem to confirm the suspicion that BNNTs were negatively affecting grain fusion of the sample by disrupting particle contact. While this is only one test and it cannot fully confirm the hypothesis, it raises several questions that future work can strive to answer. Batch 3 also demonstrated once again that the BNNTs can survive the sintering process.

THIS PAGE INTENTIONALLY LEFT BLANK

V. CONCLUSION AND FUTURE WORK

A. CONCLUSION

The core objective of this work was to confirm that hydroxyapatite could be properly sintered without degrading any BNNT additives. In its most basic sense this objective was achieved by evidence in Batches 2 and 3. In these tests both SEM and XRD evidence was found that confirmed the presence of intact BNNTs post-sintering. While the majority of the BNNTs were found to have been oxidized in the debinding and sintering processes, it demonstrated that sintering with BNNTs can be done. From the work it was determined that the temperature had little to no effect on whether the BNNTs survive, it was instead dictated by the presence of oxygen. In Batch 1, the tube furnace was operated according to the user manual, at a negative starting gauge pressure. This exacerbated a small leak in the system, resulting in almost complete oxidization of the Batch 1 samples. However, when the tube furnace was maintained at a positive gauge pressure the leak was mitigated to the point where intact BNNTs were discovered in the samples of Batches 2 and 3. As a result, the BNNTs survival rate can easily be improved under more exact conditions.

The secondary objective was to identify the ideal method by which to sinter. This work focused on three factors that influence the final percent theoretical density of the hydroxyapatite. First, was the temperature which was varied in Batch 1 from 900ºC to 1100ºC. The tube furnace had a maximum extended operating temperature of 1100ºC so higher temperature testing was not possible with the equipment available. From testing it appeared that temperature had negligible effect on the final density. Upon further research other work saw the greatest increase in final densities when sintering occurred above 1250ºC [12]. This confirmed the hypothesis that the equipment limitations were preventing densification up to industry standards. However, Batch 1 did demonstrate that the additively manufactured parts could achieve similar percent densities when compared to traditional manufactured parts. Second was the sintering medium which was examined in Batch 2. In this batch both samples were sintered at 1000ºC for 2 hours. One sample was completely covered in boron nitride powder, while the other was not placed in a medium.

No distinguishable difference in density was detected. Initially, BNNTs were found in the sample with boron nitride medium only; however, BNNTs were eventually discovered in both samples with the XRD. More samples and more mediums should be tested to determine whether the sintering medium has any effect on grain fusion or if it can act as an oxygen shield, protecting the BNNTs. Third, was the effect that BNNTs had on the sintering process of hydroxyapatite which was examined in Batch 3. In this test, both samples were sintered without any medium at 1000ºC for 2 hours. One of these samples was printed with 4w% BNNTs just as all previous samples, while the other sample was printed without BNNTs entirely. In this case the sample with no BNNTs was found to have a theoretical percent density that was 6.59% higher than its counterpart with BNNTs. This indicates either a difference in printing materials led to the difference or the BNNTs disrupted proper grain fusion within the sample. Much like Batch 2, this was only one sample. To better confirm the suspicion that BNNTs negatively affect grain fusion, more testing would be required.

In conclusion, this work was able to accomplish its primary goal, to demonstrate that hydroxyapatite could be sintered while maintaining intact BNNTs in the ceramic. While determining an ideal sintering process was less successful, it was able to raise some important questions that can guide future work.

B. FUTURE WORK

The main challenge faced in this work surrounded the equipment, particularly the tube furnace. First, the furnace used was limited to 1100ºC, which limited the amount of grain fusion that could be achieved. Second, the furnace appeared to have an incredibly small leak somewhere in the system that risked exposing the samples to oxygen. Future work should use a more airtight system that can allow for higher temperatures. This will allow for a better analysis of the theoretical percent density.

The focus of Batch 2 was to analyze the effects of sintering mediums on the samples. Future work should focus on expanding the types of media used to include materials with a wide variation in thermal conductivities. It would be interesting to see how the thermal conductivity of the medium would affect the rate of grain fusion during

sintering. Future work should also include many more samples to be used in order to create a better understanding of the trends. This would reduce the risks of outliers and other errors.

During testing some samples appeared to have BNNTs fused to hydroxyapatite grains. Upon further research it was found that hydroxyapatite can release hydroxide ions above 1000ºC. The current hypothesis is that these ions were diffusing through the hydroxyapatite grains where they bond to the BNNTs on the surface of the grains. Further research should conduct a thermal analysis of hydroxyapatite and BNNTs to validate or disprove this hypothesis.

Batch 3 focused on how BNNTs affected the grain fusion process of hydroxyapatite during sintering. Based on the results, it seems that BNNTs could negatively affect the sintering process. Future work should examine this with far more samples and ensure that the materials used in the printing process were identical. It would also be interesting if future work analyzed several different nanomaterials with differing geometries. BNNTs are 1D nanomaterials, but would 0D, 2D, or 3D nanomaterials have different effects on grain fusion? This is perhaps the most interesting question raised by this work and would be a great starting point for future work.

THIS PAGE INTENTIONALLY LEFT BLANK

APPENDIX. ADDITIONAL SEM IMAGES

The following images show the initial testing green sample prior to debinding or sintering.

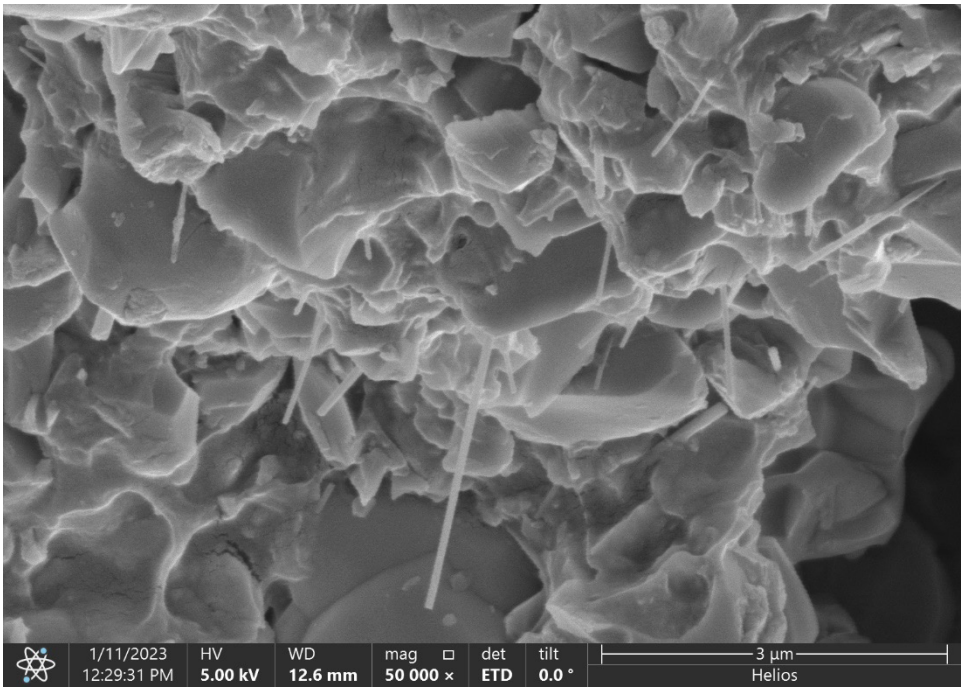

Figure 40. Initial Testing Green Sample (x50000)

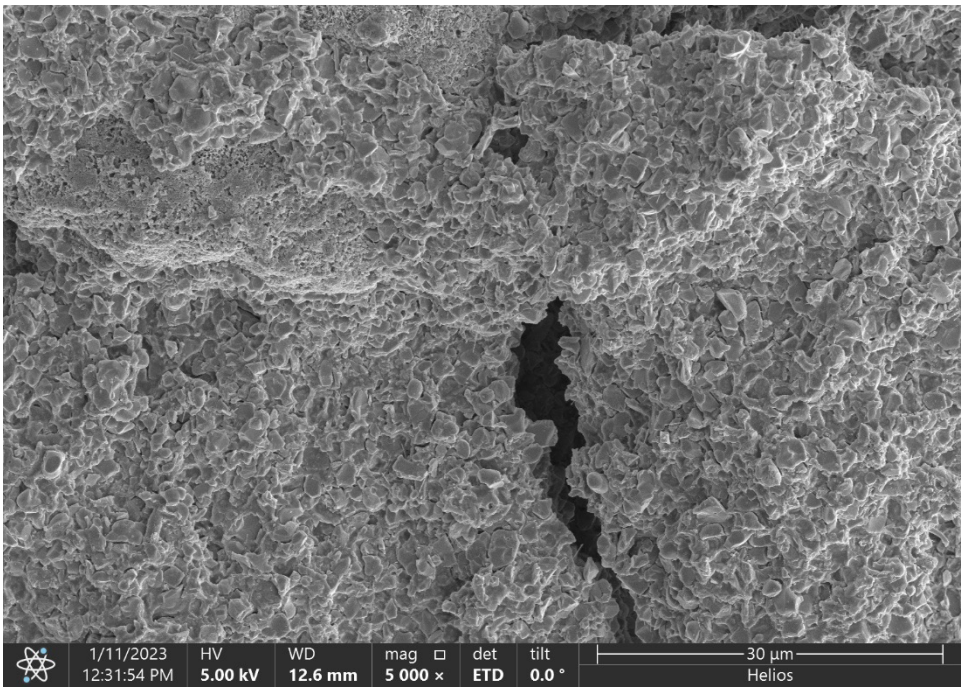

Figure 41. Initial Testing Green Sample (x5000)

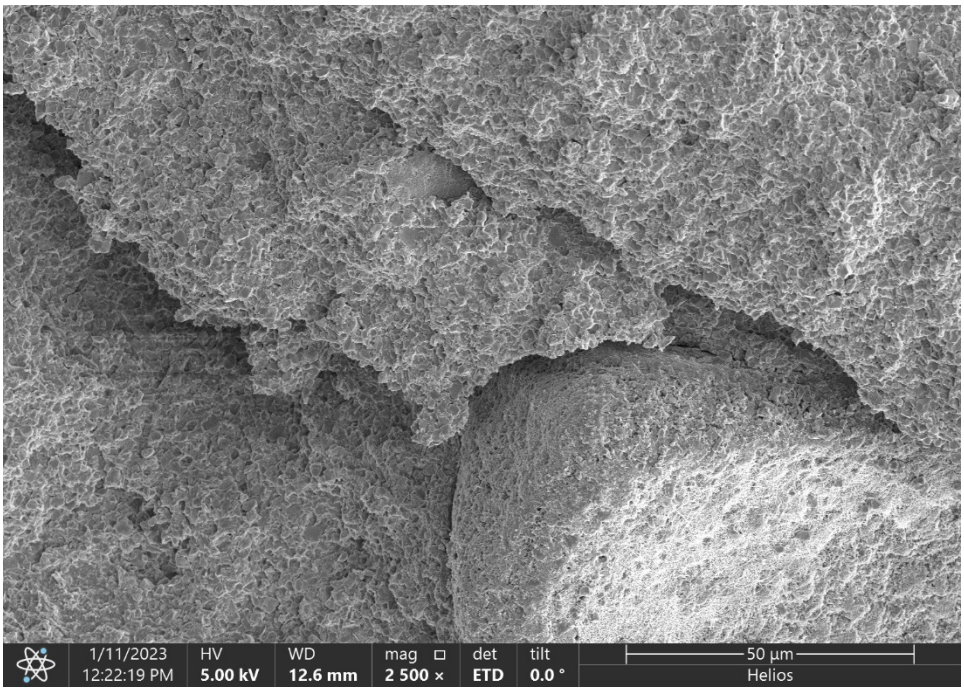

Figure 42. Initial Testing Green Sample (x2500)

The following images show the initial testing sample that was debinded in air.

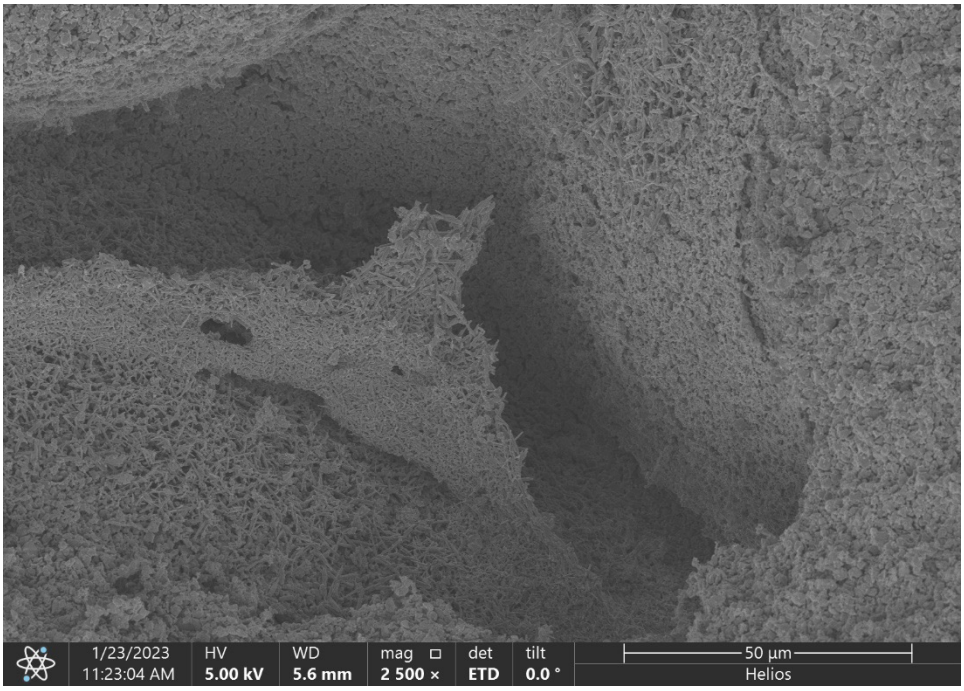

Figure 43. Initial Testing Sample that Was Debinded in Air (x2500)

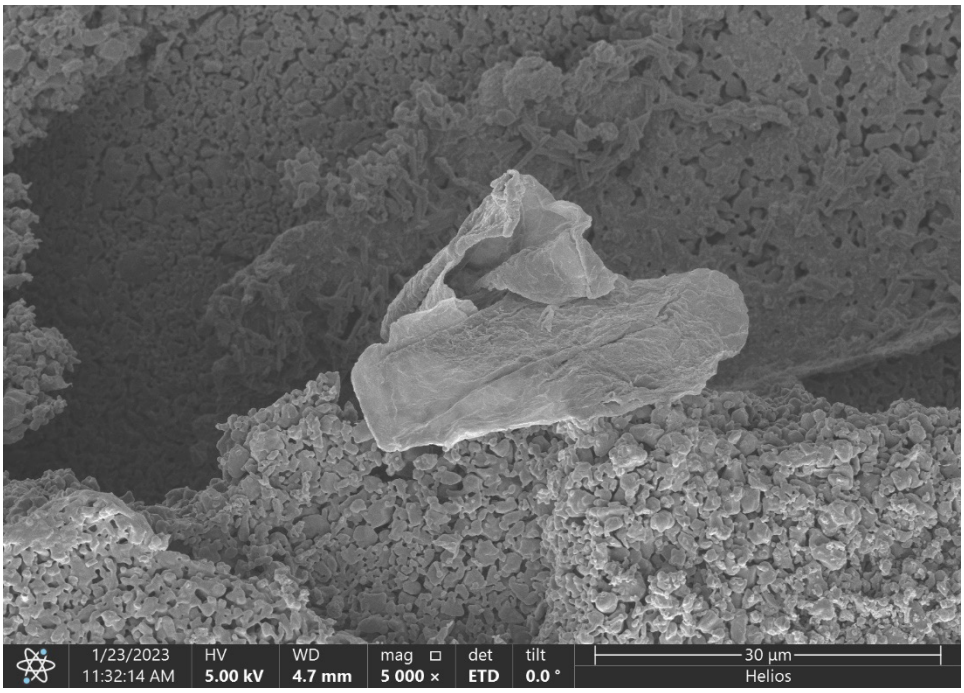

Figure 44. Initial Testing Sample that Was Debinded in Air (x5000)

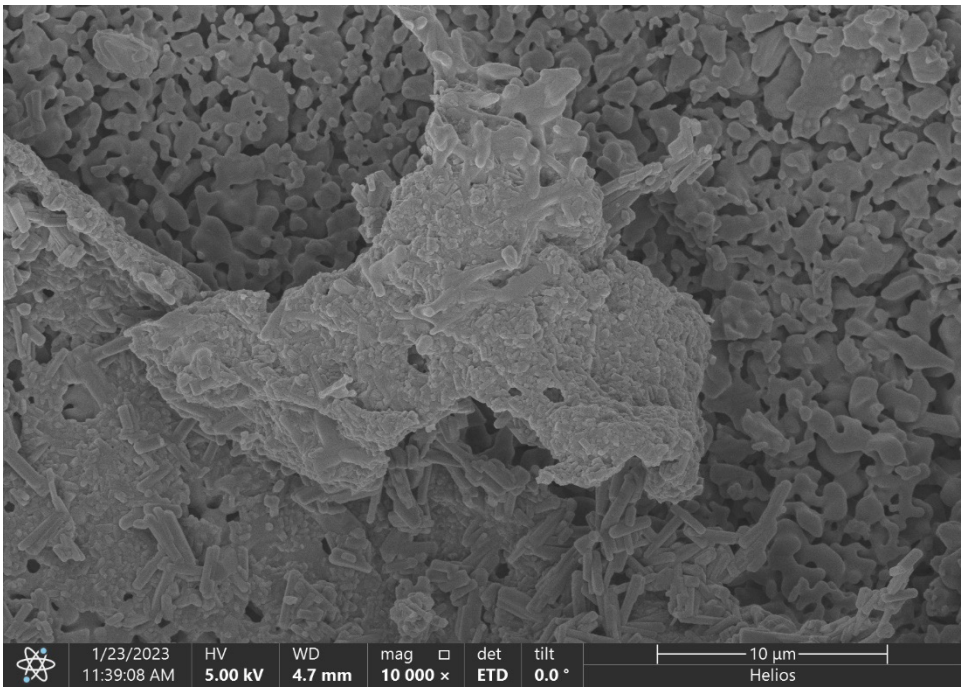

Figure 45. Initial Testing Sample that Was Debinded in Air (x10000)

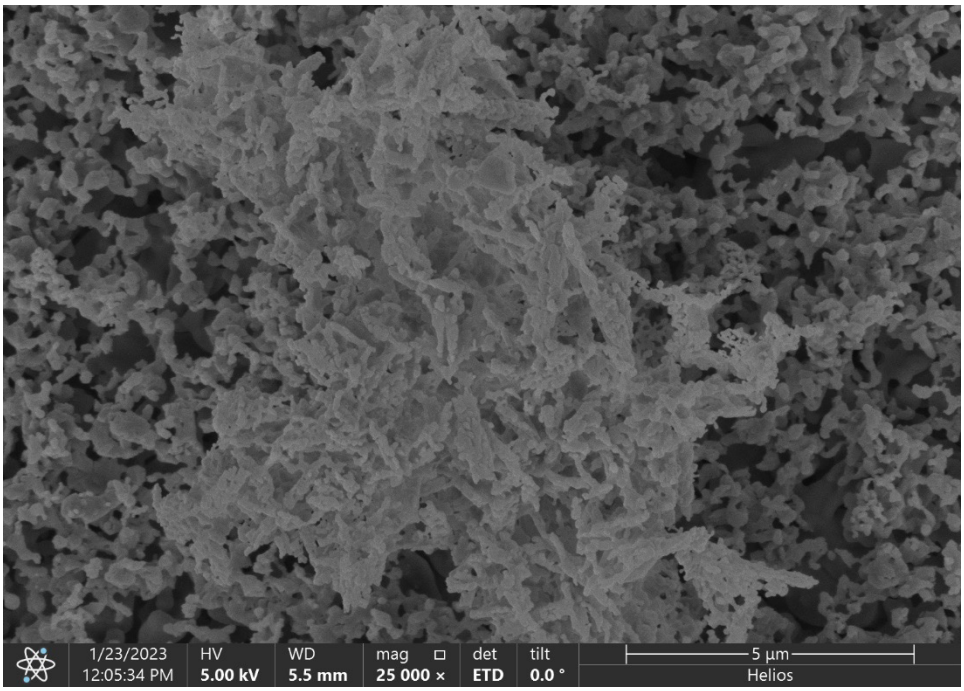

Figure 46. Initial Testing Sample that Was Debinded in Air (x25000)

The following images show the initial testing sample that was debinded in argon gas.

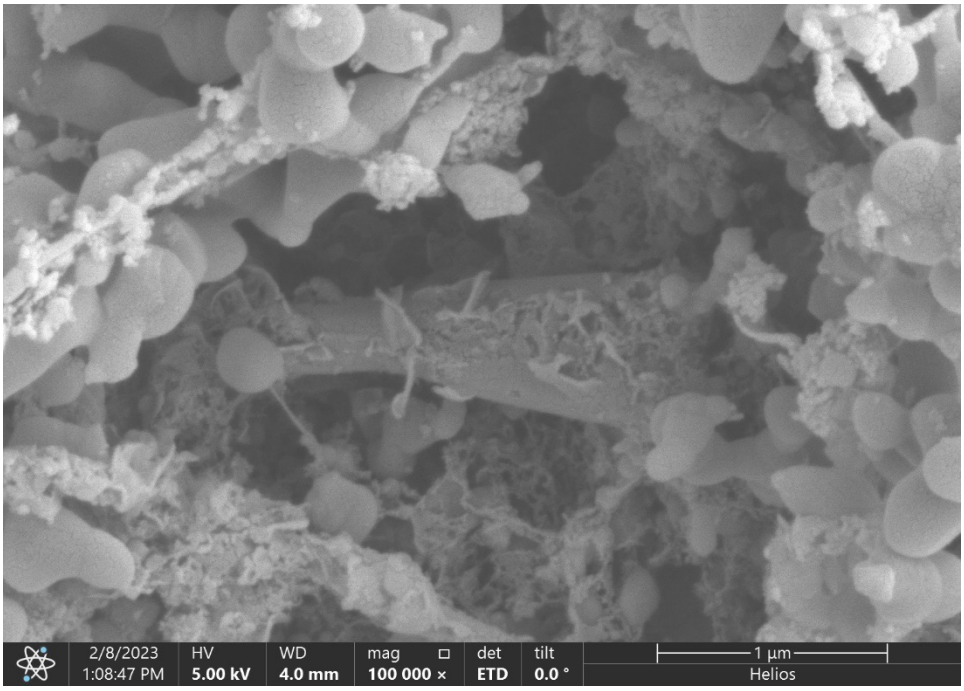

Figure 47. Initial Testing Sample that Was Debinded in Argon (x100000)

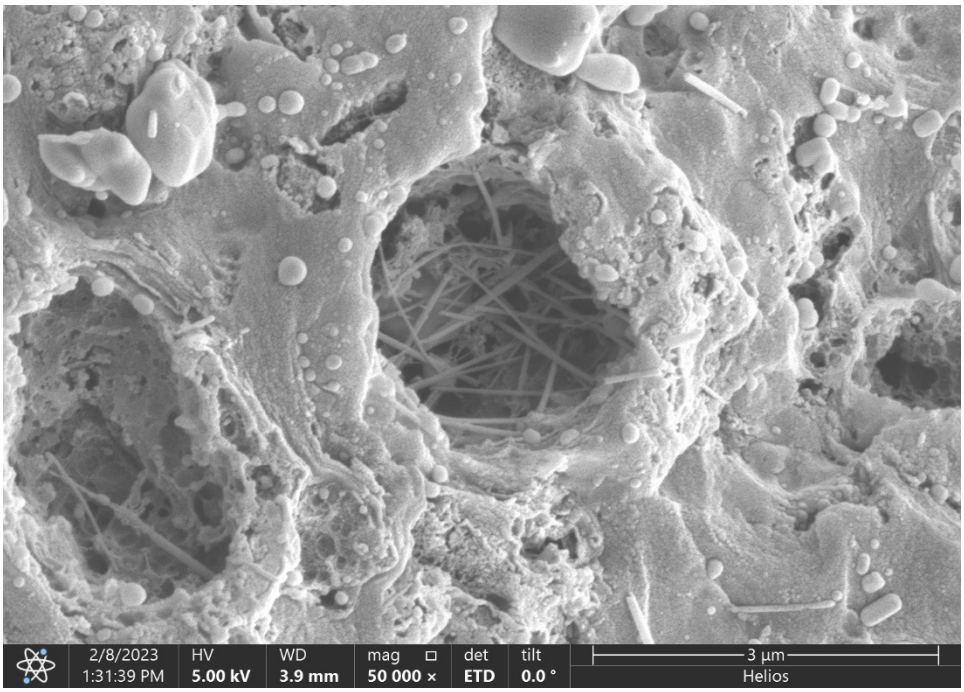

Figure 48. Initial Testing Sample that Was Debinded in Argon (x50000)

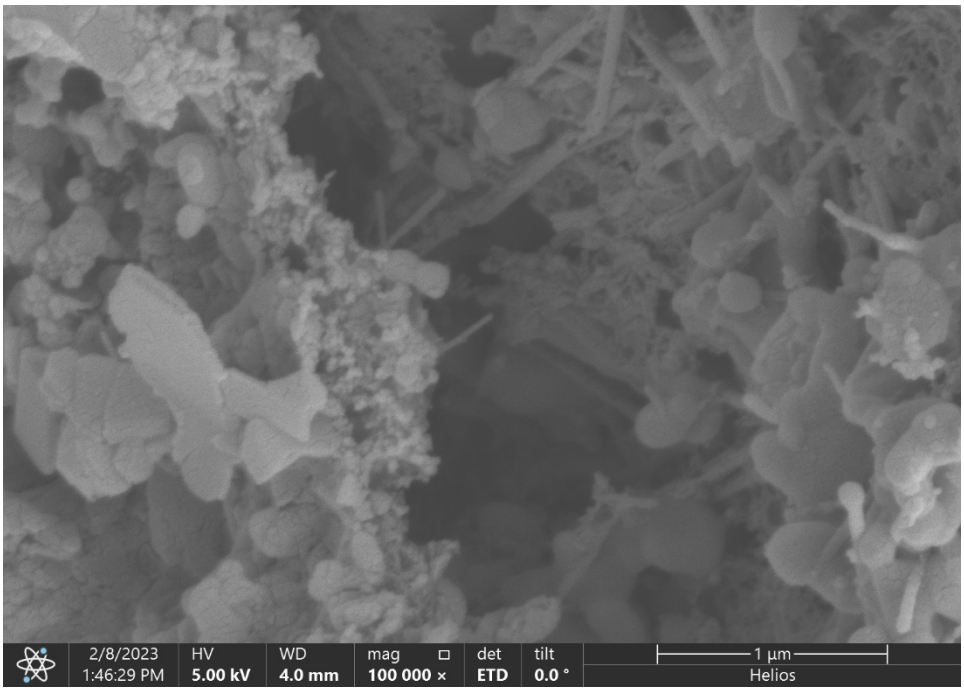

Figure 49. Initial Testing Sample that Was Debinded in Argon (x100000)

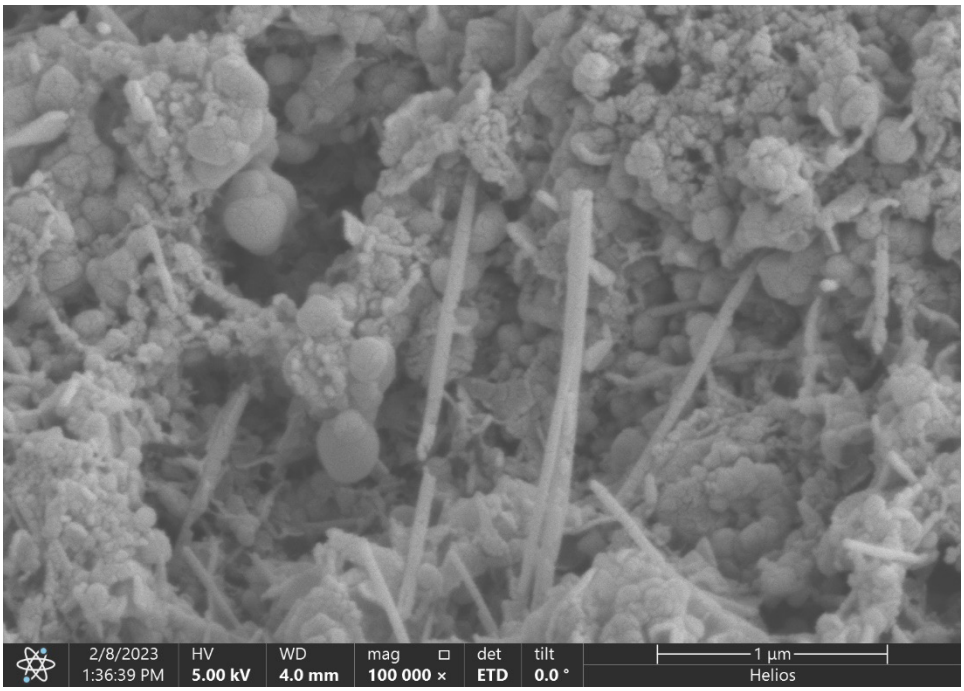

Figure 50. Initial Testing Sample that Was Debinded in Argon (x100000)

The following images show the sample sintered at 900ºC from Batch 1.

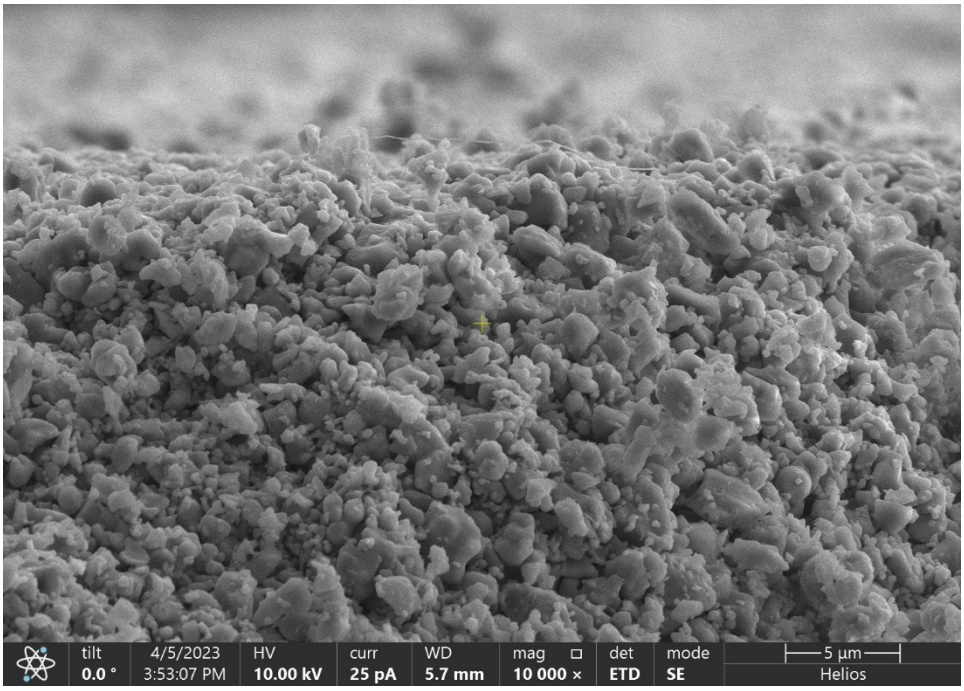

Figure 51. Sample Sintered at 900ºC from Batch 1 (x10000)

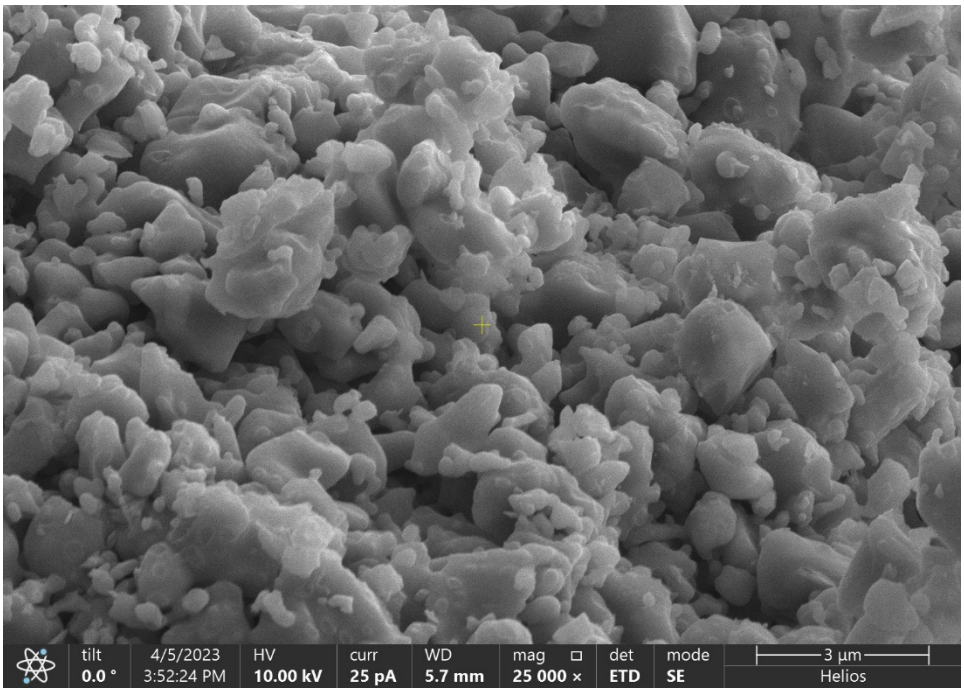

Figure 52. Sample Sintered at 900ºC from Batch 1 (x25000)

The following images show the sample sintered at 950ºC from Batch 1.

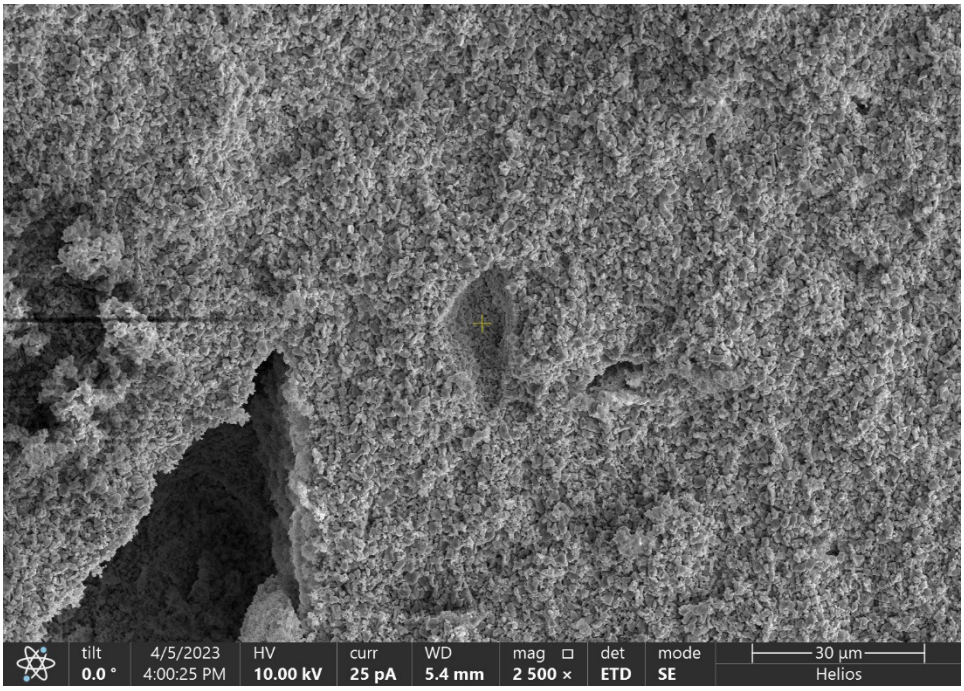

Figure 53. Sample Sintered at 950ºC from Batch 1 (x2500)

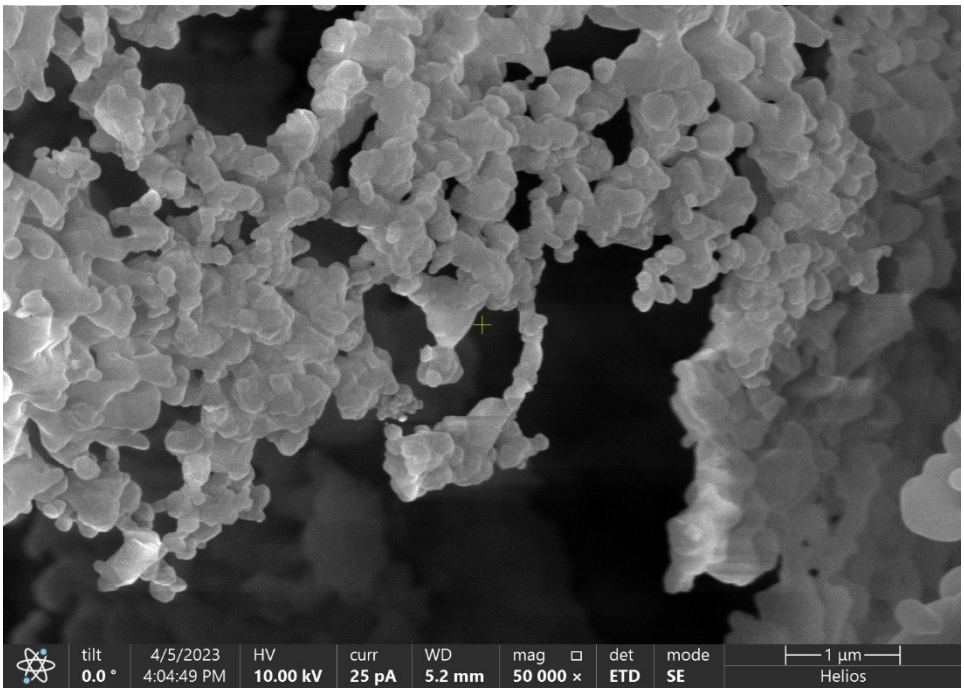

Figure 54. Sample Sintered at 950ºC from Batch 1 (x50000)

The following images show the sample sintered at 1000ºC from Batch 1.

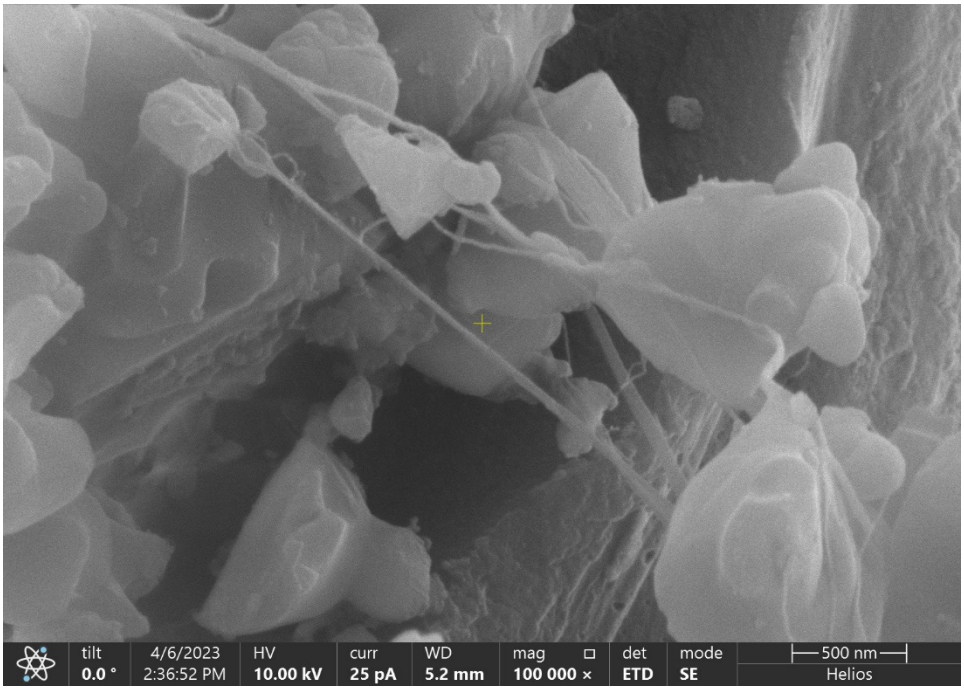

Figure 55. Sample Sintered at 1000ºC from Batch 1 (x100000)

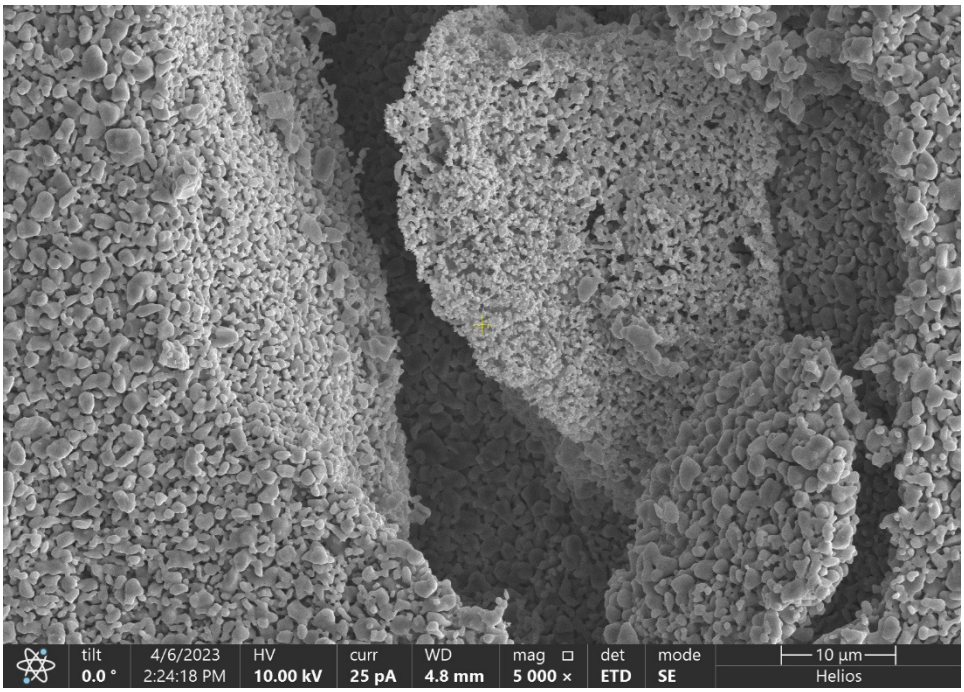

Figure 56. Sample Sintered at 1000ºC from Batch 1 (x5000)

The following images show the sample sintered at 1050ºC from Batch 1.

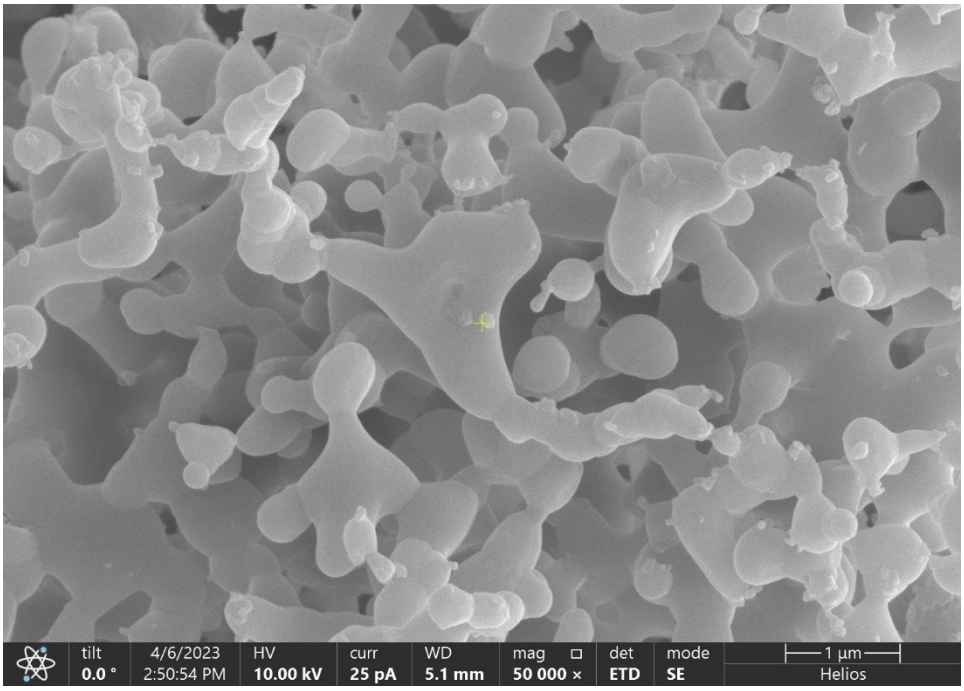

Figure 57. Sample Sintered at 1050ºC from Batch 1 (x50000)

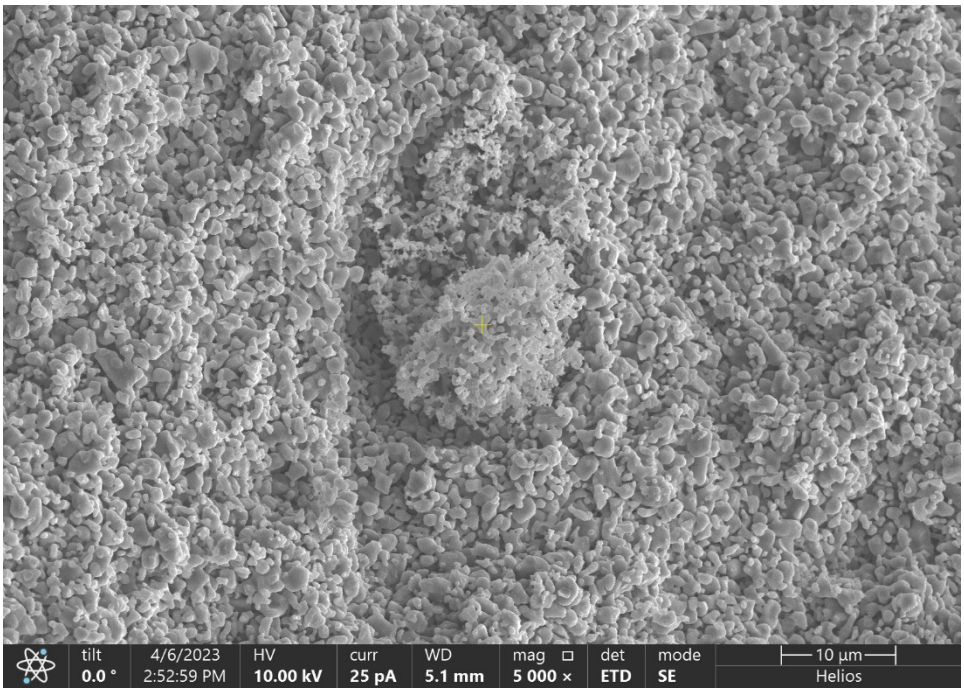

Figure 58. Sample Sintered at 1050ºC from Batch 1 (x5000)

The following images show the sample sintered at 1100ºC from Batch 1.

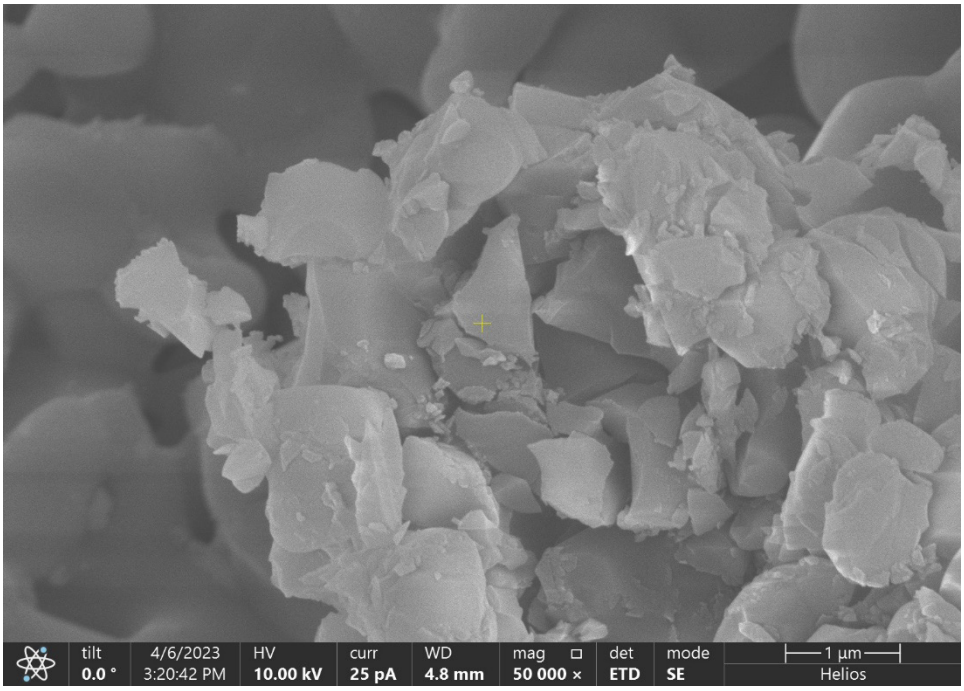

Figure 59. Sample Sintered at 1100ºC from Batch 1 (x50000)

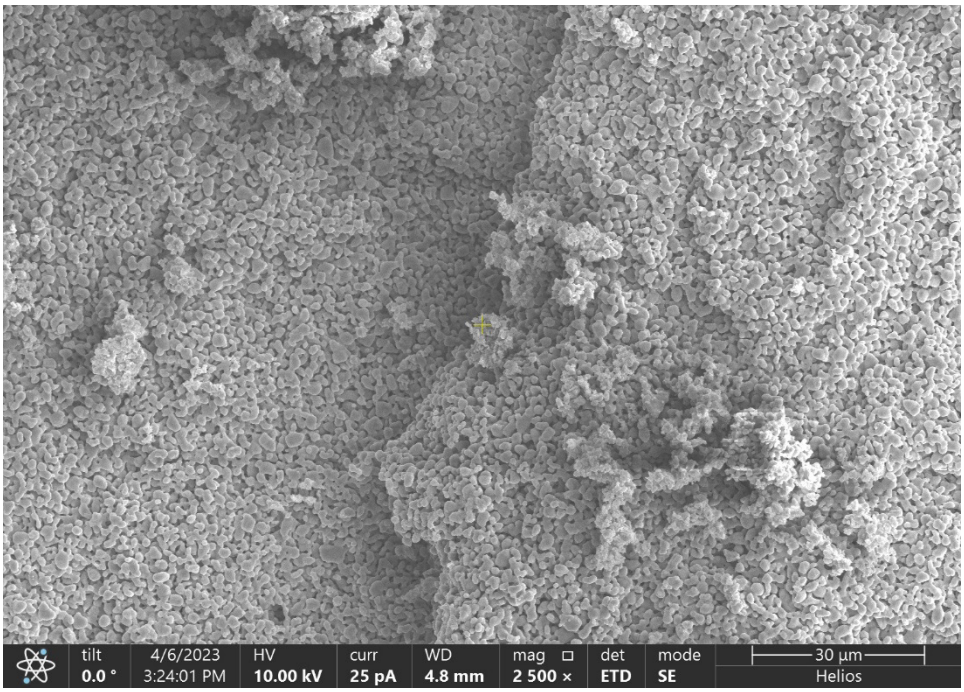

Figure 60. Sample Sintered at 1100ºC from Batch 1 (x2500)

The following images show the sample sintered in no medium from Batch 2.

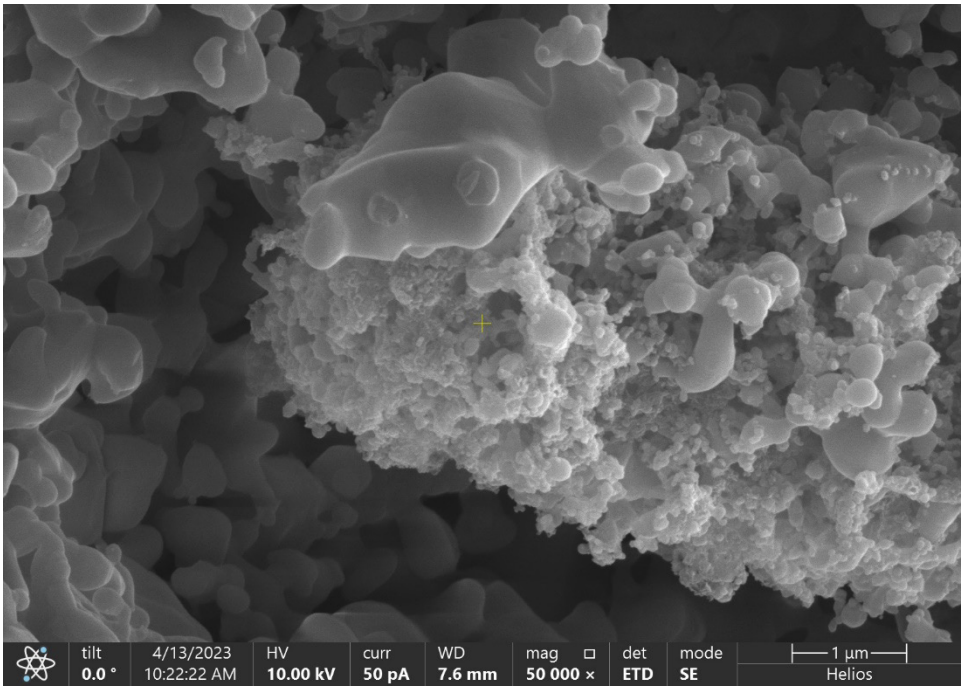

Figure 61. Sample Sintered with No Medium in Batch 2 (x50000)

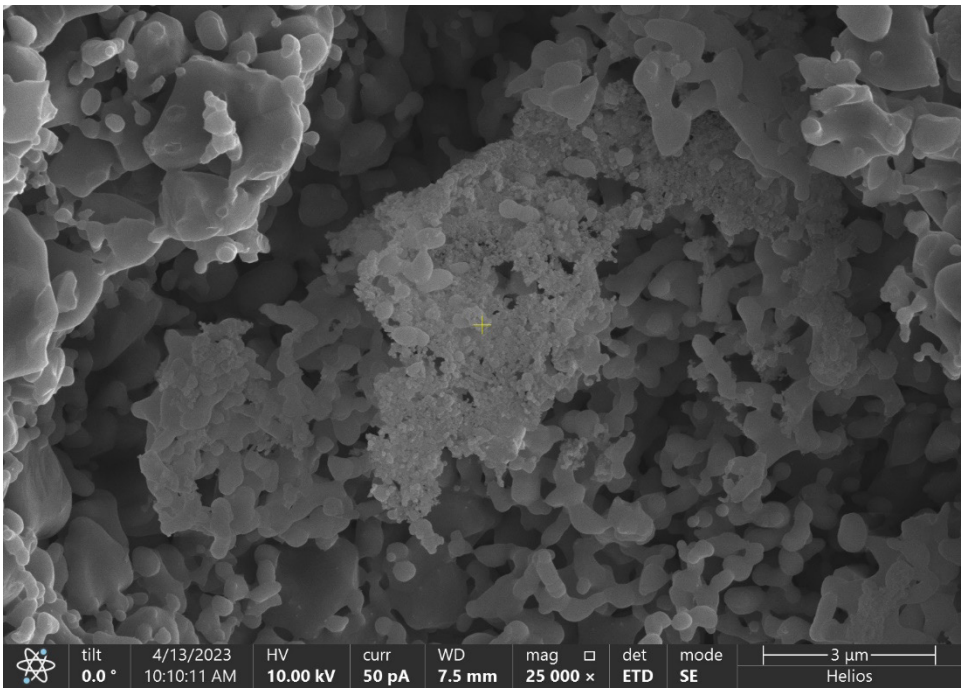

Figure 62. Sample Sintered with No Medium in Batch 2 (x25000)

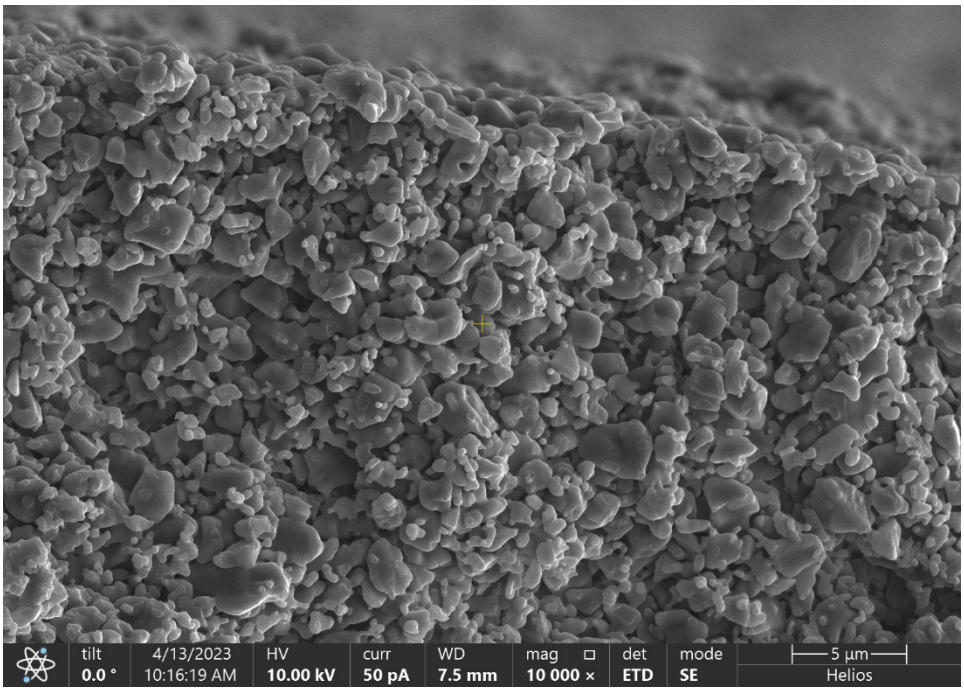

Figure 63. Sample Sintered with No Medium in Batch 2 (x10000)

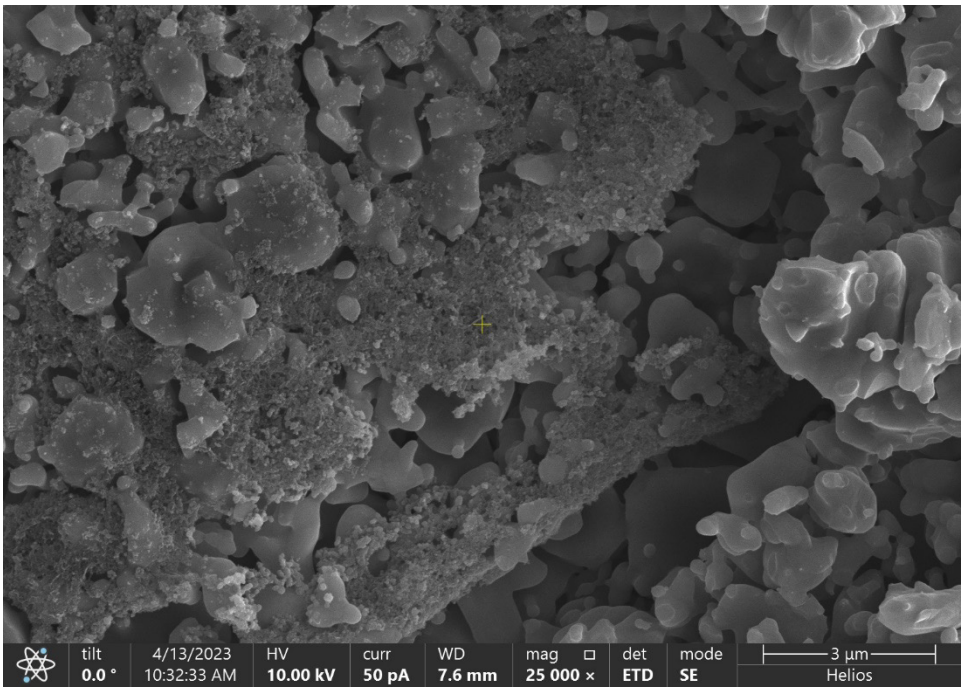

Figure 64. Sample Sintered with No Medium in Batch 2 (x25000)

The following images show the sample sintered in boron nitride medium from Batch 2.

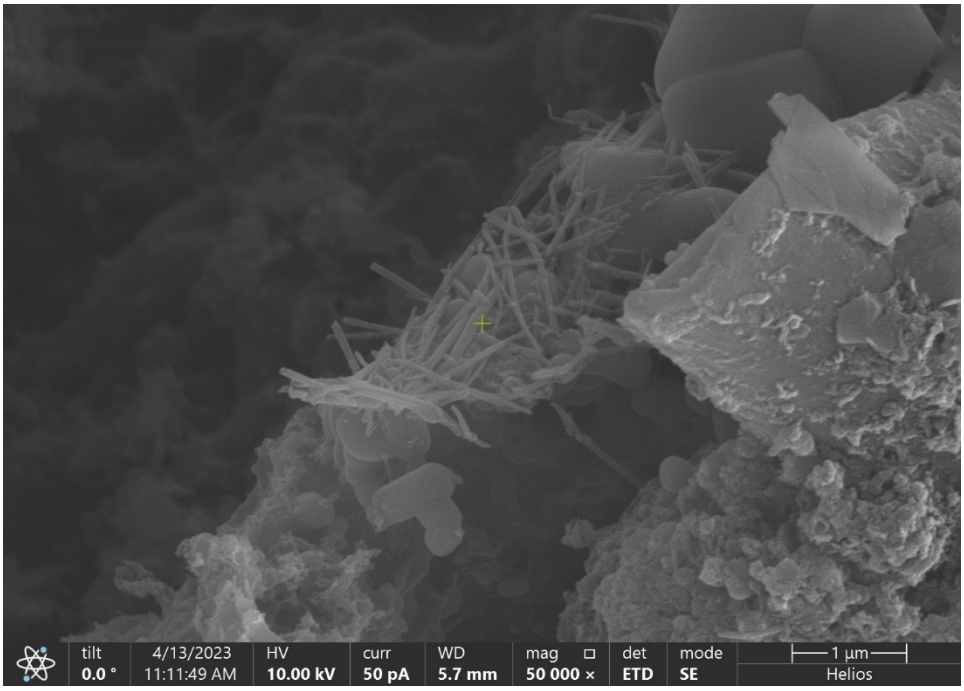

Figure 65. Sample Sintered with Boron Nitride Medium in Batch 2 (x50000)

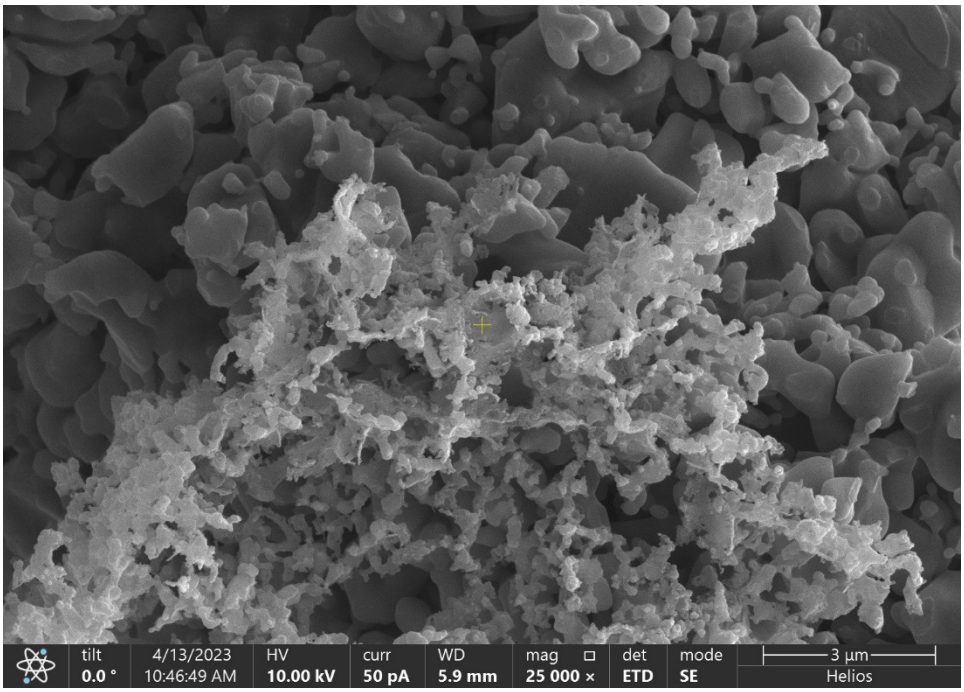

Figure 66. Sample Sintered with Boron Nitride Medium in Batch 2 (x25000)

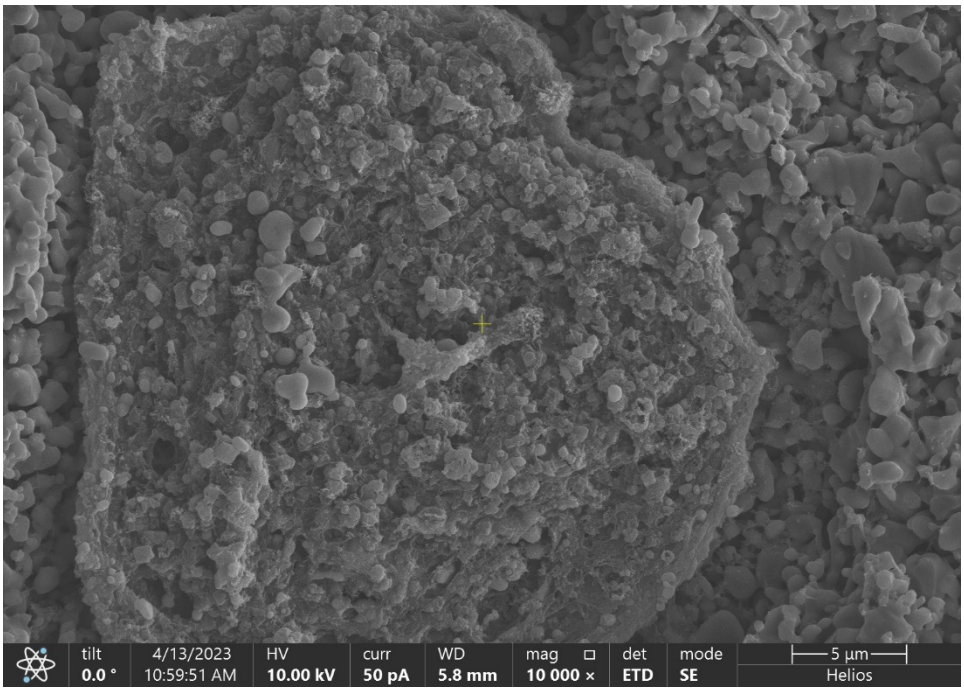

Figure 67. Sample Sintered with Boron Nitride Medium in Batch 2 (x10000)

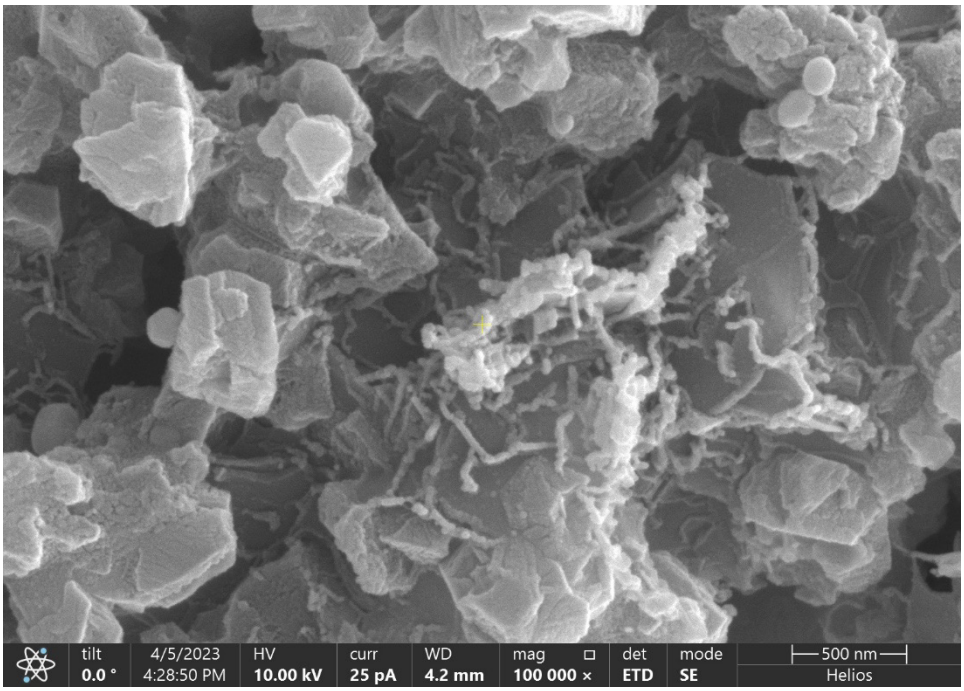

Figure 68. Sample Sintered with Boron Nitride Medium in Batch 2 (x100000)

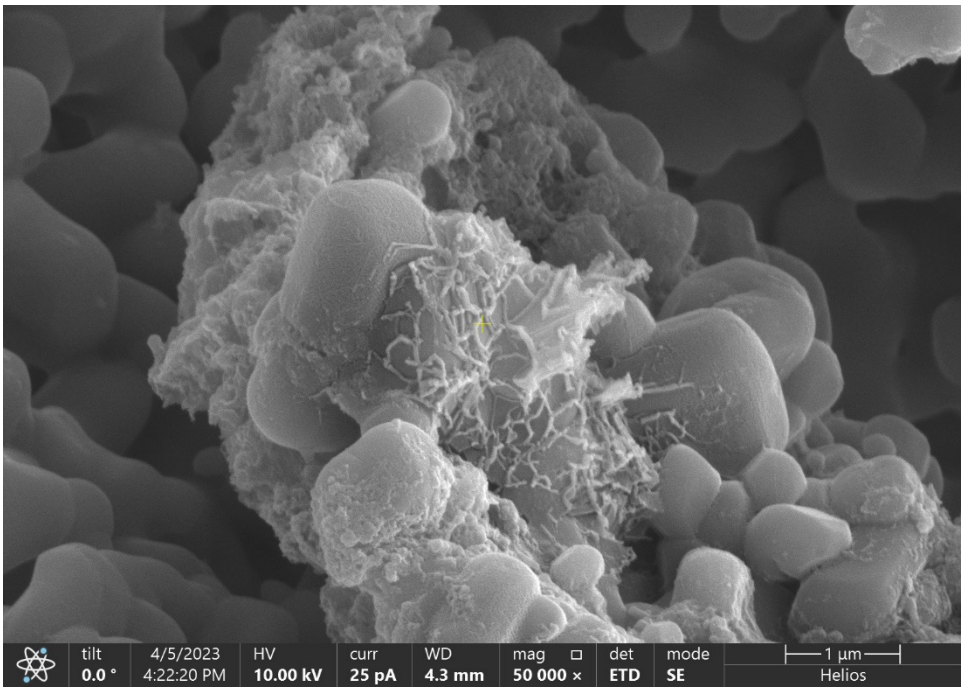

Figure 69. Sample Sintered with Boron Nitride Medium in Batch 2 (x50000)

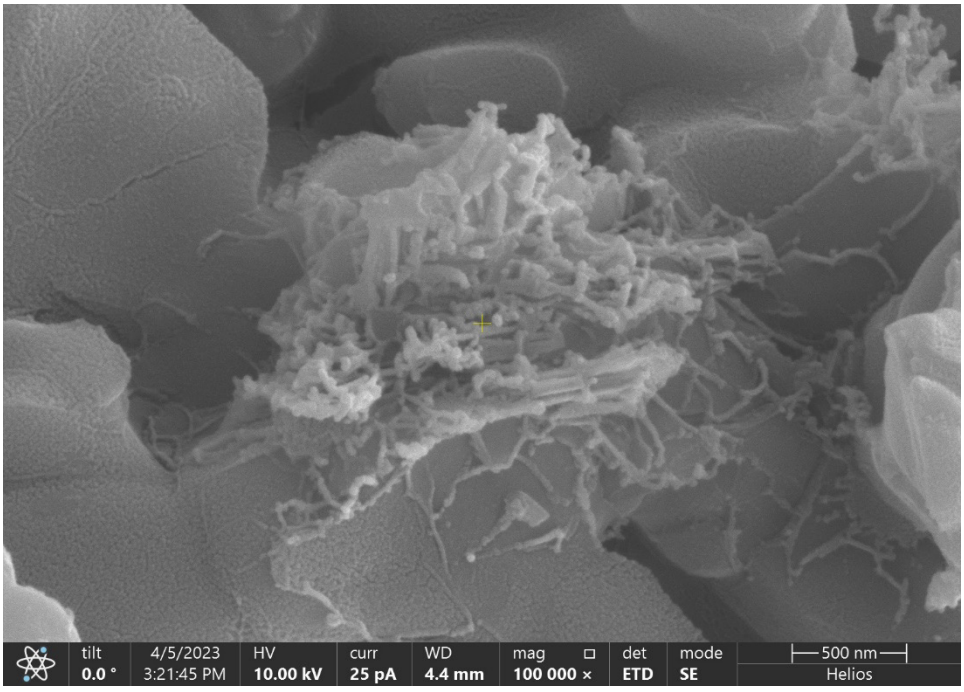

Figure 70. Sample Sintered with Boron Nitride Medium in Batch 2 (x100000)

The following images show the sample with BNNTs present in Batch 3.

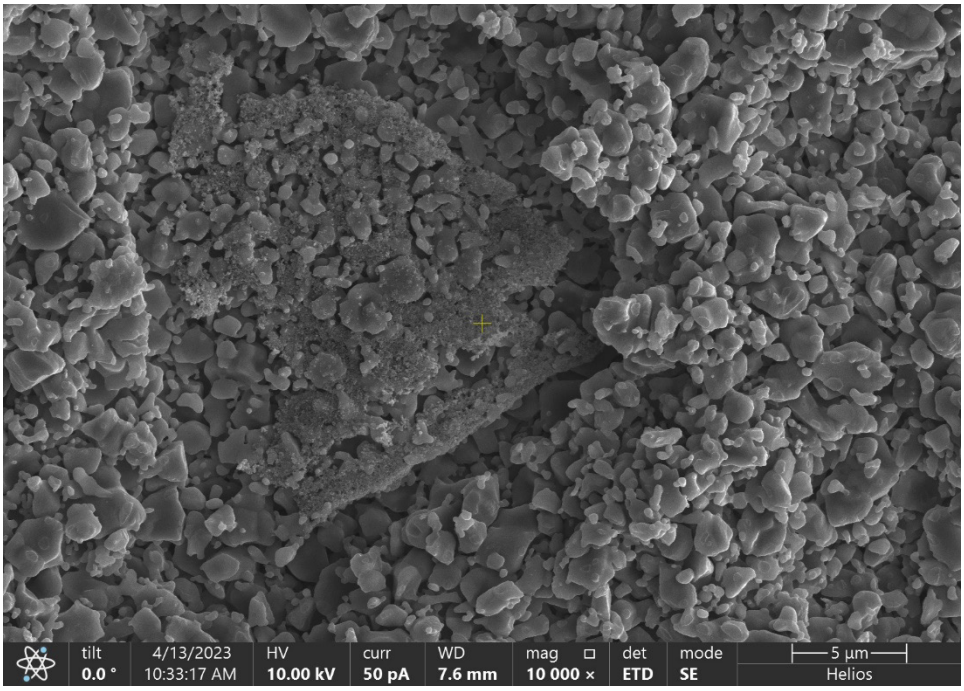

Figure 71. Sample with BNNTs Present in Batch 3 (x10000)

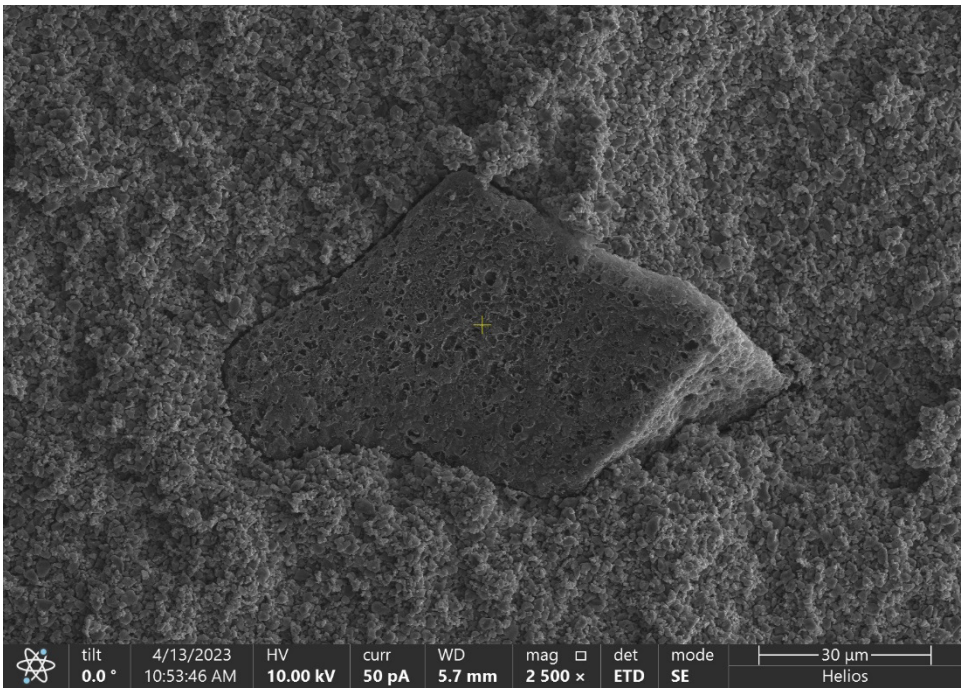

Figure 72. Sample with BNNTs Present in Batch 3 (x2500)

The following images show the sample with no BNNTs present in Batch 3.

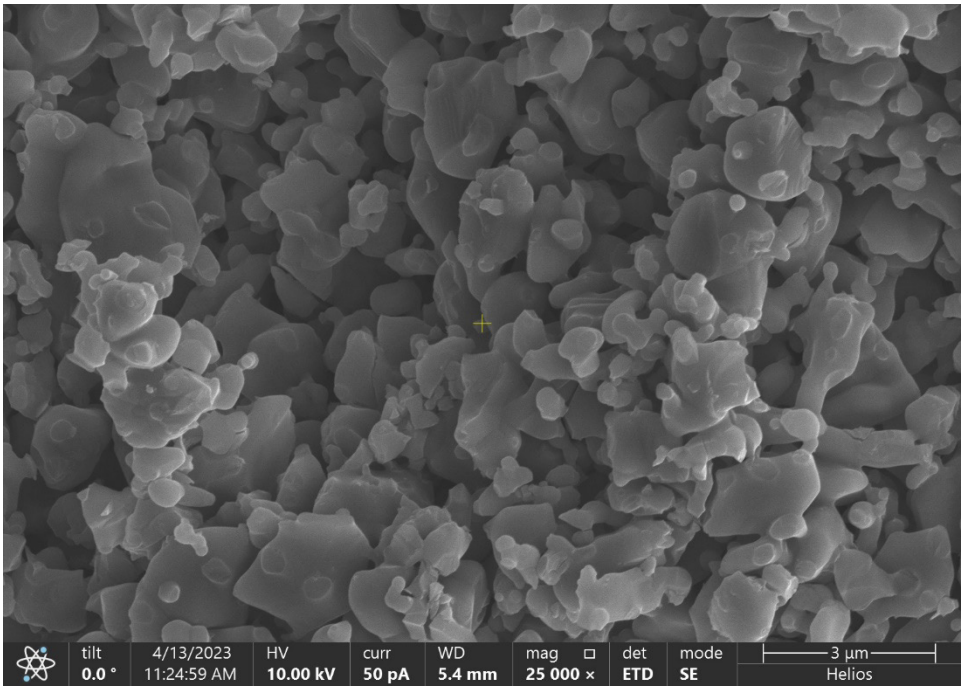

Figure 73. Sample with No BNNTs Present in Batch 3 (x25000)

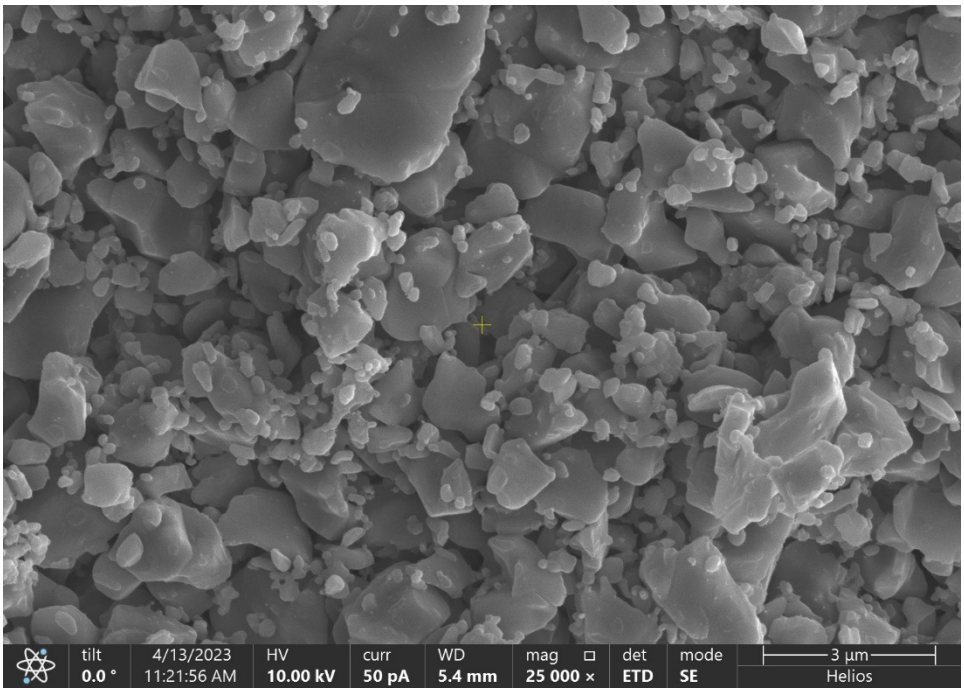

Figure 74. Sample with No BNNTs Present in Batch 3 (x25000)

LIST OF REFERENCES

[1] B. Swain, S. Bhuyan, R. Behera, S. Mohapatra, and A. Behera, "Wear: A serious problem in industry," in *Tribology in Materials and Manufacturing – Wear, Friction and Lubrication,* A. Patnaik, Eds. London, UK: IntechOpen, 2020, pp. 1–20.

[2] Department of Defense, "Defense Management: The Department of Defense's Annual Corrosion Budget Report," Washington, DC, 2012 [Online]. Available: https://apps.dtic.mil/sti/citations/ADA564923

[3] M. Fontana, *Corrosion Engineering*. New York, NY, USA: McGraw Hill, 1985.

[4] Massachusetts Institute of Technology, "Explained: hydrophobic and hydrophilic," July 16, 2013 [Online]. Available: https://news.mit.edu/2013/hydrophobic-and-hydrophilic-explained-0716

[5] Z. Zhao, Y. Liu, Y. Shao, Y. Wang, and B. Liu, "Relationship between hydrophobicity and drag reduction of SiO2/HLR-Si coatings," *Colloids Surf. Physicochem. Eng. Asp.*, vol. 642, Jun. 2022, [Online]. Available: https://doi.org/10.1016/j.colsurfa.2022.128668

[6] D. Aronov, R. Rosen, E. Z. Ron, and G. Rosenman, "Tunable hydroxyapatite wettability: effect on adhesion of biological molecules," *Process Biochem.*, vol. 41, no. 12, pp. 2367–2372, Dec. 2006, https://doi.org/10.1016/j.procbio.2006.06.006

[7] L. H. Li and Y. Chen, "Superhydrophobic properties of nonaligned boron nitride nanotube films," *Langmuir*, vol. 26, no. 7, pp. 5135–5140, Apr. 2010, https://doi.org/10.1021/la903604w

[8] G. Randle, "Thermally conductive ceramics," Precision Ceramics USA, May 20, 2021 [Online]. Available: https://precision-ceramics.com/thermally-conductive-ceramics/

[9] W.L. Wang, "Microstructure and mechanical properties of alumina ceramics reinforced by boron nitride nanotubes," *J. Eur. Ceram. Soc.*, vol. 31, no. 13, pp. 2277–2284, Nov. 2011 [Online]. Available: https://doi.org/10.1016/j.jeurceramsoc.2011.05.042

[10] T. Terao, C. Zhi, Y. Bando, M. Mitome, C. Tang, and D. Golberg, "Alignment of boron nitride nanotubes in polymeric composite films for thermal conductivity improvement," *J. Phys. Chem. C*, vol. 114, no. 10, pp. 4340–4344, Mar. 2010 [Online]. Available: https://doi.org/10.1021/jp911431f

[11] N. Kostoglou, "Boron nitride nanotubes versus carbon nanotubes: A thermal stability and oxidation behavior study," *Nanomaterials*, vol. 10, no. 12, pp. 2435, Dec. 2020 [Online]. Available: https://doi.org/10.3390/nano10122435

[12] G. Muralithran and S. Ramesh, "The effects of sintering temperature on the properties of hydroxyapatite," *Ceram. Int.*, vol. 26, no. 2, pp. 221–230, Mar. 2000 [Online]. Available: https://doi.org/10.1016/S0272-8842(99)00046-2

[13] National Institute of Standards and Technology, "Additive manufacturing of ceramics," August 4, 2021 [Online]. Available: https://www.nist.gov/programs-projects/additive-manufacturing-ceramics

[14] S. Hernandez, "Choosing a ceramic AM technology: An application-centered approach," Aniwaa, July 2020 [Online]. Available: https://www.aniwaa.com/insight/3d-printers/ceramic-additive-manufacturing-technologies/

[15] M. N. Rahaman, *Sintering of Ceramics*. Boca Raton, FL, USA: CRC Press, 2008.

[16] M. Nichols, "5 industries that benefit from ceramics 3d printing," Fabbaloo, May 01, 2020 [Online]. Available: https://www.fabbaloo.com/2020/05/5-industries-that-benefit-from-ceramics-3d-printing

[17] Vantage Market Research, "3D printing ceramic market – global industry assessment and forecast," January 1, 2022 [Online]. Available: https://www.vantagemarketresearch.com/industry-report/3d-printing-ceramic-market-1190#:~:text=Global%203D%20Printing%20Ceramic%20market,26.80%25%20during%20the%20forecast%20period

[18] R. Z. Legeros and J. P. Legeros, "Hydroxyapatite," in *Bioceramics and their Clinical Applications*, T. Kokubo, Ed. Boca Raton, FL, USA: CRC Press, 2008.

[19] National Center for Biotechnology Information, "Hydroxyapatite," [Online]. Available: https://pubchem.ncbi.nlm.nih.gov/compound/14781

[20] S. Rujitanapanich, P. Kumpapan, and P. Wanjanoi, "Synthesis of hydroxyapatite from oyster shell via precipitation," *Energy Procedia*, vol. 56, pp. 112–117, Dec. 2014 [Online]. Available: https://doi.org/10.1016/j.egypro.2014.07.138

[21] H. Kim, R. P. Camata, Y. K. Vohra, and W. R. Lacefield, "Control of phase composition in hydroxyapatite/tetracalcium phosphate biphasic thin coatings for biomedical applications," *J. Mater. Sci. Mater. Med.*, vol. 16, no. 10, pp. 961–966, Oct. 2005 [Online]. Available: https://doi.org/10.1007/s10856-005-4430-3

[22] D. Indrani, B. Soegijono, W. Adi, and N. Trout, "Phase composition and crystallinity of hydroxyapatite with various heat treatment temperatures," *Int. J. Appl. Pharm.*, vol. 9, p. 87, Jan. 2018 [Online]. Available: https://doi.org/10.22159/ijap.2017.v9s2.21

[23] MatWeb, "Calcium hydroxyapatite, Ca10(PO4)6(OH)2," [Online]. Available: https://www.matweb.com/search/datasheet_print.aspx?matguid=e1654c43ab994d7fab5e0f9aabe4dddc

[24] N. V. Bulina, "A study of thermal stability of hydroxyapatite," *Minerals*, vol. 11, no. 12, pp. 1310, Dec. 2021 [Online]. Available: https://doi.org/10.3390/min11121310

[25] C. J. Liao, F. H. Lin, K. S. Chen, and J. S. Sun, "Thermal decomposition and reconstitution of hydroxyapatite in air atmosphere," *Biomaterials*, vol. 20, no. 19, pp. 1807–1813, Oct. 1999 [Online]. Available: https://doi.org/10.1016/s0142-9612(99)00076-9

[26] AZO Materials, "Hydroxyapatite – properties and applications," Feb. 23, 2001 [Online]. Available: https://www.azom.com/article.aspx?ArticleID=107

[27] A. A. Campbell, "Bioceramics for implant coatings," *Mater. Today*, vol. 6, no. 11, pp. 26–30, Nov. 2003 [Online]. Available: https://doi.org/10.1016/S1369-7021(03)01128-3

[28] R. Dziak, K. Mohan, B. Almaghrabi, and Y. Park, "Nanoceramics for bone regeneration in the oral and craniomaxillofacial complex," in *Nanobiomaterials in Clinical Dentistry,* K. Subramani, W. Ahmed, and K. Hartsfield, Eds. Norwich, NY, USA: William Andrew, 2013, pp.289-409.

[29] BNNT Materials, "BNNT background and historical timeline," 2023 [Online]. Available: https://www.bnnt.com/resources/bnnt-background-and-historical-timeline

[30] B. Ghamsari, X. Xu, L. Gilburd, G. Walker, and P. Berini, "Mid-infrared surface phonon polaritons in boron-nitride nanotubes," *J. Opt.*, vol. 16, no.11, pp. 4008, Nov. 2014 [Online]. Available: https://doi.org/10.1088/2040-8978/16/11/114008

[31] M. Ishigami, S. Aloni, and A. Zettl, "Properties of boron nitride nanotubes," in *AIP Conference Proceedings*, pp. 94–99, 2003 [Online]. Available: https://doi.org/10.1063/1.1639682

[32] E. A. Turhan, A. E. Pazarçeviren, Z. Evis, and A. Tezcaner, "Properties and applications of boron nitride nanotubes," *Nanotechnology*, vol. 33, no. 24, pp. 2001, Mar. 2022 [Online]. Available: https://doi.org/10.1088/1361-6528/ac5839

[33] American Elements, "Boron Nitride Nanotubes," 2023 [Online]. Available: https://www.americanelements.com/boron-nitride-nanotubes-10043-11-5

[34] X. Chen and C. Ke, "Structural and physical properties of boron nitride nanotubes and their applications in nanocomposites," in *Boron Nitride Nanotubes in Nanomedicine*, G. Ciofani and V. Mattoli, Eds., in Micro and Nano Technologies. Boston: William Andrew Publishing, 2016, pp. 183–199 [Online]. Available: https://doi.org/10.1016/B978-0-323-38945-7.00012-2

[35] D. Zhang *et al.*, "Emerging Applications of Boron Nitride Nanotubes in Energy Harvesting, Electronics, and Biomedicine," *ACS Omega*, vol. 6, no. 32, pp. 20722–20728, Aug. 2021 [Online]. Available: https://doi.org/10.1021/acsomega.1c02586

[36] Lithoz, "3D printing for ceramics," 2023 [Online]. Available: https://lithoz.com/en/

[37] T. Einhauer, "LithaBone HA 480 | Ceramic 3D Printing," Sep. 21, 2022 [Online]. Available: https://lithoz.com/en/materials/lithabone-ha-480

[38] T. Einhauer, "LCM Technology," Apr. 15, 2022 [Online]. Available: https://lithoz.com/en/technology/lcm-technology

[39] Y. Chen, J. Zou, S. J. Campbell, and G. Le Caer, "Boron nitride nanotubes: Pronounced resistance to oxidation," *Appl. Phys. Lett.*, vol. 84, no. 13, pp. 2430–2432, Mar. 2004 [Online]. Available: https://doi.org/10.1063/1.1667278

[40] B. Pourmollaabbassi, S. Karbasi, and B. Hashemibeni, "Evaluate the growth and adhesion of osteoblast cells on nanocomposite scaffold of hydroxyapatite/titania coated with poly hydroxybutyrate," *Adv. Biomed. Res.*, vol. 5, pp. 156, Sep. 2016 [Online]. Available: https://doi.org/10.4103/2277-9175.188486

[41] J. Wang, Y. Gu, L. Zhang, G. Zhao, and Z. Zhang, "Synthesis of boron nitride nanotubes by self-propagation high-temperature synthesis and annealing method," Hindawi, January 18, 2011 [Online]. Available: https://www.hindawi.com/journals/jnm/2010/540456/fig3/

[42] W. M. Silva, H. Ribeiro, and J. J. Taha-Tijerina, "Potential production of theranostic boron nitride nanotubes (64cu-bnnts) radiolabeled by neutron capture," *Nanomaterials*, vol. 11, no. 11, p. 2907, Oct. 2021 [Online]. Available: https://doi.org/10.3390/nano11112907

[43] B. Karki, S. H. Dhobi, K. Yadav, S. P. Gupta, J. J. Nakarmi, and A. Pal, "Comparative study of boron oxides crystal with different sources x-ray production sources (Cu, Ag, Mo, and Fe)," *Mater. Lett. X*, vol. 13, pp. 100–110, Mar. 2022 [Online]. Available: https://doi.org/10.1016/j.mlblux.2021.100110

INITIAL DISTRIBUTION LIST

1. Defense Technical Information Center
   Ft. Belvoir, Virginia

2. Dudley Knox Library
   Naval Postgraduate School
   Monterey, California